Akademia Nauk Stosowanych w Nowym Sączu

Journal of Engineering, Energy and Informatics

No. 1/2025 (4)

Nowy Sącz, November 2025

Published by
Akademia Nauk Stosowanych w Nowym Sączu
ul. Staszica 1, 33-300 Nowy Sącz, tel.: 18 443 45 45, e-mail: sog@ans-ns.edu.pl

ISSN 2720-4162

Publisher's address
Wydawnictwo Naukowe Akademii Nauk Stosowanych w Nowym Sączu
ul. Staszica 1, 33-300 Nowy Sącz, tel.: +48 18 443 45 45, e-mail: wn@ans-ns.edu.pl, tbolanowska@ans-ns.edu.pl
wydawnictwo.ans-ns.edu.pl

Editorial Committee address
ul. Zamenhofa 1A, 33-300 Nowy Sącz, tel.: +48 18 547 29 08, e-mail: jeei@ans-ns.edu.pl, http://jeei.ans-ns.edu.pl

Printed by
Wydawnictwo i drukarnia NOVA SANDEC s.c.
Mariusz Kałyniuk, Roman Kałyniuk
ul. Lwowska 14, 33-300 Nowy Sącz, tel.: 18 441 02 88, e-mail: biuro@novasandec.pl

Contents

Anna KOCHANEK[1], **Natalia ZYGMUNT**[2]

[1] University of Applied Sciences in Nowy Sącz, Faculty of Engineering Sciences, Zamenhofa 1a, 33-300 Nowy Sącz, e-mail: akochanek@ans-ns.edu.pl
[2] University of Applied Sciences in Nowy Sącz, Faculty of Engineering Sciences, Zamenhofa 1a, 33-300 Nowy Sącz, e-mail: motyka.marek2801@gmail.com

Aspects of risk management in engineering projects based on survey research and the AHP method

Abstract

The aim of this article is to present risk management practices used in large engineering projects and to identify key factors influencing the success of these projects. The article is based on a survey conducted among engineering professionals and a decision analysis performed using the AHP method. The first part discusses selected methods and approaches to risk management. The empirical part presents the results of the survey, which show the awareness and practices of risk management among the respondents. The article concludes with an AHP hierarchical analysis, which identified the most important success factors in project risk management.

Keywords: risk management, engineering projects, AHP, survey analysis, project success.

Aspekty zarządzania ryzykiem w projektach inżynieryjnych na podstawie badań ankietowych i metody AHP

Streszczenie

Celem niniejszego artykułu jest przedstawienie praktyk zarządzania ryzykiem stosowanych w dużych projektach inżynieryjnych i identyfikacja kluczowych czynników wpływających na sukces tych przedsięwzięć. Artykuł opiera się na badaniach ankietowych przeprowadzonych wśród specjalistów z branży inżynieryjnej oraz analizie decyzyjnej przeprowadzonej metodą AHP. W pierwszej części omówiono wybrane metody i podejścia do zarządzania ryzykiem. W części empirycznej zaprezentowano wyniki badań ankietowych, które ukazują świadomość i praktyki zarządzania ryzykiem wśród respondentów. Artykuł kończy się analizą hierarchiczną AHP, która pozwoliła wyłonić najważniejsze czynniki sukcesu w zarządzaniu ryzykiem projektowym.

Słowa kluczowe: zarządzanie ryzykiem, projekty inżynieryjne, AHP, analiza ankietowa, sukces projektu.

1. Introduction

Contemporary engineering projects are characterized by high complexity, a high level of innovation, and significant financial outlays. Risk management plays a key role in their implementation, enabling the minimization of potential losses and maximization of the chances of success. The implementation of effective methods for identifying, analyzing, and responding to risk has become an indispensable part of project management.

The aim of this article is to analyze current risk management practices based on empirical research and to use the AHP method to identify the most important risk factors. The study was conducted among practitioners in the engineering industry, which allows for conclusions based on the professional experience of the respondents.

2. Literature review

Project management is a rapidly developing field of knowledge, particularly important in the context of engineering projects, which are characterized by high complexity, large scope, and strict time and budget constraints. Projects are defined as unique, temporary endeavors aimed at achieving specific goals within limited time, financial, and resource constraints. Figure 1 illustrates the key characteristics that define a project.

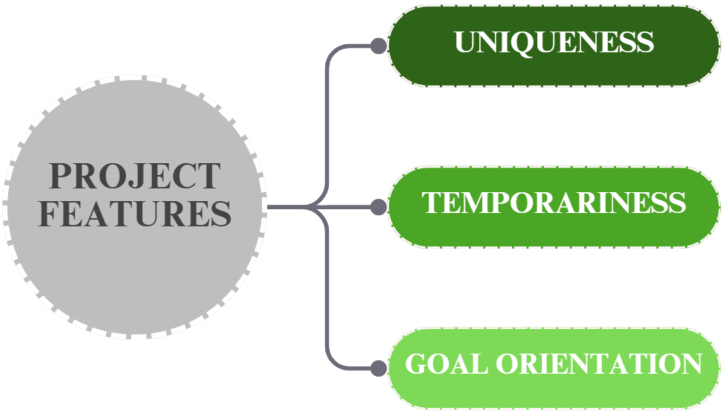

Figure 1. Diagram showing the features of the project

(source: own study based on PMI, 2021)

The first step in project management is to precisely define its objectives. Project objectives must comply with the SMART principle (Figure 2), i.e., they must be specific, measurable, achievable, realistic, and time-bound. Clearly formulating objectives allows for better organization of activities and their monitoring during implementation (Turner, 2016).

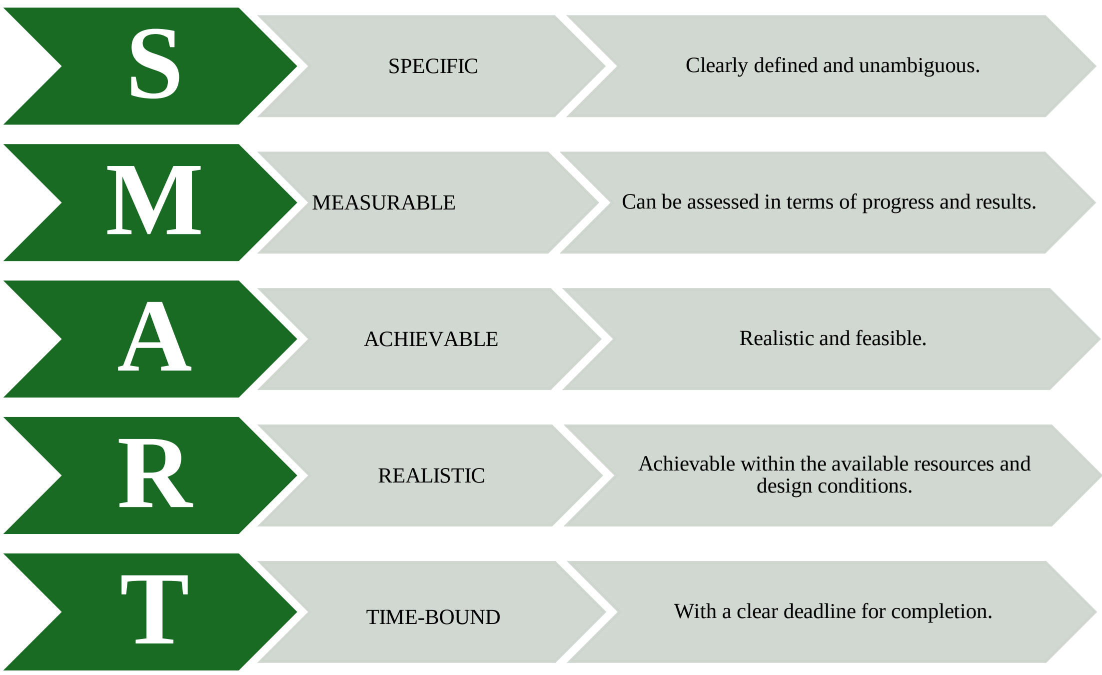

Figure 2. The SMART principle

(source: own study based on Turner, 2016)

In project management literature, risk is defined as an uncertain event or circumstance that, if it occurs, may affect the implementation of a project in both a negative and positive way (PMI, 2021). This means that risk is not only a threat, but can also be an opportunity to improve project performance by taking advantage of favorable circumstances. In the context of project management, risk is an important element of the so-called “iron triangle,” which includes time, budget, and project scope. A diagram illustrating the triangle of constraints is shown in Figure 3.

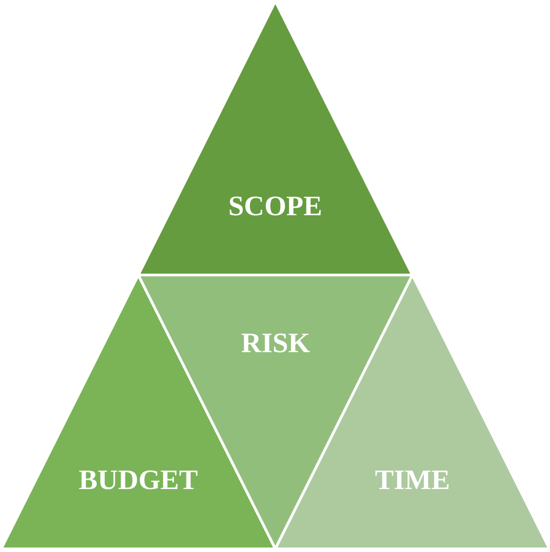

Figure 3. Diagram showing the triangle of constraints

(source: own study based on Petrenko, 2024)

Contemporary approaches to project management emphasize the need for flexibility, iteration, and value orientation, which translates into the selection of appropriate methodologies, including PMBOK, PRINCE2, and Agile. Table 1 presents a summary of the key features of the three most commonly used approaches to project management, with particular emphasis on risk management aspects. This comparison allows us to see both the differences and the potential for combining best practices depending on the nature of the project.

Table 1

Comparison of risk management methods

Criteria	PRINCE2	PMBOK	Agile
Structure	Standardized, process-based	Flexible, modular	Iterative, agile
Approach to risk	Documentation and control	Qualitative and quantitative analysis	Continuous adaptation and communication
Risk identification	Documentation analysis, consultations	Workshops, statistical analyses	Meetings, retrospectives
Risk assessment	Probability and impact	Qualitative and quantitative analysis	Subjective assessment by the team
Response planning	Risk management strategy	Contingency plans, corrective actions	Dynamic adjustment
Monitoring	Construction projects, IT, administration	Engineering projects, large organizations	IT, software development

(source: own elaboration)

The literature points to various approaches to risk analysis, including qualitative and quantitative assessment methods. The most commonly used ones include: SWOT analysis, PESTEL analysis, FMEA method, Monte Carlo analysis, risk matrices, earned value analysis (EVM), decision trees, and brainstorming. The choice of a specific method depends on the specifics of the project, available data, and the level of organizational maturity.

In the context of engineering projects, structural methods are particularly important, as they allow for a systematic approach to the identification and assessment of technical, financial, scheduling, and environmental risks. FMEA (Failure Mode and Effects Analysis) is one of the methods that is highly regarded in technical circles due to its transparency and practicality. Risk matrices, commonly used in qualitative analyses, allow for the assessment of the probability of a given risk occurring and the scale of its potential impact.

Project risk management, although well described in theory in the literature, often encounters organizational barriers in practice. In many cases, risk management procedures are not integrated into day-to-day project management, and actions are only taken after disruptions have occurred. The key factors influencing the effectiveness of risk management remain the organizational culture and the competencies of the project team.

3. Test results and interpretation

An analysis of the responses obtained from 162 respondents allows us to draw several key conclusions regarding the state of risk management in large engineering projects in Poland. Although the overall awareness of risk among the survey participants was high, the actual implementation of formal procedures and tools remains limited. In question 16, respondents were asked to assess the level of risk awareness in the organization where they work. The results are presented in Figure 4. The largest number of respondents, 38.9%, assessed the level of risk awareness as high. Another large group, accounting for 29.6% of the total, indicated a medium level. 21% of respondents described risk awareness in their organization as very high. It is worth noting that only 9.9% of survey participants indicated a low level, while a very low level was indicated by a marginal number of respondents – less than 1%.

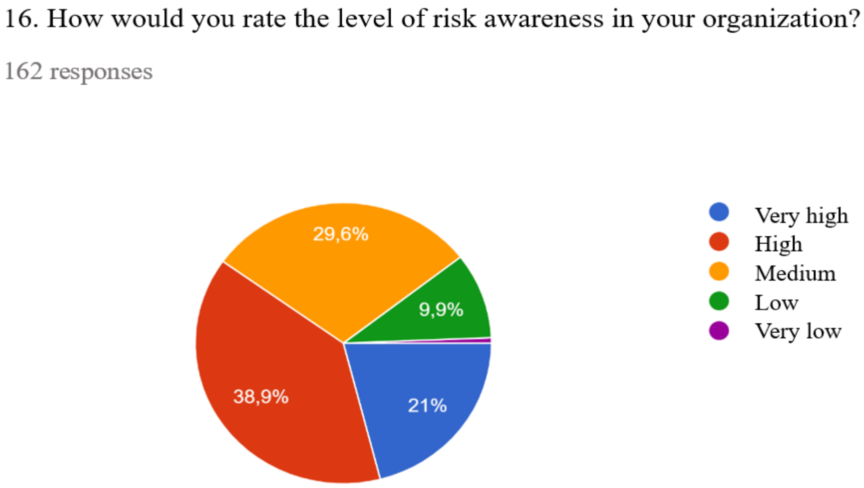

Figure 4. Assessment of risk awareness within the organization

(source: own elaboration)

The collected data indicate that the vast majority of respondents (nearly 60%) perceive the level of risk awareness in their organization as high or very high. This is a positive sign, indicating the growing importance of risk management and probably well-functioning information and education mechanisms for risk identification and assessment.

However, nearly 30% of respondents rate risk awareness as average, and nearly 10% as low, which may suggest the existence of certain barriers or differences in the perception of risk between departments, organizational levels, or depending on the individual experiences of employees. This may also indicate a need for further educational activities and a systematic approach to building a risk management culture.

Figure 5 shows the risk identification methods used in projects implemented by respondents. The question allowed for more than one answer to be selected, which is why the total percentage exceeds 100%.

The most frequently indicated method was SWOT analysis – 35.8% of survey participants declared using this technique. The second most popular was FMEA (Failure Mode and Effects Analysis) with a result of 31.5%, which indicates the widespread use of analytical approaches to assessing technical and operational risks. The Delphi method was indicated by 27.2% of respondents, and the Ishikawa diagram (cause--and-effect) by 22.2%. The relatively least frequently used method was Monte Carlo analysis, which is used by 14.8% of respondents.

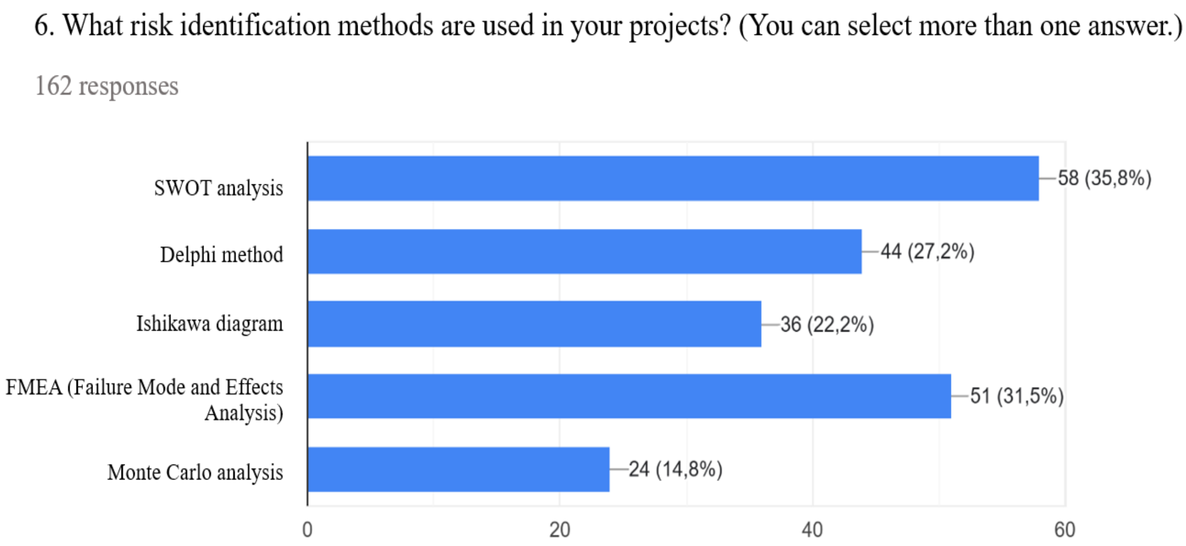

Figure 5. The most commonly used methods of risk identification in projects

(source: own elaboration)

The results show that respondents use a variety of risk identification methods, combining qualitative approaches (SWOT, Delphi, Ishikawa) with quantitative ones (FMEA, Monte Carlo). The popularity of SWOT may be due to its simplicity and versatility, while FMEA and Delphi reflect a desire for a more systematic and expert assessment of risks.

The relatively low use of Monte Carlo analysis may indicate limited availability of specialized tools or a lack of competence in probabilistic methods. The results suggest a need for further training and integration of more advanced analytical methods in project organizations.

Figure 6 shows respondents' answers regarding the most serious barriers to effective risk management in their organizations. The most frequently cited limitation is a limited risk management budget – this factor was indicated by 45.1% of respondents. In second place was insufficient data for analysis – 30.2% of responses.

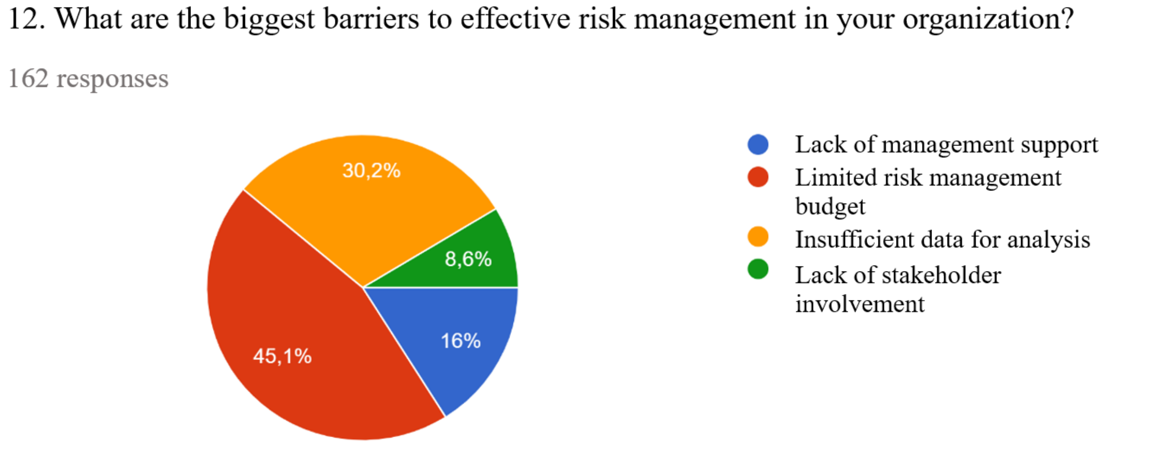

Figure 6. The most common barriers to effective risk management

(source: own elaboration)

The results clearly indicate that the biggest obstacle to implementing effective risk management is financial constraints, which can limit access to training, analytical tools, and human resources. The lack of data is another serious challenge, pointing to inadequate risk monitoring and reporting practices.

The relatively small number of responses indicating a lack of commitment from management or stakeholders may suggest that, although risk management has structural support, its effectiveness is limited primarily by systemic and organizational factors rather than people's attitudes.

In question 26, respondents were asked to indicate how often risk reviews are conducted in engineering projects in their organizations. The distribution of responses is shown in Figure 7.

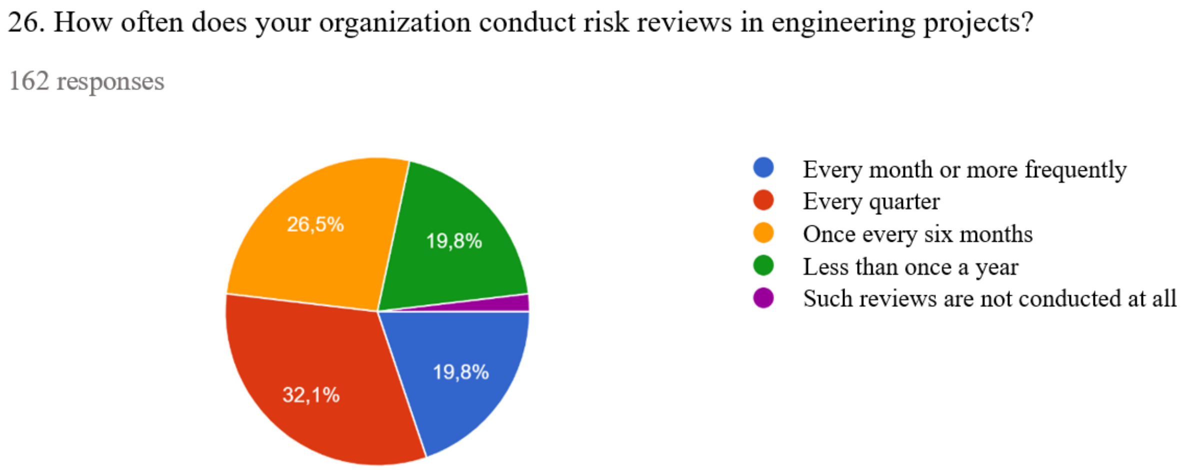

Figure 7. Frequency of risk reviews in engineering projects

(source: own elaboration)

The most frequently indicated answer is a quarterly risk review (32.1%), which can be considered a relatively optimal frequency in the context of large engineering projects, where risks change cyclically, but not necessarily at very short intervals. Slightly fewer, 26.5% of respondents, indicate reviews once every six months, which may be insufficient for dynamic projects. In turn, almost 20% of respondents declare monthly or more frequent reviews, which indicates a high level of commitment and organizational maturity in the area of risk monitoring.

However, it is worth noting that a total of almost 22% of organizations review risks less than once a year or not at all, which may indicate insufficient supervision of risks in design processes or a lack of a systematic approach to their management.

Analysis of the survey results enabled the formulation of important observations regarding risk management practices in engineering projects. The research sample included a diverse group of respondents in terms of professional experience, project roles, and industries, which strengthens the reliability and multifaceted nature of the data obtained.

Most participants in the study confirmed the existence of formal risk management policies in their organizations, but their actual application is sometimes limited. This indicates a discrepancy between the declarative and operational levels of risk management. The respondents emphasized that the effectiveness of these activities depends not only on the choice of methodology (e.g. FMEA, PRINCE2, PMBOK), but also on its consistent implementation and support from the organization.

The main barriers to effective risk management identified include: limited resources (budget, time), lack of specialized tools, resistance from teams, and insufficiently rapid response to threats. The role of organizational culture proved to be equally important – open communication and team involvement are prerequisites for the effectiveness of the entire process.

Respondents most often use general tools such as spreadsheets or Microsoft Project, while specialized software (e.g., Primavera Risk Analysis, Tableau) is used sporadically. Nevertheless, there is a noticeable trend toward digitization – many organizations are planning to implement new technologies to support risk management, including solutions based on predictive analytics and artificial intelligence.

Key findings:

- Risk management is present in most organizations, but its practical implementation can be inconsistent.
- The most commonly used methodologies are FMEA, PRINCE2, and PMBOK, which are particularly valued in technical projects.
- The main obstacles are lack of resources, organizational resistance, limited tools, and slow response times.
- Organizational culture and open communication are essential for effective risk management.
- There is a widespread belief in the need to improve current practices.
- Digital technologies, including automation, predictive analytics, and Big Data, are considered key areas for development.

Practical recommendations:
- Enforce the application of risk management procedures in project practice.
- Invest in modern IT tools that support risk analysis and monitoring.
- Develop the competencies of project teams, including in the areas of communication and working in conditions of uncertainty.
- Ensure organizational flexibility to enable rapid response to threats.
- Build a culture of openness to risk by encouraging active reporting of uncertainty.
- Standardize the approach to risk management within the organization, especially in multi-disciplinary projects.

The collected data clearly indicate that although the importance of risk management is recognized by most survey participants, its implementation remains selective, strongly dependent on the specific nature of the organization, the type of project, and the awareness of management. The results justify the need for further support for organizations – both through training and the selection of appropriate tools and system procedures.

4. Analysis of risk management methods using the AHP method

This chapter presents a comparative analysis of four popular risk management methodologies: PRINCE2, PMBOK, Agile, and FMEA, using the Analytic Hierarchy Process (AHP) method. The aim of the study was to determine which of the analyzed methodologies best meets the criteria for effective risk management in projects.

The analysis adopted six key criteria that are essential for effective risk management:

1. Methodology structure – transparency, completeness, and consistency of the methodology structure,
2. Approach to risk – systematic actions and compliance with best practices,
3. Risk identification – effectiveness in recognizing potential threats,
4. Risk assessment – depth and accuracy of risk analysis,
5. Response planning – flexibility and adequacy of remedial actions,
6. Monitoring – effectiveness in tracking and reporting risks.

The Saaty scale (1-9) was used to assign weights to individual criteria. Based on expert assessment, the following comparison matrix was created in Table 2.

Table 2

Criteria pair comparison matrix

Criteria	Structure	Approach	Identification	Assessment	Response planning	Monitoring
Structure	1	0,5	1	1	2	1
Approach	2	1	2	2	2	2
Identification	1	0,5	1	1	2	1
Assessment	1	0,5	1	1	2	1
Response planning	0,5	0,5	0,5	0,5	1	0,5
Monitoring	1	0,5	1	1	2	1
Sum	6,5	3,5	6,5	6,5	11	6,5

(source: own elaboration)

Based on expert assessments, a matrix of comparisons of pairs of criteria was developed in accordance with Saaty's scale. The results were normalized and the following AHP weights were determined in Table 3.

Table 3

Comparison matrix and criteria weights

Criteria	AHP weight
Approach to risk	0,2393
Risk assessment	0,1764
Response planning	0,1490
Methodology structure	0,1451
Risk identification	0,1451
Monitoring	0,1451

(source: own elaboration)

Each methodology was assigned a score based on a subjective expert assessment in Table 4.

Table 4

Scoring of methods against criteria (scale 1-5)

Criteria	PRINCE2	PMBOK	Agile	FMEA
Methodology structure	5	4	3	3
Approach to risk	4	5	3	4
Risk identification	4	5	4	5
Risk assessment	4	5	3	5
Response planning	4	5	5	5
Monitoring	4	5	3	4

(source: own elaboration)

The preference index was calculated using the following formula:

$$W = \sum_{Y=1}^{n} P_{XY} \cdot W_Y \qquad (1)$$

where:

P_{XY} – point assessment of method X in relation to criteria Y,

W_Y – weight assigned to the criteria Y.

PMBOK=4×0.1451+5×0.2393+5×0.1451+5×0.1764+5×0.1490+5×0.1451=4.8549
FMEA=3×0.1451+4×0.2393+5×0.1451+5×0.1764+5×0.1490+4×0.1451=4.3254
PRINCE2=5×0.1451+4×0.2393+4×0.1451+4×0.1764+4×0.1490+4×0.1451=4.1451
Agile=3×0.1451+3×0.2393+4×0.1451+3×0.1764+5×0.1490+3×0.1451=3.4431

The final values are as follows:

- PMBOK – 4.85
- FMEA – 4.33
- PRINCE2 – 4.15
- Agile – 3.44

The AHP analysis shows that PMBOK is the most comprehensive and effective risk management methodology. It received the highest final score, which proves its strong process-based approach, broad scope of risk assessment, and well-developed planning and monitoring mechanisms.

Second place went to the FMEA method, which stands out for its excellent effectiveness in identifying and analyzing threats. Its specialized nature makes it particularly useful in engineering and manufacturing environments, despite its less complex management structure compared to PMBOK.

The PRINCE2 methodology took third place, offering a well-organized approach to risk, especially in the context of administrative and infrastructure projects.

Agile methodology came last in the ranking. Although very flexible and agile, it focuses less on formal and systematic risk management. Its approach works better in environments requiring rapid iterations than in projects requiring precise risk analysis.

The use of the AHP method enabled a transparent, multi-criteria analysis to be carried out, which can support project managers in selecting the most appropriate risk management methodology, tailored to the specific nature of the organization or industry.

5. Conclusions

The aim of this article was to analyze the risk management methods used in engineering projects, with particular emphasis on the level of organizational awareness, the effectiveness of the tools used, and their compliance with applicable standards. The empirical research conducted allowed us to assess the degree of risk management implementation in practice and identify areas requiring improvement.

The results indicate the growing popularity of tools such as FMEA, PRINCE2, PMBOK, and SWOT analysis, with FMEA gaining particular recognition for its simplicity and effectiveness in the context of technical risk. At the same time, as many as 90.7% of respondents expressed the need to improve current practices, confirming the growing awareness of the importance of effective risk management. Despite this, only 30.2% of respondents rated the level of risk awareness in their organization as very high, indicating a need for further educational and organizational measures.

Some organizations do not conduct systematic risk reviews, which increases the vulnerability of projects to disruptions. In response to these challenges, a comparative analysis of four risk management methodologies (PMBOK, PRINCE2, Agile, and FMEA) was also carried out using the AHP method. Six decision criteria were taken into account, which enabled an objective assessment and selection of an approach tailored to the specific nature of the project.

Based on the analyses, the following practical recommendations were formulated:

– implementing regular and cyclical risk reviews at all stages of the project;
– integrating risk management with scheduling and cost control (e.g., through EVM);
– developing a risk management culture through training and team communication;
– using a variety of tools, such as risk matrices, FMEA, and Monte Carlo simulations.

In summary, risk management should be viewed not as a formal obligation, but as a strategic tool supporting project decision-making. Effective identification, assessment, and response to risk increase the chances of completing projects within budget, on schedule, and within scope. The findings of this article can serve as a starting point for further research and practical support for organizations seeking mature solutions in the area of risk management.

References

Anderson, D.J. (2010). *Kanban: Successful Evolutionary Change for Your Technology Business*. Washington DC: Blue Hole Press.

Aven, T. (2016). *Risk assessment and risk management: Review of recent advances on their foundation. European Journal of Operational Research, 253*(1), 1-13. DOI: https://doi.org/10.1016/j.ejor.2015.12.023.

Axelos. (2017). *Managing Successful Projects with PRINCE2*. London: TSO.

Beck, K., Beedle, M., van Bennekum, A., Cockburn, A., Cunningham, W., Fowler, M., Jeffries, R. (2001). *Manifest Agile*. Agile Alliance. Retrieved from: http://agilemanifesto.org.

Bennett, R., Lemoine, G. (2011). *PRINCE2: A Practical Handbook*. London: Kogan Page.

Boothroyd, K., Thompson, C. (2024). *Fundamentals of risk management: Understanding, evaluating and implementing effective enterprise risk management (7th ed.)*. London, New York: Kogan Page.

Chapman, C., Ward, S. (2011). *How to Manage Project Opportunity and Risk: Why Uncertainty Management Can Be a Much Better Approach than Risk Management*. Chichester, UK: Wiley.

Cohn, M. (2009). *Succeeding with Agile: Software Development Using Scrum*. Ann Arbor: Addison-Wesley.

Derby, E., Larsen, D. (2016). *Agile Retrospectives: Making Good Teams Great*. Raleigh: Pragmatic Bookshelf.

Gido, J., Clements, J.P. (2014). *Successful Project Management*. Stamford: Cengage Learning.

Highsmith, J. (2010). *Agile Project Management: Creating Innovative Products*. Boston: Addison-Wesley.

Hillson, D. (2012). *Practical Project Risk Management: The ATOM Methodology*. Tysons Corner, VA: Management Concepts Press.

Hillson, D. (2016). *The Risk Management Handbook: A Practical Guide to Managing the Multiple Dimensions of Risk*. London: Kogan Page.

Hillson, D. (2024). *Managing Risk in Projects*. London: Routledge.

Hillson, D., Murray-Webster, R. (2007). *Understanding and Managing Risk Attitude*. London: Routledge.

Hopkin, P. (2018). *Fundamentals of Risk Management: Understanding, Evaluating and Implementing Effective Risk Management*. London, New York: Kogan Page.

ISO. (2018). *ISO 31000:2018 Risk Management – Guidelines*. Genewa: International Organization for Standardization.

Kendrick, T. (2024). *Identifying and Managing Project Risk: Essential Tools for Failure-Proofing Your Project*. New York: AMACOM.

Kerzner, H. (2022). *Project Management: A Systems Approach to Planning, Scheduling, and Controlling*. Hoboken, New Jersey: Wiley.

Kutsch, E., Hall, M. (2010). Bridging the Risk Gap: The Failure of Risk Management in Information Systems Projects. *Research-Technology Management*, 57(2), 26-32. DOI: https://doi.org/10.5437/08956308X5702133.

Larson, E.W., Gray, C.F. (2014). *Project Management: The Managerial Process*. New York: McGraw-Hill Education.

Lock, D. (2013). *Project Management*. Burlington: Routledge.

McDermott, R., Mikulak, R.J., Beauregard, M. (2008). *The Basics of FMEA*. New York: CRC Press.

Office of Government Commerce (OGC). (2009). *Managing Successful Projects with PRINCE2*. London: TSO.

Petrenko, T. (2024). Working with constraints in project management. *Zeszyty Naukowe Wyższej Szkoły Bankowej w Poznaniu, 100*(1), 1-7.

PMI (Project Management Institute). (2017). *A Guide to the Project Management Body of Knowledge (PMBOK® Guide)* (6th ed.). Newtown Square: PMI.

PMI (Project Management Institute). (2021). *A Guide to the Project Management Body of Knowledge (PMBOK® Guide)* (7th ed.). Newtown Square: PMI.

Pritchard, C.L. (2014). *Risk Management: Concepts and Guidance*. London, New York: CRC Press.

Schwalbe, K. (2015). *Information Technology Project Management* (8th ed.). Bolston: Cengage Learning.

Smith, N.J., Merna T., Jobling, P. (2014). *Managing Risk in Construction Projects*. Chichester: Wiley-Blackwell.

Stamatis, D.H. (2003). *Failure Mode and Effect Analysis: FMEA from Theory to Execution*. Milwaukee: ASQ Quality Press.

Tchankova, L. (2002). *Risk identification – basic stage in risk management. Environmental Management and Health, 13*(3), 290-297. DOI: https://doi.org/10.1108/09566160210431088.

Turner, J.R. (2013). *Gower Handbook of Project Management*. London, New York: Routledge.

Vose, D. (2008). *Risk Analysis: A Quantitative Guide*. Chichester: Wiley.

Walker, A. (2015). *Project Management in Construction*. Chichester: Wiley.

Winch, G.M. (2009). *Managing Construction Projects. 2nd Edition*. Chichester: Wiley-Blackwell.

Iga PIETRUCHA[1], **Jan MATUŁA**[2]

[1] University of Applied Sciences in Nowy Sącz, Faculty of Engineering Sciences, Zamenhofa 1a, 33-300 Nowy Sącz, e-mail: ipietrucha@ans-ns.edu.pl
[2] University of Applied Sciences in Nowy Sącz, Faculty of Engineering Sciences, Zamenhofa 1a, 33-300 Nowy Sącz, e-mail: jasiek.matula@wp.pl

Prototype of a system that tracks the sun's rays

Abstract

The article presents the design and implementation of a prototype tracking system for photovoltaic panels, whose task is to track the movement of the Sun and improve energy conversion efficiency. Traditional PV installations are characterized by limited efficiency resulting from the fixed orientation of the modules, which leads to a decrease in energy production during the day. The developed system uses an Arduino Leonardo microcontroller, MG995 servo mechanisms, and four photoresistors acting as light intensity sensors. The algorithm, implemented in C++, analyzes sensor readings and dynamically corrects the position of the platform in two axes, ensuring that the panels are maintained in the direction of maximum radiation. Tests conducted on the constructed prototype confirmed the effectiveness of the system – the platform responded smoothly and stably to changing lighting conditions. The results indicate that the use of tracking systems in real photovoltaic farms can increase energy yields by 20-35% compared to static installations. They are particularly important in Poland, where seasonal variability in sunlight means that tracking systems can significantly improve the profitability of investments.

Key words: photovoltaics, energy production, microcontroller, tracking system.

Prototyp systemu nadążającego za promieniami słonecznymi

Streszczenie

W artykule przedstawiono projekt oraz implementację prototypu systemu nadążnego dla paneli fotowoltaicznych, którego zadaniem jest śledzenie ruchu Słońca i poprawa efektywności konwersji energii. Tradycyjne instalacje PV charakteryzują się ograniczoną wydajnością wynikającą z nieruchomej orientacji modułów, co prowadzi do spadku produkcji energii w ciągu dnia. Opracowany system wykorzystuje mikrokontroler Arduino Leonardo, serwomechanizmy MG995 oraz cztery fotorezystory pełniące rolę czujników natężenia światła. Zaimplementowany w języku C++ algorytm analizuje odczyty z sensorów i dynamicznie koryguje położenie platformy w dwóch osiach, zapewniając utrzymanie paneli w kierunku maksymalnego promieniowania. Badania przeprowadzone na skonstruowanym prototypie potwierdziły skuteczność działania systemu – platforma reagowała płynnie i stabilnie na zmieniające się warunki oświetlenia. Wyniki wskazują, że zastosowanie systemów nadążnych w rzeczywistych farmach fotowoltaicznych może zwiększyć uzyski energii o 20-35% w porównaniu do instalacji statycznych. Szczególne znaczenie mają one w Polsce, gdzie sezonowa zmienność nasłonecznienia sprawia, że systemy śledzące mogą istotnie poprawić opłacalność inwestycji.

Słowa kluczowe: fotowoltaika, produkcja energii, mikrokontroler, system nadążny.

1. Introduction

Global demand for electricity is constantly growing, while at the same time issues such as climate change, CO_2 emissions, and the need for energy transition are becoming increasingly important. In this context, renewable energy sources (RES) are becoming a key element of many countries' strategies. One of the fastest growing technologies in the RES sector is photovoltaics. Thanks to falling PV cell production costs, regulatory support, and subsidy programs, photovoltaics in Poland is developing very dynamically (Bachanek, 2025).

In Poland, the technical potential of solar energy is ~153,484 PJ, which corresponds to approx. 42,634 TWh – an amount that could cover approx. 26% of the country's annual electricity consumption (Igliński, 2023). Despite this potential, there are several limitations: seasonal and daily changes in sunlight, meteorological conditions, angles of incidence of sunlight, as well as the orientation and inclination of the panels. In static photovoltaic installations, the panels are positioned once, which gives good efficiency during periods of maximum sunlight, but less good efficiency in the morning, evening, and winter months. To overcome these limitations, the concept of solar tracking systems is being developed. These systems allow for dynamic adjustment of the orientation of the panels relative to the position of the sun, which can significantly increase energy yield. The literature shows that with a single axis of rotation, an increase in efficiency of 10-20% can be achieved, and with dual-axis systems, even 30-40% compared to static panels. Research by Harazin and co-authors has shown that the gains from trackers are particularly high in the morning and evening, when static panels are less efficient (Harazin, 2022).

In addition to improving efficiency, tracking systems also pose technical and economic challenges: installation and maintenance costs, weather resistance, precision of mechanisms, and energy consumption of the control system itself. In Poland, where the climate is temperate and seasonal sunshine varies greatly, these systems seem to make particular sense – they can allow for better use of morning and evening hours and improve performance in the transitional months of spring and fall (Kumba, 2024).

This article focuses on the development and testing of a prototype tracking system based on an Arduino Leonardo microcontroller, servo mechanisms, and photoresistors. The aim is to verify whether such a solution can be practical and effective as an educational model or on a small scale, with the possibility of scaling or modification for larger installations. Both the theoretical and design assumptions as well as the preliminary test results will be presented, which will allow for the assessment of the potential of such a system in conditions typical for Poland.

2. Purpose and scope

The aim of this article is to present the design and implementation of a prototype tracking system for photovoltaic panels, whose task is to increase the efficiency of solar energy conversion by dynamically adjusting the position of the modules relative to the radiation source. The research was conducted to test the practical application of such systems in laboratory conditions and to assess their potential efficiency in real installations.

The research part includes an analysis of the theoretical principles of photovoltaic systems and trackers, the characteristics of the electronic and mechanical components used, a description of the control algorithm, and a presentation of the prototype test results. The article also includes references to the literature on the subject, presenting the benefits of using tracking systems, as well as a discussion of the possibilities for further development of the solution towards its practical implementation in photovoltaic (PV) installations.

3. Basic concepts

Solar radiation is the primary source of renewable energy available on Earth. Its total power reaching the upper layers of the atmosphere averages 1361 W/m² and is referred to as the solar constant (Kopp, 2011). However, this value varies significantly depending on latitude, season, atmospheric conditions, and the angle of incidence of sunlight, as shown in Figure 1.

The energy emitted by the Sun is electromagnetic radiation, which covers a wide range of wavelengths – from ultraviolet (UV) radiation, through visible radiation, to infrared (IR) radiation. Visible radiation (approx. 43%) and infrared radiation (approx. 49%) account for the largest share of the solar spectrum, while ultraviolet radiation accounts for only a few percent of the total energy (Duffie, 2013).

The amount of energy reaching the Earth's surface is significantly affected by the atmosphere, which partially absorbs and scatters electromagnetic waves. As a result, the radiation power at ground level rarely exceeds 1000 W/m². In practice, when designing photovoltaic systems, the values of average annual irradiation expressed in kWh/m²/year are used, which depend on the location.

The key properties of solar radiation from the point of view of renewable energy include:

- radiation intensity – most often expressed in W/m², determining the instantaneous power density;
- wave spectrum – the distribution of energy as a function of wavelength, which determines the conversion efficiency in PV cells;
- angle of incidence – determining how much of the radiation is absorbed by the panel surface;
- polarization and scattering – related to the interaction of the atmosphere, which can change the direction and quality of radiation;
- temporal variability – resulting from the daily and annual cycles and meteorological conditions.

Understanding these properties is crucial for the design of tracking systems, whose task is to position the panels so that the angle of incidence of the sun's rays is as close to perpendicular as possible. In this way, it is possible to increase energy yields compared to static systems. Studies have shown that optimal panel positioning can increase the amount of energy produced by up to 20-40%, depending on latitude and climatic conditions (Bamisile, 2025).

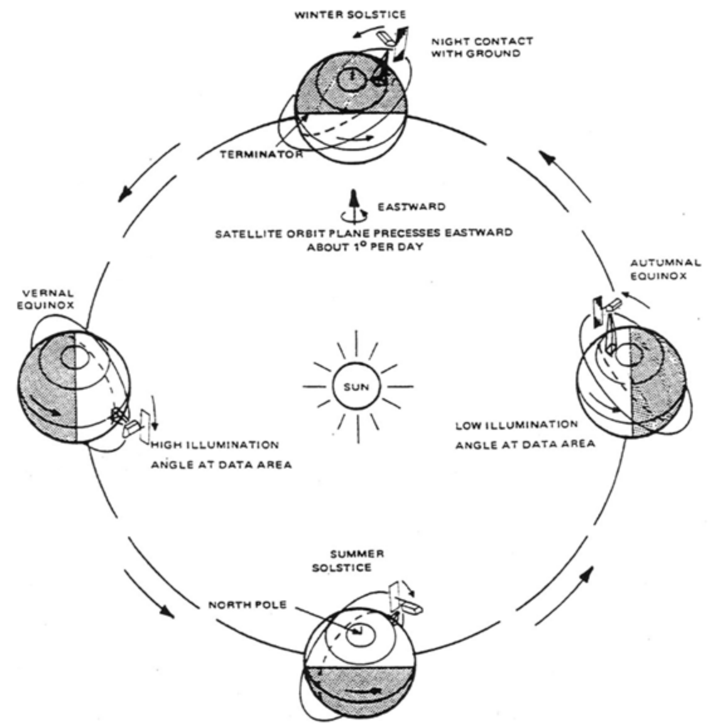

Figure 1. Illumination of the Earth from different angles throughout the year

(source: https://landsat.gsfc.nasa.gov/article/seasonal-illumination-variations/)

4. Type of photovoltaic systems

Depending on the design, photovoltaic systems vary in terms of investment costs, complexity, and energy efficiency. The simplest are stationary installations, in which the panels are mounted at a fixed angle. More advanced solutions include single-axis systems, which track the sun's movement along a single axis, and dual-axis systems, which ensure that the orientation of the panels is fully aligned with the position of the sun in the sky. The table summarizes the basic characteristics of these three types of systems, along with their advantages and limitations (Duffie, 2013).

Table 1

Types of photovoltaic systems

System type	Investment cost	Construction complexity	Energy yield increase	Advantages	Disadvantages
Fixed system	Low	Low	0% (base value)	Low price, no moving parts, simple installation, low failure rate	No sun tracking, limited efficiency
Single-axis system	Medium	Medium	+10-25%	Better efficiency than fixed systems, cost/efficiency compromise	Higher cost, maintenance required, moving parts susceptible to damage
Dual-axis system	High	High	+25-40%	Highest efficiency, full sun tracking	Very high cost, complex mechanics, risk of failure, high maintenance requirements

(source: own study based on Duffie, 2013)

5. Energy conversion and photovoltaic cell construction

Solar radiation is a form of electromagnetic waves emitted by the Sun as a result of nuclear fusion reactions taking place inside it. This energy, currently considered one of the most important renewable energy sources, can be converted into electricity using photovoltaic technology. PV cells, made of semiconductor materials, use the photoelectric effect – under the influence of incident solar radiation, an electromotive force is generated, which allows the production of voltage and electrical power. This phenomenon results from the movement of charge carriers between two layers of semiconductors with opposite types of conductivity: p and n. This results in a potential difference, leading to the generation of direct current. In order for it to power electrical devices or be fed into the grid, it is then converted by an inverter into alternating current with parameters compatible with the power grid (Luque, 2014; Platt, 2016).

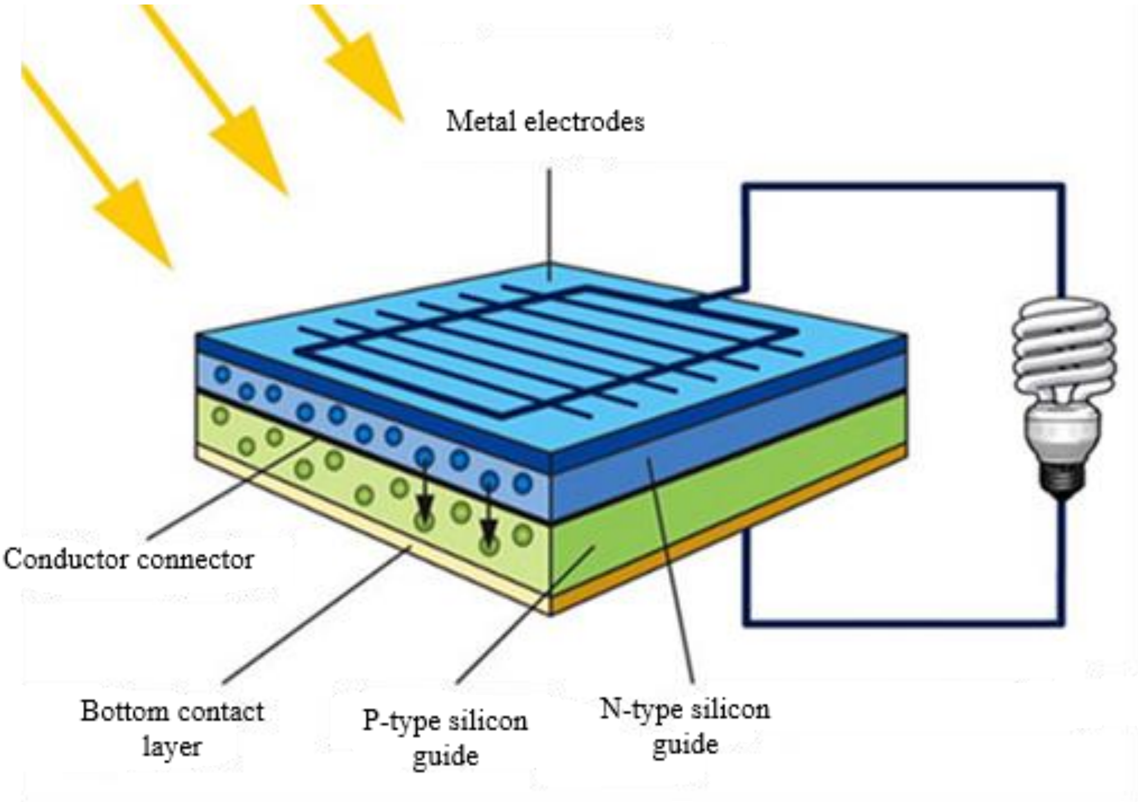

Figure 2. Structure of a photovoltaic cell

(source: http://fundacjaenergia.pl/baza-wiedzy/technologie/energia-slonca/konwersja-fotowoltaiczna)

6. Sun exposure in Polish regions

Assessing the potential of solar power plants requires an analysis of radiation resources in a given region. Although the solar constant at the edge of the atmosphere is approximately 1367 W/m², an average of about 1000 W/m² reaches the Earth's surface due to absorption and scattering in the atmosphere. In Poland, the average annual radiation is approx. 990 kWh/m², of which nearly 77% occurs during the summer season and only 23% during the winter. The annual number of hours of sunshine ranges from 1300 to 1900, with an average of 1600, of which about 75% occurs between April and September (Tytko, 2023). Regional variations in sunshine values in Poland are shown in Figure 3.

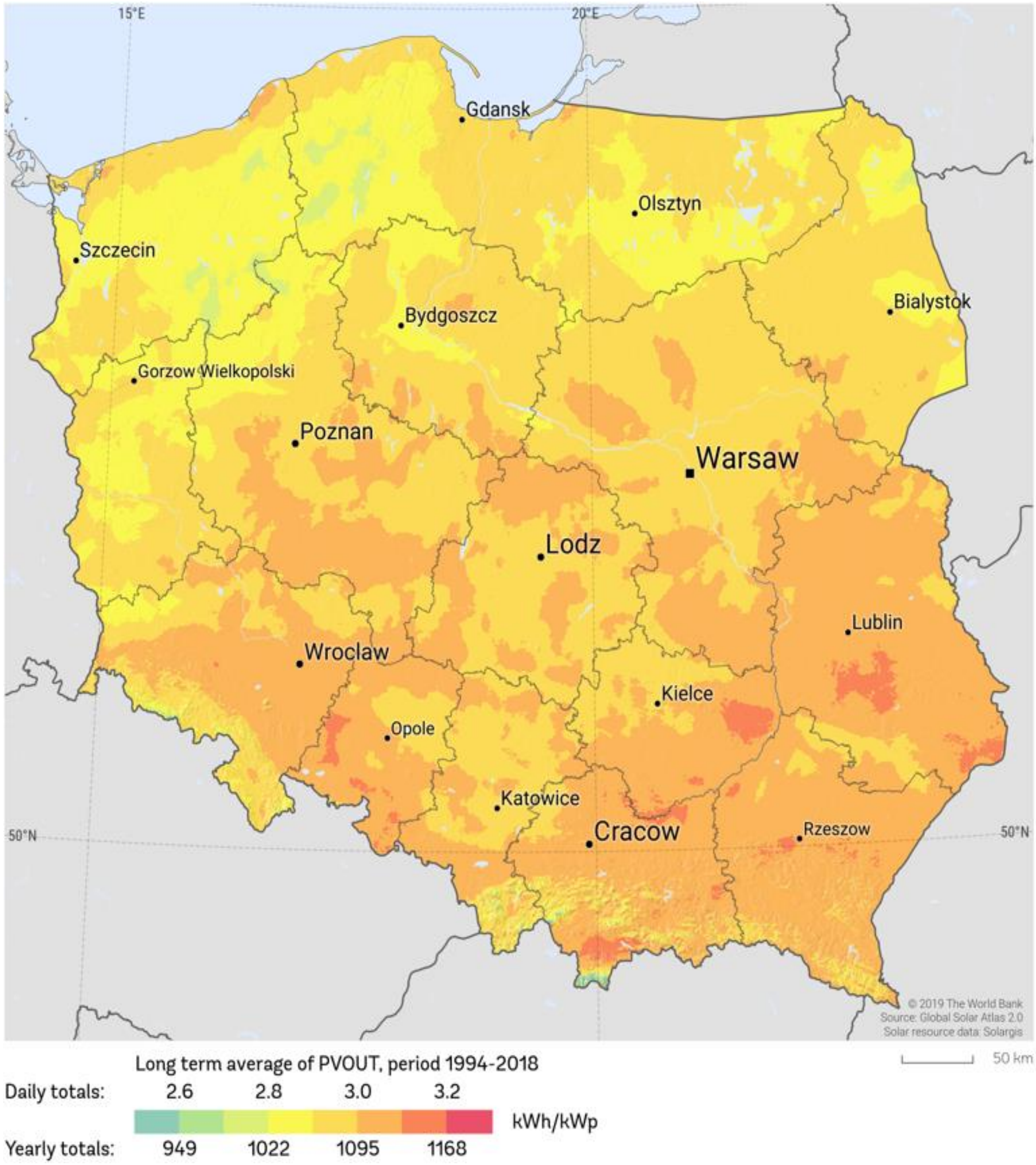

Figure 3. Photovoltaic energy potential in Poland

(source: https://solargis.com/maps-and-gis-data/download/poland)

7. Sunshine in European regions

Although sunlight conditions in Poland are less favorable than in southern European countries, photovoltaic installations remain profitable. Annual radiation totals average between 1,000 and 1,300 kWh/m², which ensures effective electricity production. However, there are significant regional differences – the highest values are recorded in southern provinces, such as Małopolska, while in northern regions, e.g., Warmia and Mazury, sunlight is significantly lower (Tytko, 2024). The differences in photovoltaic potential between Poland and other European countries are shown in Figure 4.

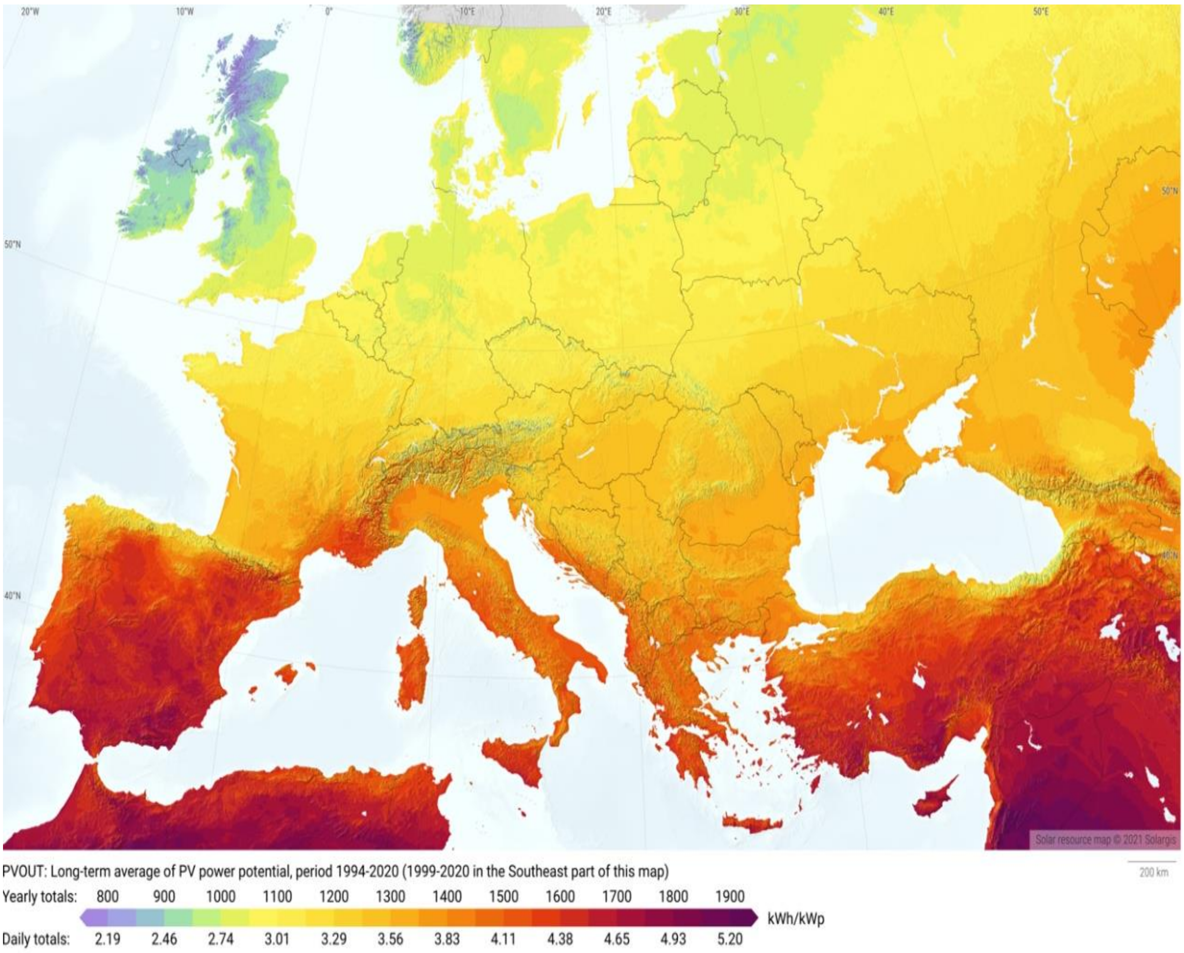

Figure 4. Photovoltaic energy potential in Europe
(source: https://solargis.com/maps-and-gis-data/download/europe)

8. Prototype implementation

In order to verify the theoretical assumptions in practice, a mock-up of a tracking system for a photovoltaic panel was designed and built. The structure was based on a lightweight support platform that could rotate in two axes – horizontal and vertical. Four photoresistors were mounted on the platform, located at the corners of a cross--shaped separation screen. Their task was to detect differences in the intensity of light coming from different directions. This arrangement of sensors allowed for precise determination of the dominant direction of solar radiation or its artificial source.

The signals from the photoresistors were processed by an Arduino Leonardo microcontroller, which implemented the control algorithm. The C++ program compared the voltage values corresponding to the light intensity on individual sensors. If the difference between the readings exceeded a set threshold, a control signal was generated for the corresponding MG995 servo mechanism. This made it possible to smoothly rotate the platform towards the light source, while limiting unnecessary movements caused by temporary measurement disturbances.

Two servo mechanisms were used to implement the movement: one responsible for changing the angle in the vertical axis and the other in the horizontal axis. The use of high-torque servos ensured stable operation. The system was powered by an LM2596 converter, which provided stable voltage for the servo mechanisms and microcontroller.

The tests were carried out in laboratory conditions, using an artificial light source simulating solar radiation. The prototype demonstrated the ability to respond efficiently to changes in the direction of light incidence. When the source was moved to the left, right, up, or down, the platform rotated in the appropriate direction until the sensor readings were equalized. In the case of uniform illumination, the system remained at rest, which proves that the algorithm worked correctly.

The results of the experiment confirmed the correct operation of the designed solution. The prototype met the assumed requirements – it was able to track the light source in two axes and maintain a position ensuring maximum exposure of the panel surface. However, it should be noted that due to the laboratory nature of the tests and the scale of the design, actual application would require further work related to weather resistance, mechanical strength, and optimization of energy consumption by the control system.

9. List of components used to build the prototype

The circuit design consists of the following components:

– Arduino microcontroller (Leonardo).
– 5-10KΩ photoresistor (4 pcs.).
– MG995 servo motors (2 pcs.).
– Voltage converter for powering the servos.
– Cables.
– 100Ω resistor (4 pcs.).
– Servo mounting kit allowing tilt in two planes.
– Servo tester.
– Base for mounting the entire system.

Figure 5. Prototype of the tracking system

(source: own study)

10. Circuit connection diagram

The diagram below shows the actual connection of the circuit, measuring the light intensity on four photoresistors (LDR1, LDR2, LDR3, LDR4). Then, the servo mechanisms (Servo1, Servo2) change their angles based on the data collected from the photoresistors and change the position of the platform so that the light intensity falling on these four sensors is as uniform as possible.

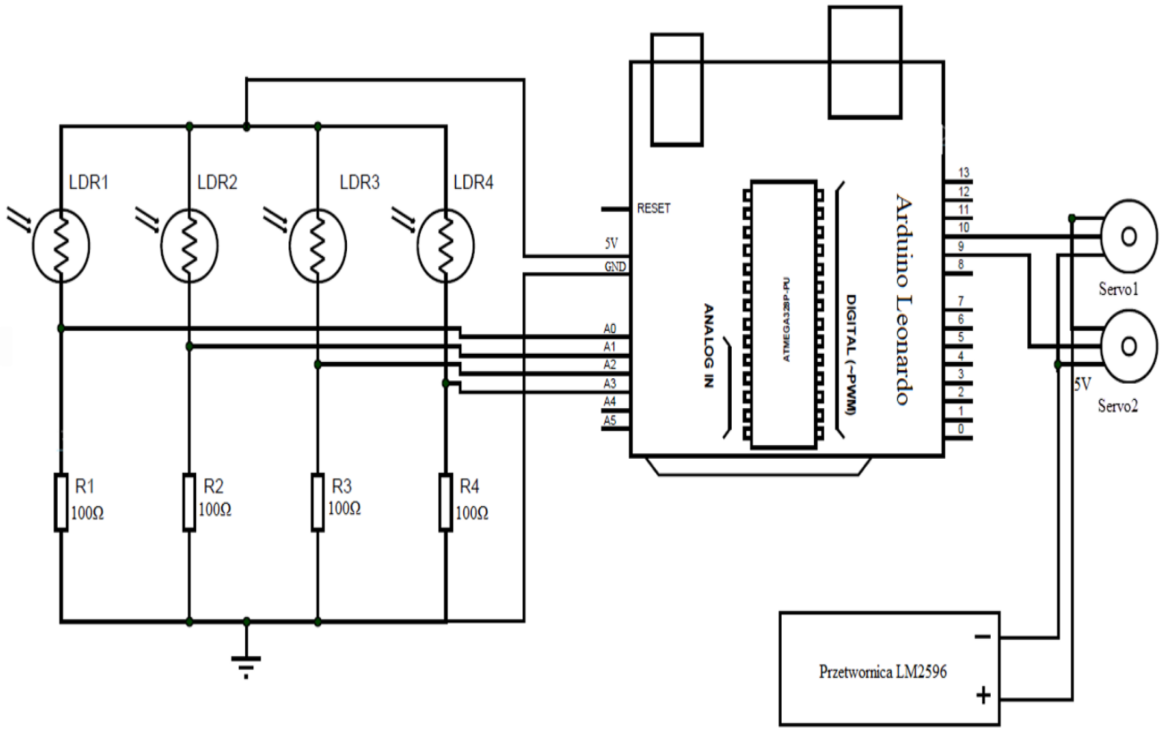

Figure 6. Circuit connection diagram

(source: own study)

11. Program code

The code for the system control program is presented below. The program was written in C++ for the Arduino platform and is responsible for reading data from light sensors and positioning servos accordingly.

```
#include <Servo.h>
int czulosc = 15;
Servo servohori;
int servoh = 0;
int servohLimitHigh = 160;
int servohLimitLow = 20;
Servo servoverti;
int servov = 0;
int servovLimitHigh = 120;
int servovLimitLow = 50;

int ldrtopl = 2;
int ldrtopr = 1;
int ldrbotl = 3;
int ldrbotr = 0;
```

```
void setup() {
  Serial.begin(9600);
  servohori.attach(10);
  servohori.write(90);
  servoverti.attach(9);
  servoverti.write(90);
  delay(500);
}

void loop() {
  servoh = servohori.read();
  servov = servoverti.read();

  int topl = analogRead(ldrtopl);
  int topr = analogRead(ldrtopr);
  int botl = analogRead(ldrbotl);
  int botr = analogRead(ldrbotr);

  int srtop = (topl + topr) / 2;
  int srbot = (botl + botr) / 2;
  int srleft = (topl + botl) / 2;
  int srright = (topr + botr) / 2;

  if (abs(srtop - srbot) > czulosc) {
    if (srtop > srbot) {
      servoverti.write(servov + 1);
      if (servov > servovLimitHigh) {
        servov = servovLimitHigh;
        servoverti.write(servov);
      }
      delay(10);
    }
    else if (srbot > srtop) {
      servoverti.write(servov - 1);
      if (servov < servovLimitLow) {
        servov = servovLimitLow;
        servoverti.write(servov);
      }
      delay(10);
    }
    else {
      servoverti.write(servov);
    }
  }

  if (abs(srleft - srright) > czulosc) {
    if (srleft < srright) {
      servohori.write(servoh + 1);
      if (servoh > servohLimitHigh) {
        servoh = servohLimitHigh;
```

```
      servohori.write(servoh);
    }
    delay(10);
  }
  else if (srright < srleft) {
    servohori.write(servoh - 1);
    if (servoh < servohLimitLow) {
      servoh = servohLimitLow;
      servohori.write(servoh);
    }
    delay(10);
  }
  else {
    servohori.write(servoh);
  }
}

delay(50);
Serial.print("Kąt poziomy: ");
Serial.println(servoh);
Serial.print("Kąt pionowy: ");
Serial.println(servov);
}
```

12. Conclusions

The research conducted and the implementation of the prototype tracking system confirmed that dynamic tracking of the Sun's position significantly increases the efficiency of photovoltaic panels compared to traditional static systems. A mock-up built on the basis of an Arduino Leonardo microcontroller, light sensors, and servo mechanisms proved the practical possibility of precisely adjusting the angle of inclination of the platform in two axes, which translated into the optimization of solar energy conversion conditions. An analysis of the literature and available data on sunshine in Poland indicates that, despite the moderate climate, the use of sun tracking technology can increase energy yields by 20-40%. This is particularly important in domestic conditions, as it increases the profitability of investments in photovoltaics, especially in winter and transitional months when the amount of solar energy is limited. The project confirms the potential of an interdisciplinary approach combining elements of electronics, automation, and renewable energy sources. At the same time, it points to directions for further research, including the development of more advanced control algorithms, integration with real PV installations, and miniaturization and optimization of mechanical systems. The results of the work provide a solid basis for further analysis of the application of tracking systems in Polish conditions and their adaptation to industrial scale.

References

Bachanek, K.H., Drożdż, W., Kolon, M. (2025). Development of Renewable Energy Sources in Poland and Stability of Power Grids–Challenges, Technologies, and Adaptation Strategies. *Energies, 18*(8), 2036. DOI: https://doi.org/10.3390/en18082036.

Bamisile, O., Acen, C., Cai, D., Huang, Q., Staffell, I. (2025). The environmental factors affecting solar photovoltaic output. *Renewable and Sustainable Energy Reviews, 208*, 115073. DOI: https://doi.org/10.1016/j.rser.2024.115073.

Duffie, J.A., Beckman, W.A. (2013). *Solar Engineering of Thermal Processes*. Wiley.

Harazin, J., Wróbel, A. (2022). Analysis and study of the potential increase in energy output generated by prototype solar tracking, roof mounted solar panels. *F1000Research, 9*, 1381. DOI: https://doi.org/10.12688/f1000research.27641.2.

Igliński, B., Piechota, G., Kiełkowska, U., Kujawski, W., Pietrzak, M.B., Skrzatek, M. (2023). The assessment of solar photovoltaic in Poland: the photovoltaics potential, perspectives and development. *Clean Techn Environ Policy, 25*, 281-298. DOI: https://doi.org/10.1007/s10098-022-02403-0.

Kopp, G., Lean, J.L. (2011). A new, lower value of Total solar irradiance: Evidence and climate significance. *Geophysical Research Letters, 38*(1). DOI: https://doi.org/10.1029/2010GL045777.

Kumba, K., Upender, P., Buduma, P., Sarkar, M., Simon, P.S., Gundu, V. (2024). Solar tracking systems: Advancements, challenges, and future directions: A review. *Energy Reports, 12*, 3566-3583. DOI: https://doi.org/10.1016/j.egyr.2024.09.038.

Luque, A., Hegedus, S. (2014). *Handbook of Photovoltaic Science*. England: Wiley.

Platt, C. (2016). *Make: Electronic* (*Elektronika od praktyki do teorii*). Gliwice: Helion.

Tytko, R. (2023). *Urządzenia i systemy energetyki odnawialnej*. Kraków: Eco Investment.

Tytko, R. (2024). *Urządzenia i systemy energetyki odnawialnej*. Kraków: Eco Investment.

http://fundacjaenergia.pl/baza-wiedzy/technologie/energia-slonca/konwersja-fotowoltaiczna.

https://landsat.gsfc.nasa.gov/article/seasonal-illumination-variations/.

https://solargis.com/maps-and-gis-data/download/europe.

https://solargis.com/maps-and-gis-data/download/poland.

Anna KOCHANEK[1], **Marek MOTYKA**[2]

[1] University of Applied Sciences in Nowy Sącz, Faculty of Engineering Sciences, Zamenhofa 1a, 33-300 Nowy Sącz, e-mail: akochanek@ans-ns.edu.pl
[2] University of Applied Sciences in Nowy Sącz, Faculty of Engineering Sciences, Zamenhofa 1a, 33-300 Nowy Sącz, e-mail: motyka.marek2801@gmail.com

Application of the ESP32 microcontroller and FDM technology in the development of an electrotechnical harness connection tester

Abstract

The article describes the design and construction of a prototype device for testing electrical harness connections. The tester combines the functionality of the ESP32 microcontroller with the flexibility of additive manufacturing technology used in the FDM method. A specialized PCB board was created in KiCAD, which integrates the ESP32 with input and output expanders, while the housing and mechanical components were manufactured using 3D printing technology. The software, written in C++, runs in the Arduino environment, allowing for intuitive operation of the device using a 2.8-inch touch screen and configuration files stored on an SD card. Functional tests confirmed that the device is capable of testing sixty-four wire connections, proving its practical application. A cost analysis showed that the total expenditure on the prototype was approximately PLN 770, which is significantly lower than commercial testers available on the market. The results of the research indicate that the combination of microcontrollers and 3D printing is an innovative and cost-effective solution for small and medium-sized companies.

Keywords: Additive manufacturing, FDM 3D printing, ESP32 microcontroller, Wire harness tester, PCB design, Prototyping, Touchscreen interface, Low-cost instrumentation.

Zastosowanie mikrokontrolera ESP32 i technologii FDM w budowie testera połączeń wiązek elektrotechnicznych

Streszczenie

Artykuł opisuje projekt oraz budowę prototypu urządzenia przeznaczonego do testowania połączeń wiązek elektrycznych. Tester łączy w sobie funkcjonalność mikrokontrolera ESP32 oraz elastyczność technologii przyrostowych stosowanej w metodzie FDM. Stworzono specjalistyczną płytkę PCB w programie KiCAD, która integruje ESP32 wraz z ekspanderami wejść i wyjść, natomiast obudowa i elementy mechaniczne zostały wyprodukowane w technologii druku 3D. Oprogramowanie napisane w języku C++ działa w środowisku Arduino, co pozwala na intuicyjną obsługę urządzenia przy użyciu 2,8-calowego ekranu dotykowego oraz plików konfiguracyjnych przechowywanych na karcie SD. Testy funkcjonalne potwierdziły, że urządzenie jest w stanie sprawdzić 64 połączenia przewodów, co dowodzi jego praktycznego zastosowania. Analiza kosztów wykazała, że całkowity wydatek na prototyp wyniósł około 770 zł, co jest kwotą znacznie niższą w porównaniu do komercyjnych testerów dostępnych na rynku. Wyniki badań wskazują, że połączenie mikrokontrolerów z drukowaniem 3D stanowi nowatorskie oraz kosztowo efektywne rozwiązanie dla małych i średnich firm.

Słowa kluczowe: wytwarzanie przyrostowe, druk 3D FDM, mikrokontroler ESP32, tester wiązek elektrotechnicznych, projektowanie PCB, prototypowanie, interfejs dotykowy, niskokosztowa aparatura pomiarowa.

1. Introduction

1.1. Importance of additive manufacturing in engineering

Additive technologies, commonly referred to as 3D printing, have become a key achievement in modern engineering and manufacturing. Their ability to produce components layer by layer allows for efficient prototyping, small-scale serial production, and flexible design adaptation (Gibson et al., 2021; Ngo et al., 2018). The use of 3D printing continues to evolve, ranging from the aerospace and automotive industries to medicine and consumer goods manufacturing.

One of the most important benefits of additive technologies is a significant reduction in product development time. Engineers can go from a digital design to a physical prototype in just a few hours, making this method the foundation of rapid prototyping and supporting innovation in various industries (Shahrubudin et al., 2019; Naghshineh, 2025).

Additive technologies also offer both environmental and economic benefits. Unlike subtractive methods, they produce significantly less waste, require less material, and in some cases also less energy. For this reason, 3D printing is seen as a technology that promotes sustainable development and reduces the negative environmental impact of manufacturing processes (Frazier, 2014; Shah, 2024; Javaid, 2021).

All these features mean that additive technologies are no longer considered a niche solution but are an integral part of modern engineering. Their growing importance reflects general trends in industry, where flexibility, cost-effectiveness, and sustainability play a key role.

1.2. FDM technology in prototyping

Among the various additive manufacturing methods, Fused Deposition Modeling (FDM) stands out as one of the most used techniques, primarily due to its low cost, ease of use, and the wide availability of printers on the market. FDM printers enable the creation of durable prototypes and functional parts directly from thermoplastic materials such as PLA, ABS, or PET-G (Bochnia, Kozior, 2024; Siemiński, Budzik, 2015). This technology has become a valuable tool for engineers and researchers in the design of enclosures, holders, and test equipment.

The popularity of FDM stems not only from the low cost of purchasing equipment and materials, but also from the wide selection of filaments available for processing. In addition to basic materials such as PLA and ABS, modern printers also support engineering materials, including polycarbonate (PC), polyamide (PA, nylon), and thermoplastic elastomers such as TPU, which significantly expand the industrial applications of this technology (Zhang et al., 2025). The literature also highlights the use of carbon fiber composites, which increase the stiffness and mechanical strength of prints (Budzik, 2013).

Despite its numerous advantages, FDM technology has its limitations. These include relatively low printing speed, anisotropy of mechanical properties resulting from the layered structure of the model, and visible layer lines on the surface, which can negatively affect the aesthetics and precision of the manufactured elements (Ngo et al., 2018). In addition, dimensional precision in FDM is lower than in resin-based technologies such as SLA or DLP (Zieliński, 2022).

Despite these limitations, due to its low cost, flexibility, and ease of access, FDM remains the most popular 3D printing technology. It is used not only in rapid prototyping and education, but also in low-volume production and even in the manufacture of end-use parts for industry (Šercer et al., 2019).

1.3. Wire harnesses and need for testing

Cable harnesses are a key component of modern electrical and electronic systems. They are responsible for the reliable transmission of both signals and energy in areas such as automotive, aviation, household appliances, and industrial automation. Problems with cable connections can lead to system failures, safety hazards, or costly downtime. Therefore, effective harness testing is an essential step in quality assurance processes (Frazier, 2014; Shahrubudin et al., 2019).

1.4. Commercial solutions and their limitations

Professional electrical harness testers are available on the market, offered by companies such as Weetech (e.g., model WK260). These devices offer precise measurements and extensive capabilities, but their price is significantly high, often reaching tens of thousands of euros. Such costs make them inaccessible to small and medium-sized companies that are looking for easier and more affordable solutions.

1.5. Justification for the implementation of the project

The presented project addresses a specific gap by offering the design and creation of a low-cost harness connection tester. The device is based on the ESP32 microcontroller, which provides multiple inputs and outputs, as well as the ability to communicate via Wi-Fi and Bluetooth while maintaining high computing performance at a low price. In addition, the tester's housing and structural components were manufactured using FDM 3D printing technology, which enabled rapid and economical prototyping (Gibson et al., 2021; Bochnia, Kozior, 2024). The combination of these two technologies has resulted in an innovative, inexpensive, and functional device for testing electrical harnesses.

2. Purpose and scope of the research

The main purpose of the research was to develop and implement a prototype device for testing electrical harness connections, combining the advantages of the budget ESP32 microcontroller with the versatility of FDM 3D printing technology. This device was designed to support the testing of harnesses used in low-voltage and low-current applications, offering both functionality and affordability.

The specific objectives included:

- Design and commission a custom printed circuit board (PCB) using KiCAD software, integrating an ESP32 microcontroller, input/output expanders, and basic security components.
- Development of modular software in C++ using the Arduino framework and the Visual Studio Code development environment.
- Designing the case and structural elements of the tester in Fusion 360 software, then manufacturing them using FDM technology on a Prusa MK3S+ 3D printer.
- Functional tests of the prototype were conducted, which included verification of up to sixty-four possible connections, corresponding to 128 measuring points.
- Conducting an economic analysis of the device and comparing its costs and functionality with other testers available on the market.

The scope of the research covered a complex engineering process, which included individual stages, from concept formulation and electronic system design, through software development and additive manufacturing of the housing, to the assembly, validation, and cost analysis of the final prototype. This comprehensive approach reflects the interdisciplinary nature of modern mechatronics, in which electronics, programming, and additive manufacturing are tightly integrated (Siemiński, Budzik, 2015; Gibson et al., 2021; Bochnia, Kozior, 2024).

3. Research/project methodology

3.1. ESP32-based control unit and functional design

The device is based on the ESP32 Devkit V1 microcontroller. It was chosen as the central control unit due to the substantial number of available GPIO lines and its serial communication capabilities. In order to enable testing of more connections than those directly available in the microcontroller itself, 16 PCF8574 expanders were used, which were connected within the I²C bus. This solution made it possible to increase the number of available input/output lines (GPIO) to 128, which corresponds to the possibility of setting up sixty-four test connections in a paired configuration.

A 2.8-inch graphic display operating in the SPI standard is used to operate the user interface. The display has been integrated with:

- an SD memory card reader for storing test configuration files;
- a touch panel for interactive operation of the device.

The CSV configuration files contain a list of test programs as well as additional data on wire harnesses. After loading the data from the SD card, the user can select the appropriate test program via the touch screen. The system then provides the user with information on the status of all analyzed connections.

ESP32 plays a key role in coordinating the operation of all system modules. It is responsible for sending signals to I²C expanders, receiving feedback from tested connections, communicating with the display via the SPI bus, and interpreting information from the memory card. This type of architecture enables modularity and facilitates project scaling, while ensuring intuitive operation thanks to the use of a touchscreen graphical interface.

3.2. Software and development environment

The tester software was designed in C++ using the Visual Studio Code environment, enhanced with the PlatformIO extension. This extension enables effective library management and code compilation. The Arduino framework was used to manage the microcontroller, which enables effective integration with hardware modules and provides broad access to ready-made libraries.

The code structure has been designed in a modular way, which ensures transparency and ease of further expansion. The following parts of the program have been distinguished:

- display and touch panel support – responsible for the user interface, displaying messages, and selecting the test program;
- connection test logic – control of signals sent by I²C expanders and interpretation of results;
- SD card support – reading configuration files in CSV format, containing a list of test programs and additional information about harnesses;
- auxiliary modules – including serial communication support, diagnostics, and error handling.

This division of the software contributes to easier maintenance and development. Changes to the test configuration can be made by editing CSV files, eliminating the need to recompile the entire software. Using a touch screen, the user can intuitively select a test program, after which the device automatically performs a verification procedure for all available connections.

3.3. PCB project

The schematic and PCB board were designed using KiCAD software, which enables the generation of comprehensive electronic documentation for the device. The project involved the integration of key system components:

- ESP32 microcontroller, acting as the central unit;
- 16 PCF8574 expanders supporting up to 128 GPIO lines via the I²C bus;
- an R-78E3.3-1.0 converter, providing a stable 3.3 V supply voltage for the circuit;
- filter capacitors, responsible for voltage stabilization;
- Zener diodes, which functioned as ESD protection for the input/output lines.

The printed circuit board (PCB) design features printed pin numbering, which facilitates the identification of individual pins during the process of connecting the tested wires. In addition, the components have been arranged appropriately to ensure optimal readability of the layout and ergonomics during the assembly process in the enclosure.

The production process for the board was outsourced to an external contractor based on the design documentation. As a result of these activities, a professionally manufactured prototype board was obtained, which is ready for integration with the other components of the device.

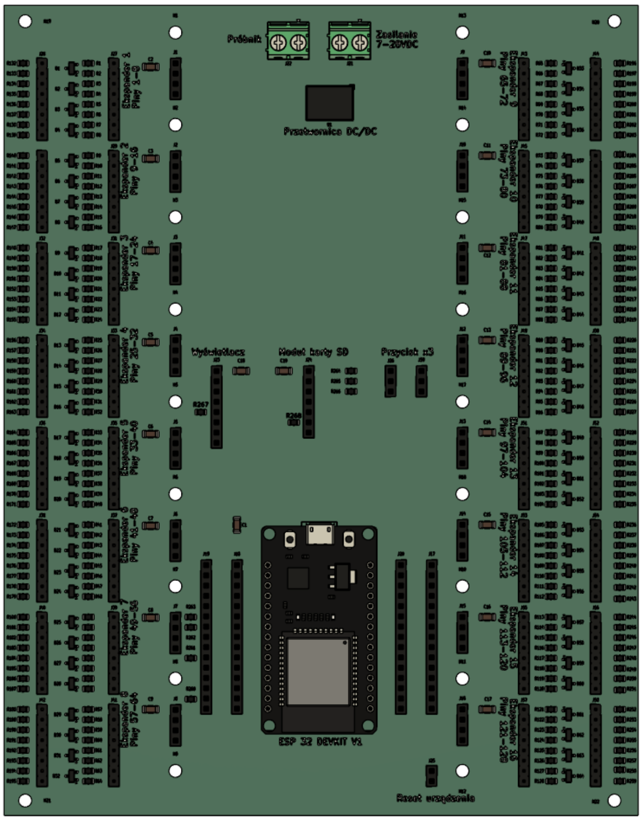

Figure 1. PCB design of the wire harness tester in KiCAD

(source: own study)

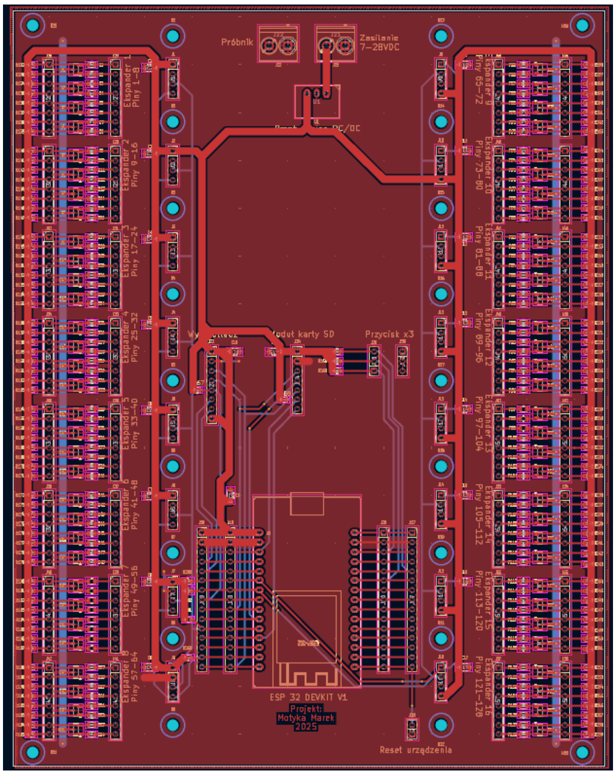

Figure 2. Visualization of PCB connections in KiCAD

(source: own study)

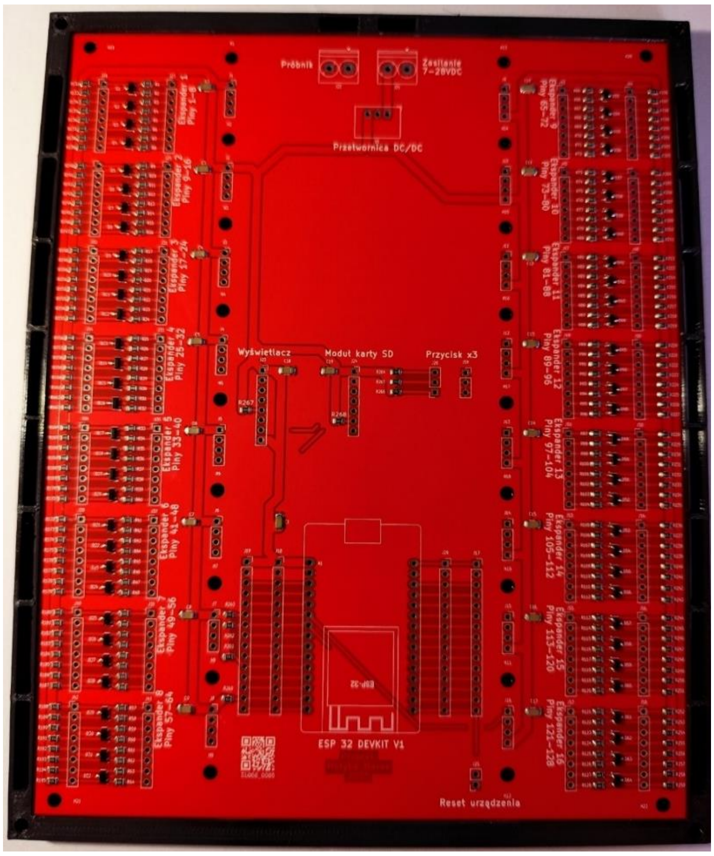

Figure 3. Assembled PCB of the wire harness tester

(source: own study)

3.4. Housing design and additive manufacturing

The tester housing and fasteners were designed in Fusion 360, which offers advanced modeling capabilities for both individual components and complex assemblies, ensuring high precision and accuracy in the design process. The basic design assumptions included:

- mechanical protection for the PCB and electronic modules;
- easy access to input and output connectors;
- easy assembly and disassembly;
- ergonomic operation and compact dimensions.

The three-dimensional models were exported to STL format and then prepared for printing using PrusaSlicer software. The production process was conducted using Fused Deposition Modeling (FDM) 3D printing technology with a Prusa MK3S+ printer.

Various printing materials were used to construct the housing and components, selected according to strength and functional requirements:

- PET-G was used as the material to produce key housing components, including the body, base, side walls, front panels, and transport handles. It was chosen for its advantageous properties, such as good mechanical strength, resistance to temperature and humidity changes, and ease of printing. Polycarbonate (PC) – used in applications involving the fastening of expanders and cable sockets. Polycarbonate has exceptionally high mechanical and impact resistance, which is a significant advantage in applications exposed to frequent connection and disconnection of cables.
- PA+15CF (carbon fiber reinforced nylon) is a material used in the production of fasteners that must meet high strength requirements, including applications such as side fasteners for structures. The addition of carbon fiber significantly increases the stiffness and mechanical strength of the components, while minimizing their tendency to deform.
- TPU was used in the construction of flexible elements, such as spacer feet and the upper housing of the USB port. Thanks to its flexibility, thermoplastic polyurethane (TPU) can absorb vibrations, provides anti-slip properties, and is highly resistant to mechanical damage caused by pressure or impact.

The use of varied materials has enabled the mechanical and functional properties of individual parts to be optimally matched to their function within the entire device. As a result, the housing combines durability, ergonomics, and aesthetic design.

4. Prototype description and results

The designed tester was implemented by mounting it on a previously developed PCB board, using expansion modules and housing components made with 3D printing technology. The central element of the device is the ESP32 Devkit V1 microcontroller, which plays a key role in coordinating the operation of all components.

The printed circuit board (PCB), designed using KiCAD software, integrates a microcontroller with sixteen PCF8574 expanders. This configuration increases the number of supported GPIO lines to 128, allowing testing on sixty-four connections. The R-78E3. 3-1. 0 converter provides a stable power supply to the circuit, while filter capacitors and Zener diodes play a key role in protecting components from interference and electrostatic surges.

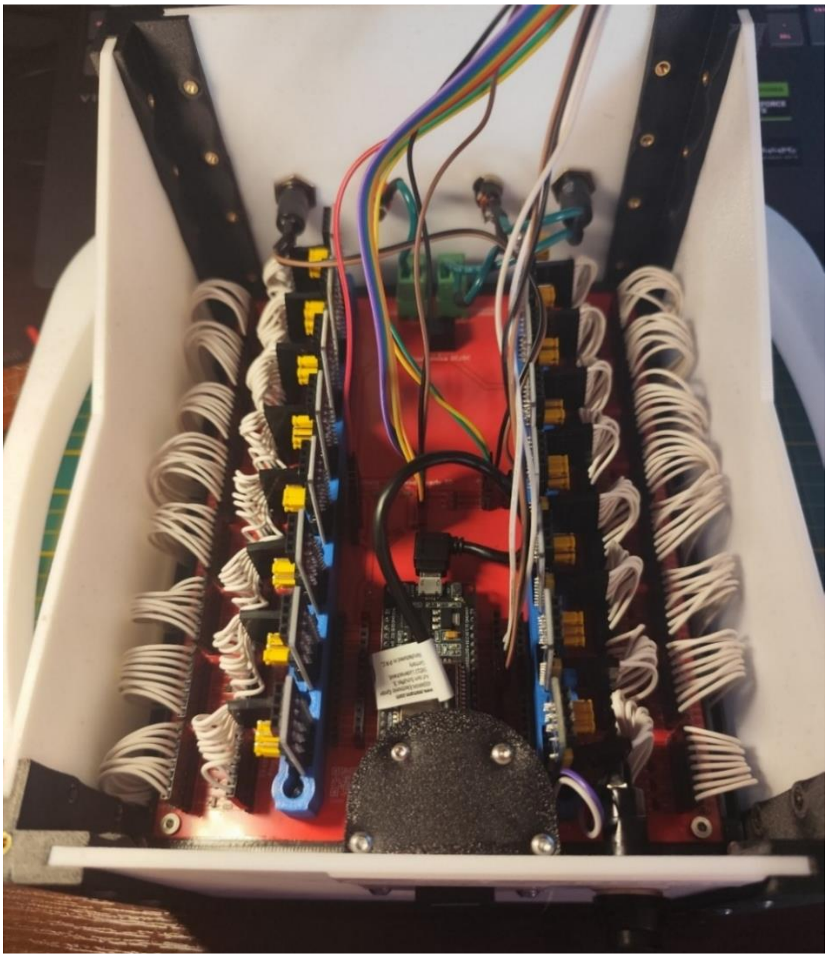

Figure 4. Internal view of the tester showing the PCB and wiring

(source: own study)

A 2.8-inch touchscreen display equipped with an SD card reader is used for user interaction. This solution enables efficient loading of test configuration files saved in CSV format, with the process being controlled via an interactive touch panel.

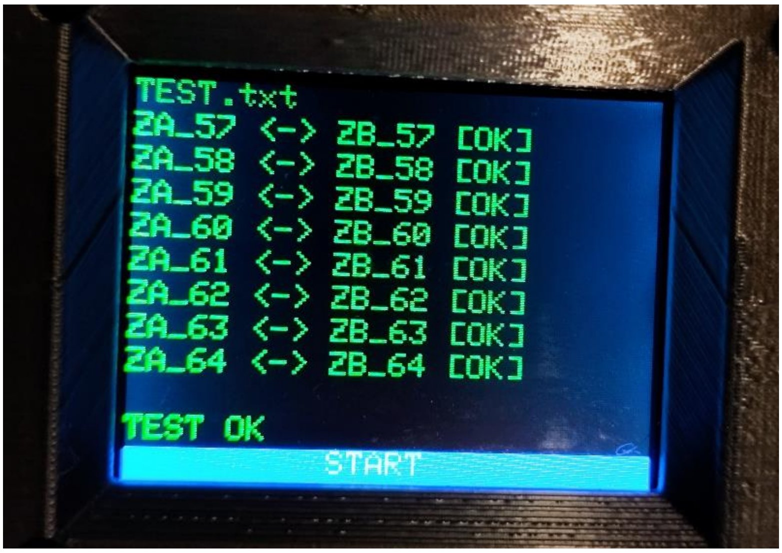

Figure 5. User interface of the 2.8-inch touch display during operation

(source: own study)

All electronic components were placed in a housing designed using Fusion 360 software and manufactured using Fused Deposition Modelling (FDM) 3D printing technology. The housing is made of components of different materials, including: PET-G, which forms the main structure and panels; polycarbonate (PC), used to manufacture expander mounts and sockets; PA+CF composite, characterized by high rigidity in structural applications; and TPU, used in the production of spacer feet and flexible covers. The material diversity used in the analysed context made it possible to achieve an optimal combination of features such as durability, functionality, and ergonomic use.

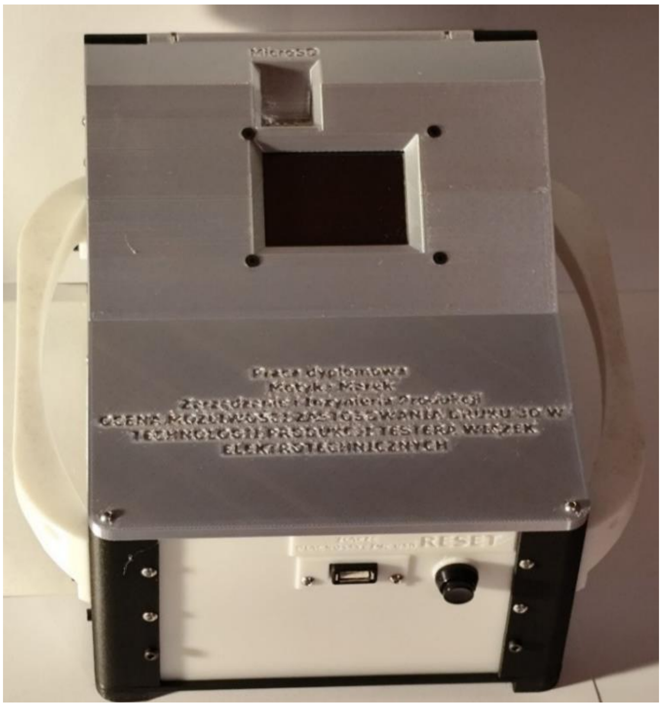

Figure 6. View of the assembled prototype of the wire harness tester

(source: own study)

The developed prototype device is distinguished by its compact design, intuitive user interface, and simplified process of connecting the tested cables. The design has been developed in such a way as to enable effective expansion of its functionality through the introduction of new test programs and modifications to the housing.

5. Economic analysis

The developed prototype of an electrical wiring connection tester was subjected to a cost analysis to assess the cost-effectiveness of its design in comparison with existing commercial solutions on the market.

The cost estimate included both electronic components and materials used in the 3D printing process. The total cost of purchasing electronic components, including the ESP32 microcontroller, PCF8574 expanders, R-78E3 converter. 3-1. 0, touch display, SD card module, and passive components such as resistors, capacitors, and diodes, amounted to several hundred zlotys. Additionally, the costs of filaments used in FDM technology (PET-G, PC, PA+CF, TPU) were considered, which in the case of the prototype were relatively low due to the limited amount of material used. The total cost of manufacturing the device was approximately PLN 770.

For comparison purposes, professional beam testers, represented by Weetech devices, are significantly more expensive. The WK260 model costs around PLN 38,000. The difference in cost is therefore significant; constructing our own prototype device has enabled us to obtain a fully functional tester at minimal expense compared to commercially available solutions.

However, it should be noted that the developed prototype does not provide such advanced functionality or the same precision as professional-grade devices. The aim of the project was to develop an economical and flexible tool for testing low-voltage and low-current harnesses that could be implemented in small and medium-sized enterprises. From a cost analysis perspective, the project showed that the integration of the ESP32 microcontroller with Fused Deposition Modelling (FDM) 3D printing technology enables the development of an innovative and economical solution that is an alternative to expensive industrial testers.

6. Opportunities for further development

The developed prototype of an electrical harness connection tester provides a foundation for further development of the technology in various directions, enabling the device to be adapted to more advanced applications. Potential areas of development may include:

- increasing the number of supported connections – by using additional I²C expanders or other microcontroller architectures;
- extending the range of functionality – adding wire resistance measurement, continuity tests with current control, and even simple insulation measurements;
- improving the user interface – developing software with more extensive menus, test reports saved in files, and wireless communication capabilities (Wi-Fi, Bluetooth);
- use of other 3D printing technologies – e.g., SLA technology for components requiring greater precision or SLS for parts with high mechanical resistance;
- integration with production systems – the ability to send test results directly to production management systems (MES/ERP), which would increase the usefulness of the device in industrial conditions.

As a result of the modifications indicated, the tester under development has the potential to evolve in the future not only into a prototyping tool, but also into a fully functional device supporting quality control processes in the electrical engineering industry.

7. Conclusions

The completed project enabled the design and construction of a prototype electrical wiring connection tester based on the ESP32 microcontroller and Fused Deposition Modeling (FDM) 3D printing technology. The device achieved its objectives, enabling effective testing of up to sixty-four wire connections in the context of low-voltage and low-current applications.

The use of the ESP32 microcontroller in combination with PCF8574 expanders has significantly increased the number of supported inputs and outputs, which has contributed to the flexibility of the device and facilitated its further development. The software, developed in C++ using the Arduino framework, enabled the creation of an intuitive user interface that is operated via a 2.8-inch touch screen and configuration files in CSV format.

The use of 3D printing technology enabled the efficient and economical production of the housing and structural components. The selection of materials such as PET-G, PC, PA+CF, and TPU made it possible to obtain diverse mechanical properties that are appropriately matched to the specific functions of individual components. This applies in particular to parameters such as strength, stiffness, flexibility, and vibration resistance.

An economic analysis showed that the total cost of the prototype was approximately PLN 770, which is a fraction of the cost of professional testers available on the market (PLN 38,000). The device can therefore be an attractive alternative for small and medium-sized enterprises that need inexpensive and functional tools for testing harnesses.

In summary, the project has demonstrated that combining microcontroller technology with additive manufacturing enables the development of innovative and low-cost engineering solutions that can be further developed and adapted to industrial needs.

References

Bochnia, J., Kozior, T. (2024). *Podstawy szybkiego prototypowania. Druk 3D. Technologia FDM/FFF*. Kielce: Politechnika Świętokrzyska.

Budzik, G. (2013). *Dokładność geometryczna łopatek turbin silników lotniczych*. Rzeszów: Oficyna Wydawnicza Politechniki Rzeszowskiej.

Frazier, W.E. (2014). Metal additive manufacturing: A review. *Journal of Materials Engineering and Performance, 23*(6), 1917-1928.

Gibson, I., Rosen, D., Stucker, B. Khorasani, M. (2021). *Additive Manufacturing Technologies: 3D Printing, Rapid Prototyping, and Direct Digital Manufacturing*. Cham: Springer.

Ngo, T.D., Kashani, A., Imbalzano, G., Nguyen, K.T.Q. Hui, D. (2018). Additive manufacturing (3D printing): A review of materials, methods, applications, and challenges. *Composites Part B: Engineering*, *143*, 172-196.

Šercer, M., Rezić, T., Godec, D., Oros, D. (2019). Microreactor production by PolyJet matrix 3D-printing technology: Hydrodynamic characterization. *Food Technology and Biotechnology, 57*(3), 362-370.

Shah, J. (2024). Environmental and economic sustainability of additive manufacturing. *Journal of Manufacturing and Materials Processing, 8*(2), 298.

Shahrubudin, N., Lee, T.C., Ramlan, R. (2019). An overview on 3D printing technology: Technological materials and applications. *Procedia Manufacturing, 35*, 1286-1296.

Siemiński, P. Budzik, G. (2015). *Techniki przyrostowe: druk 3D, drukarki 3D*. Warszawa: Oficyna Wydawnicza Politechniki Warszawskiej.

Sydor, M. (2009). *Wprowadzenie do CAD. Podstawy komputerowo wspomaganego projektowania*. Poznań: Wydawnictwo Naukowe PWN.

Zhang, F., Zhou, S.X., You, H.Y., Zhang, G., Yang, J.Q. Shi, Y.S. (2025). *3D printing of ceramic matrix composites: Strengthening and toughening strategies*. Composites Part B: Engineering.

Zieliński, D. (2022). Drukowanie trwałych elementów z żywic utwardzanych światłem lasera w technologii SLA. *Materiały & Maszyny Technologiczne, 1,* 42-44.

Sławomir JURKOWSKI[1], **Józef CIUŁA**[2]

[1] University of Applied Sciences in Nowy Sącz, Faculty of Engineering Sciences, Zamenhofa 1a, 33-300 Nowy Sącz, e-mail: sjurkowski@ans-ns.edu.pl
[2] University of Applied Sciences in Nowy Sącz, Faculty of Engineering Sciences, Zamenhofa 1a, 33-300 Nowy Sącz, email: jciula@ans-ns.edu.pl

The use of rapid prototyping methods and FEM analyses to improve aerodynamic characteristics of passenger vehicles

Abstract

The aerodynamic features of motor vehicles mainly affect two aspects: operating costs related to the drag force of the vehicle (Cx coefficient) and traction properties. The simulation tests carried out made it possible to modify body elements in order to improve the aerodynamic downforce of the rear axle of the vehicle and to evaluate the range of rear spoiler settings from the point of view of its usefulness. The research problem was the analysis of the aerodynamic features of the BMW E46 325i vehicle, based on CFD numerical analyses and the design of an active spoiler. The body of the vehicle was digitized on the basis of a point cloud using the Smarttech3D Universe optical scanner and the SpaceClaim program from the ANSYS package. Numerical calculations were carried out in the vehicle speed range of 50-245 [km/h]. Air streams flowing around the body of the vehicle were analysed. The dynamically designed rear spoiler has three positions relative to the boot lid: 0°, 10° and 20°. The analysed range of speeds and spoiler angles allowed to determine the aerodynamic downforce and the active spoiler control map, i.e. the extension of the positioning mechanism and setting the angle of the system relative to the plane of the trunk depending on the speed of the vehicle. The aerodynamic downforce ranged from 0.5 to 321 [N]. Based on the data obtained, it was found that the factory body geometry provides aerodynamic downforce of 3 to 93 [N], the use of a spoiler increases this value from 12 to 228 [N], with a decrease in the Cx coefficient from 1 to 3 [%]. The beneficial effect of using a spoiler is registered above the speed of 50 [km/h], and the optimum angle of attack of the spoiler is 10°.

Keywords: FEM, FVM, ANSYS, aerodynamics, vehicle, Cx, down force.

Zastosowanie metod szybkiego prototypowania i analiz MES do poprawy charakterystyk aerodynamicznych pojazdów osobowych

Streszczenie

Cechy aerodynamiczne pojazdów samochodowych wpływają głównie na dwa aspekty: koszty eksploatacji związane z siłą oporu powietrza (współczynnik Cx) i właściwości trakcyjne. Przeprowadzone testy symulacyjne umożliwiły modyfikację elementów nadwozia w celu poprawy siły docisku aerodynamicznego tylnej osi pojazdu oraz ocenę zakresu ustawień tylnego spoilera pod kątem ich użyteczności. Problem badawczy stanowiła analiza właściwości aerodynamicznych samochodu BMW E46 325i na podstawie analiz numerycznych CFD i projekt aktywnego spoilera.

Nadwozie pojazdu zostało zdigitalizowane na podstawie chmury punktów przy użyciu optycznego skanera Smarttech3D Universe oraz programu SpaceClaim z pakietu ANSYS. Obliczenia numeryczne przeprowadzono w zakresie prędkości pojazdu od 50 do 245 km/h, analizując przepływ strug powietrza wokół karoserii. Dynamicznie zaprojektowany tylny spoiler posiada trzy pozycje względem pokrywy bagażnika: 0°, 10° i 20°. Analizowany zakres prędkości i kątów nachylenia spoilera pozwolił określić wartości docisku aerodynamicznego oraz opracować mapę sterowania aktywnym spoilerem, obejmującą wysuw mechanizmu pozycjonującego i ustawienie kąta systemu względem płaszczyzny bagażnika w zależności od prędkości pojazdu.

Uzyskana siła docisku aerodynamicznego mieściła się w zakresie od 0,5 do 321 N. Na podstawie uzyskanych danych stwierdzono, że fabryczna geometria nadwozia generuje docisk aerodynamiczny od 3 do 93 N, natomiast zastosowanie spoilera zwiększa tę wartość do 12-228 N, przy jednoczesnym spadku współczynnika oporu Cx o 1-3%. Korzystny wpływ spoilera odnotowano przy prędkościach powyżej 50 km/h, a optymalny kąt jego nachylenia określono na 10°.

Słowa kluczowe: MES, FVM, ANSYS, aerodynamika, pojazd, Cx, siła docisku.

1. Introduction

Rapid prototyping is a technology that supports the work of modern engineers. Its basic design process includes rapid prototyping of models with appropriate geometry, data conversion and final processing (including verification). Applying 3D scanning involves collecting digital data about the shape and appearance of real objects to create digital models (Hyndhavi, Murthy, 2017). Rapid prototyping methods are also used in design work in industries that produce equipment that converts renewable energy into other forms of energy. This concerns hydropower (water turbines), biogas and biomass in combined heat and power plants (gas turbines and steam turbines) and, in particular, wind power in the blade area of wind turbines to determine the aerodynamic profile of the wind turbine. Comparison of the blade structure and its mechanical strength with the loads occurring during operation (Poole, Phillips, 2019; Ciuła et al., 2023). The process used to manufacture wind turbine blades consists of various steps, including: CAD model development procedures and 3D printing processes, printing of turbine blade geometries (enhanced production) and reinforcement of the blade structure (Bassett et al., 2015). To optimize rapid prototyping processes, virtual reality systems are increasingly used to model these processes. Such measures are intended to reduce the risks associated with prototype production in the early stages of the product development cycle. Therefore, by applying modeling and simulation in virtual systems, we reduce the number of prototyping, building, testing and testing cycles (Choi, Samavedam, 2022).

Another area related to rapid prototyping is the acquisition of input data for computational processes and the use of incremental manufacturing methods. This is especially true for three-dimensional models of real objects, such as prototype structures, objects without design documentation, or components that have been damaged and need to be rebuilt (Kowalski et al., 2022). One method of obtaining a three-dimensional model is so-called drawing from nature, which involves measuring the geometric properties of elements and then drawing the object in a CAD program. This method is commonly used in manufacturing facilities for design purposes with incomplete input data sets. A significant problem arises with objects with irregular shapes and elements that are difficult to describe using simple geometric blocks. In this case, the scanning method is still available. As basic methods of 3D scanning (Confalone et al., 2023) we can distinguish: contact method, laser (triangulation and ToF), stereo, photogrammetry, structural light scanning and computer tomography (Olejarczyk et al., 2020). In the case of incremental manufacturing methods, the most important aspect is to obtain on the basis of the cloud points a model free of discrepancies and anomalies caused by measurement errors (Rosso et al., 2020). The finite element method also requires the even distribution of the grid of triangles from which the 3D model is constructed. The size and shape of the triangles forming the surface of the object, and errors associated with uncovered surfaces, duplicated edges, etc., are crucial when working grid algorithms. These types of errors in a three--dimensional model cause the object to be divided into finite elements of low quality, which consequently increases the number calculation errors. Today, rapid prototyping methods are closely related to numerical methods, including the finite element method (FEM) (Cui, 2015). On the one hand, some numerical analyses require the import of CAD models of physical objects, on which strength, heat, flow, etc. are calculated. There is also a dependency: the results of the numerical analysis provide the basis for the redesign of the object of investigation and the empirical verification of whether the basic goals of the redesign are achieved (Pawłucki, 2015). Additive production methods can be used here (Szczepaniak et al., 2015).

2. Materials and methods

The aerodynamic characteristics of motor vehicles are mainly affected by two aspects: the operating costs associated with the vehicle's drag force (coefficient C_x) (Piechna, 2012) and with the traction properties (Gao, Xin, 2021; Anderson, 2010). The simulation studies allowed the body components to be modified to improve the aerodynamic strain on the rear axle (Katz, 1985) of the vehicle and to assess the range of rear spoiler settings (Somerfield, 2023) from the point of view of its usability (Rohl et al., 1995). Modelling of turbulent flows around moving vehicles makes it possible to analyse the correctness of determining the geometric characteristics of aerodynamic elements (Paszko, Łygas, 2016), similar analyses are being carried out on a large scale in the field of aviation (Yurkovich, 2003). The characteristics of vehicle geometry also have a significant impact on emissions of pollutants into the atmosphere, which is emphasized by (Ciuła et al., 2019; Generowicz et al., 2019).

Technical capabilities of the 3D Printing Laboratory and the Metrological Laboratory of the University of Applied Sciences in Nowy Sącz have the possibility of contact scanning using a coordinate measuring arm. Photogrammetric methods are implemented by systems based on the software Photoscan and Zephyr 3DF. In addition, the Department of Engineering Sciences is equipped with the David SLS 2 and Smarttech Universe systems for structural light scanning. For the purposes of rapid prototyping and FEM analysis, the data obtained i.e. the cloud of points identified on the surface of the measured object requires additional processing for its later use. The technical facilities of the Faculty of Engineering Sciences in this regard allow the use of both basic, commonly available methods of incremental production, such as FDM (Fused Deposition Modeling), as well as advanced technologies SLA (Stereolitography) (Yurkovich, 2003) and SLS (Selective Laser Sintering) (Tuliszka-Sznitko, 2011) and numerical calculations using the method of finite elements FEM in the ANSYS package. Numerical analyses allow for the reduction of the number of prototypes made during the redesign phase, which impacts the reduction of waste production, thus making a significant contribution to environmental protection (Przydatek et al., 2017; Kochanek, Kobylarczyk, 2024). Such an approach aligns with the idea of sustainable development described, among others, by (Kochanek et al., 2024).

The research problem was the analysis of the aerodynamic characteristics of the BMW E46 325i, based on numerical CFD analyses and the design of the active spoiler (Vreman et al., 1997). The vehicle was digitized on the basis of the point cloud using the Smarttech3D Universe optical scanner. The car body is an object that is relatively difficult to digitize with a scanner operating in structural light technology. Painted elements, chrome elements and glazing generate reflections of Gray codes, displayed by the thrower on the vehicle's surface, as a result of which the detector captures a blurred, inaccurate image of the surface. The measurement area recorded with one fixing of the scanner is effectively 300 mm per 250 mm, which in combination with large surfaces of body components, such as roof, front mask, or windows makes it difficult to impose on each other further clouds of points (no characteristic transitional elements) (Park, Kwon, 1996). In order to improve the quality of the obtained clouds of dots, the vehicle's coil is covered with a trigger used in welding for testing non--destructive bonds. In addition, the number of shots required for capturing was limited by measuring only on the right side of the car. The CAD model was obtained by copying the resulting cloud of points, making a mirror reflection, and attaching the resulted object to the original cloud. The processing of the obtained data consisted of cleaning the scans from the interference and unwanted elements that were accidentally identified, by mutually adjusting the resulting clouds, based on the characteristic points identified on the adjacent images. The CAD model building algorithm reduces the number of measurement points taken into account when determining the triangle grid, in this case a reduction of 10%. The obtained 3D model is saved in .stl format. For the purposes of producing a model on a scale using incremental methods, the model proved to be satisfactory. In the case of FEM analyses, geometry errors made it impossible to divide the object into finite elements, it was necessary to use the Space Claim program from the ANSYS package, the final effect of the work on the reproduction of the car's body is shown in Figure 1. The model optimization for numerical analysis was based on the regularization of the triangle grid, the reduction of the disproportions in the dimensions of the 3D model grid-building triangles, and the use of geometry error detection algorithms for FEM calculations (Iljaszewicz et al., 2020).

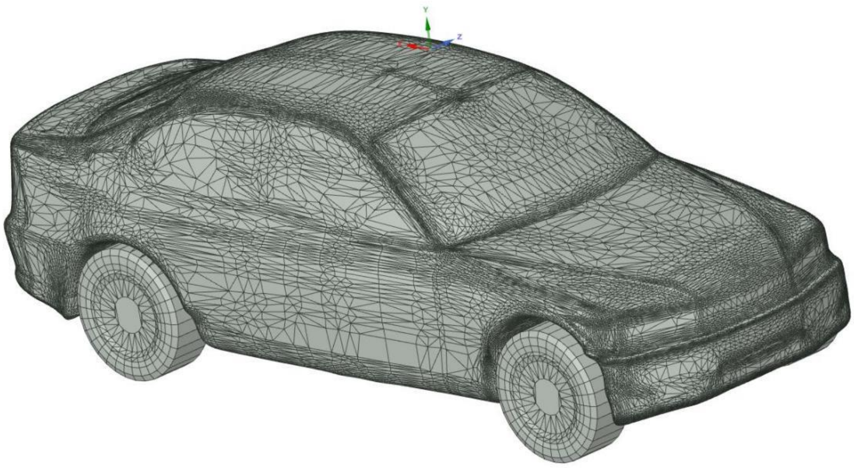

Figure 1. The three-dimensional model of the BMW E4

(source: own study)

The FEM flow analysis system was based on ANSYS software. A view of the calculation modules used in performing the calculations is shown in Figure 2. The three--dimensional model was imported using the Geometry module marked as A in Figure 2. Modules from B to I are flow analysis computing environments based on the Fluent meter.

The calculations were made on the factory geometry of the vehicle (modules B and G), on the vehicle equipped with the rear spoiler adjusted at angles of 10° (Modules C and H) and 20° (Modules D and I). The calculations were made for two turbulence models: kε and kω (Arrondeau, Rana, 2020). Due to the convergence of results obtained with different turbulence models, the article presents data for the kε model with turbulence determine by intensity and hydraulic diameter with turbulence intensity set up as 5%. In another articles we find the same turbulence models, and conclusion that kω SST model can by better in more complex flow cases (Czyż et al., 2018).

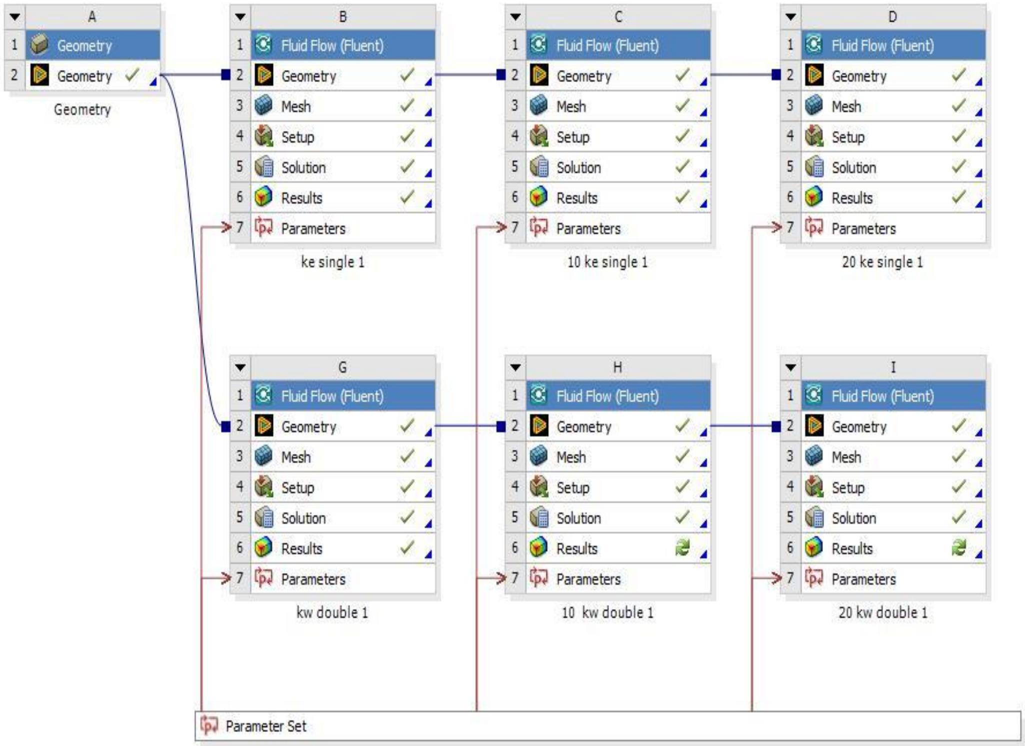

Figure 2. A connections of analysis systems in ANSYS Workbench

(source: own study)

The red arrow indicates the input data that controls the calculations, stored in the Parameter Set module (Sangeetha, 2015). In this case, the input parameter was the air flow speed of the car, for the full range of reachable speeds, in this case: 50; 100; 150; 200; 245 [km/h]. We can find another calculation with a range of vehicle speed between 20 and 325 [km/h] (Czyż et al., 2018), but in this case the lower speed is similar to the cited research, and the maximum speed is equal to the maximum reachable speed of the BMW 325i.

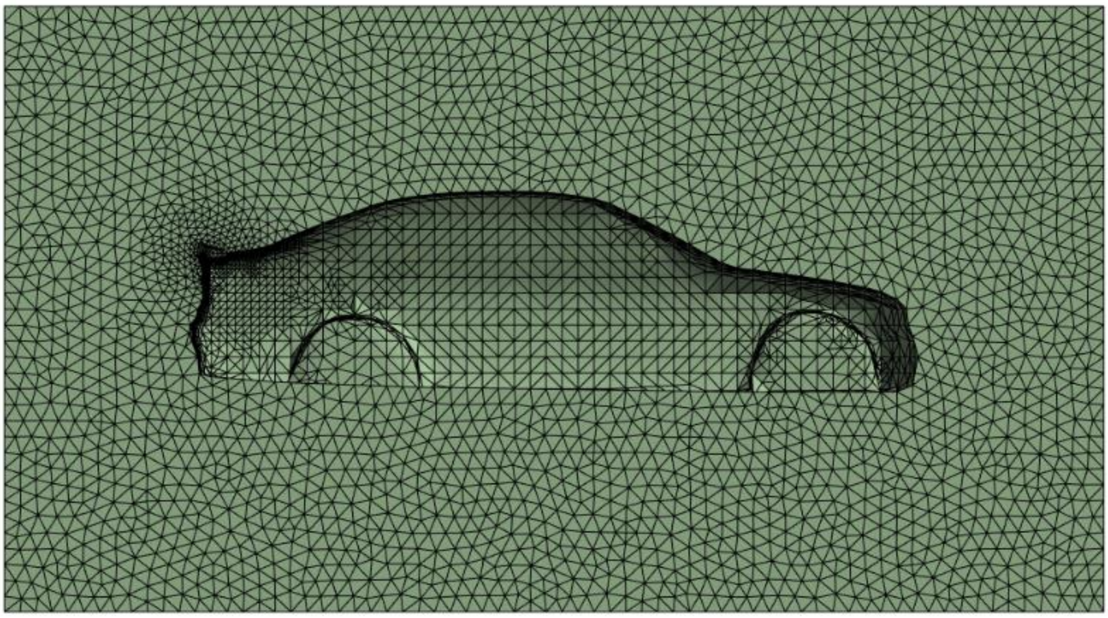

Figure 3. Divide a domain into finite elements

(source: own study)

The results after the meshing process are shown in Figure 3. We set the maximum finite element size to 72 [mm] during grid generation and enabled the grid thickening function at the Curvature Minimum Size of 4.5 [mm]. We introduced the speed of the gas through the "inlet" wall within the Parameter Set range of 50-245 [km/h]. We expanded the computing domain by 1 [m] in each direction, taking into account the vehicle dimensions. In order to limit the required measuring power, half of the model was reduced along the symmetrical plane. The minimum element quality parameter is about 0.13. There are 480092 elements, and 86873 nodes were obtained. The calculation was made with a pressure base type and steady-state conditions. It was assumed that the medium was the ideal gas (air), with a viscosity of $1.7894 \cdot 10^{-5}$ [$kg \cdot m^{-1} \cdot s^{-1}$] and a temperature of 15 [°C].

3. Results and discussion

The calculations allowed to generate flowing air strands of the geometry analysed, a representative example is shown in Figure 4. The turbulence that occurs around the vehicle can be observed visually, in addition each of the straws represents the speed of air flow represented by the colour scale.

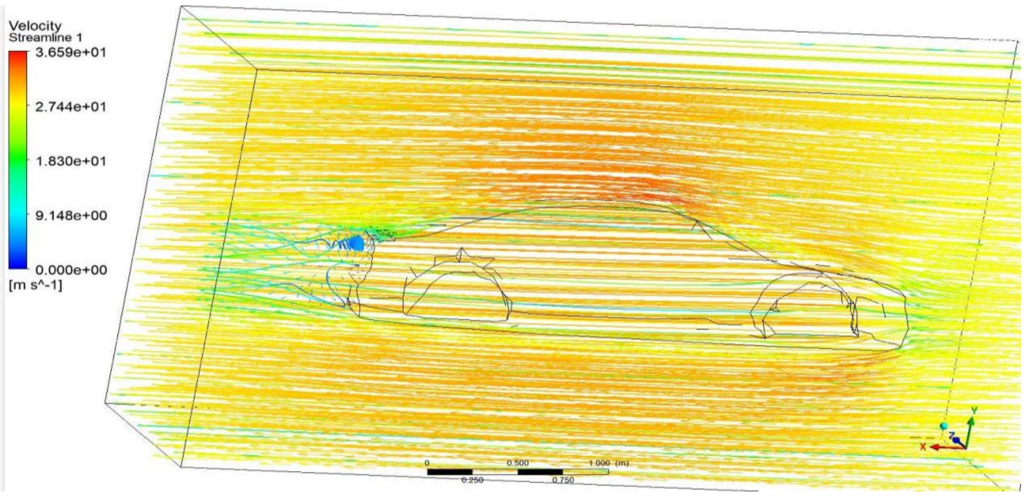

Figure 4. Visualization of air stream lines flowing through the car

(source: own study)

A visual analysis of the air strands provides the basis for determining the best position of the rear spoiler to efficiently utilize the kinetic energy of the gas. The case shown in Figure 3 indicates that the spoiler should be raised slightly in relation to the current position at the prototype stage so that a higher-speed air pipe is on the way. The analysis of the forces acting on the vehicle resulting from its aerodynamic characteristics was carried out separately for the horizontal component (the resistance force acting along the calculated axis X) and the vertical (the force of the aerodynamic pressure, operating along the axis Y). A summary of resistance data is provided in Figure 1 for three cases:

- 0° – the vehicle's factory edge (spoiler case from resting position – counting with the trunk lid);
- 10° – a spoiler in working position with an angle of impact setting of 10° in relation to the plane of the tray lid;
- 20° – a spoiler at work position with a angle of stress setting of 20° in respect of the surface of the luggage lid.

Additionally, a graph of the dependency of the resistance force on the speed of the vehicle is drawn up and is shown in Figure 5 and Table 1. It can be noticed that slight differences in resistance were obtained at angles 0° and 10°, only at a larger angle of impact the resistance begins to increase significantly. From the economic point of view, setting the spoiler at an angle of about 10° gives the best results. Further analysis should be carried out for more impact angle settings. The data obtained will be used to develop a map of the device control.

Table 1
Drag force calculated using FEM for the variable angle of the spoiler slope and different vehicle speeds

	Force of aerodynamic Resistance [N]		
	Spoiler angle		
Velocity [km/h]	**0°**	**10°**	**20°**
50	20.20	20.68	28.83
100	82.47	79.95	101.54
150	178.46	177.53	226.77
200	316.35	314.41	403.16
245	472.92	470.25	599.29

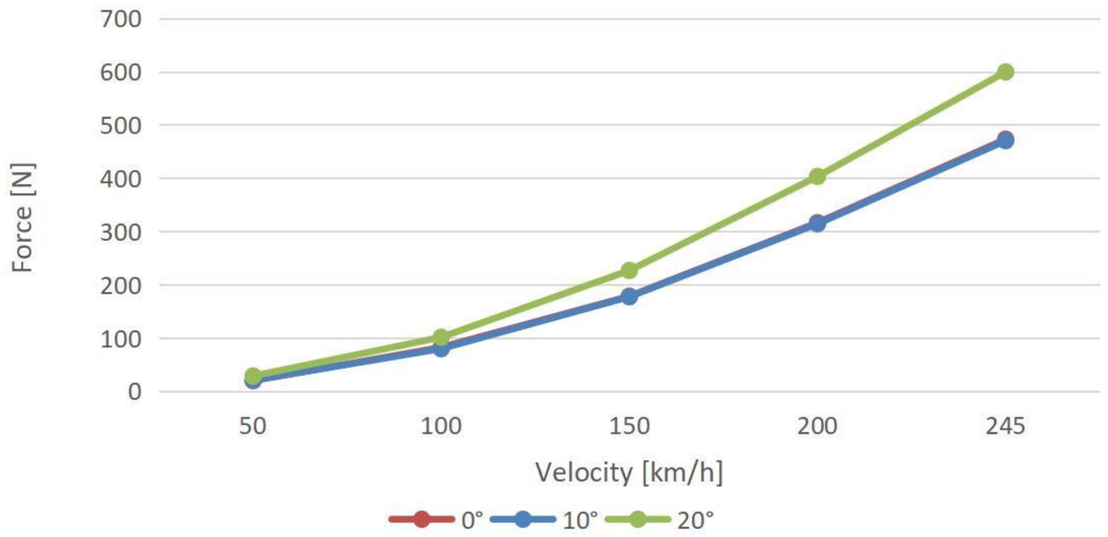

Figure 5. Dependency of drag force on vehicle speed

Table 2
Drag force calculated using FEM for the variable angle of the spoiler slope and different vehicle speeds

Force of aerodynamic resistance [N]			
Spoiler angle			
Velocity [km/h]	**0°**	**10°**	**20°**
50	-1.73	-7.54	-3.57
100	-0.26	-29.38	-17.84
150	-15.67	-63.42	-40.54
200	-28.76	-144.07	-70.26
245	-46.78	-160.51	-104.27

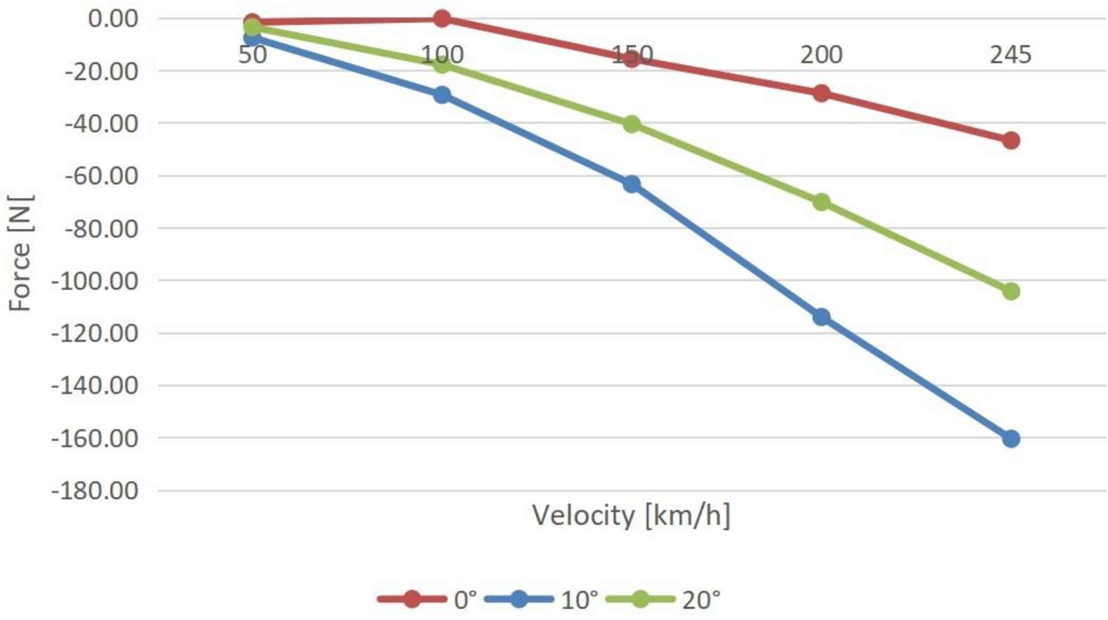

Figure 6. The impact of the aerodynamic pressure force from the spoiler impact angle

In addition, a graph of the relationship of the aerodynamic pressure force to the speed of movement of the vehicle is produced and is shown in Figure 6. It can be noticed that an increase in the force of aerodynamic pressure has already been achieved from the setting of the spoiler at an angle of 10°, while at the same time a slight increase in srag force (Figure 5), which confirms that this is the most reasonable area of the device settings. Changing the geometry of the body affects the change in the air resistance factor, this factor has a direct effect on the strength of the drag force. Car body designers, on the one hand, take into account the visual qualities, and on the other hand, the movement resistors of the vehicle, which in half make up the aerodynamic resistors (Dadbakhsh, 2017). Formula 1 allows you to calculate the strength of the drag force.

$$F_p = 0{,}5 \cdot A \cdot V^2 \cdot C_x \cdot \rho \qquad (1)$$

Where: F_p – drag force, ρ – air density depending on temperature and pressure, V – object velocity, A – front surface of the car, C_x – air resistance coefficient. Having the data on air resistance, the resistance factor C_x was calculated for the original body of the vehicle and for the geometry of the working spoiler. The calculations were performed using formula 2.

$$C_x = \frac{F_p}{0{,}5 \cdot A \cdot V^2 \cdot \rho} \qquad (2)$$

Table 3 summarizes the percentage change in the drag force factor. For the impact angle of 10° for low speeds the coefficient has deteriorated by 2.4 [%] while at speeds of about 100 [km/h] we record an improvement of the resistance factor by 3.1 [%]. By increasing the speed the change factor is negligible. At an impact angle of 10°, a significant deterioration of the C_x factor is observed, reaching 42.7 [%] at a speed of 50 [km/h].

Table 3
Change of the Cx factor calculated for the variable angle of the spoiler inclination and the different speeds of the car

Changing the C_x coefficient		
Spoiler angle		
Velocity [km/h]	**10°**	**20°**
50	2,4%	42.7%
100	-3.1%	23.1%
150	-0.5%	27.1%
200	-0.6%	27.4%
245	-0.6%	26.7%

The simulation studies were extended to include strength analyses carried out to confirm the possibility of using additive manufacturing methods in the manufacture of the rear spoiler prototype. The manufacturing technology that has been taken into account is selective plastics powder compression (SLS) (Pavan, 2017). The final manufacturing process will be carried out on the Sinterit Lisa Pro 2 device, which uses PA-12 polyamide as one of the available materials, characterized by the parameters set out in Table 4. Scientific research confirms the technical usefulness of components produced in addition to laser sintered Pa-12 powders (Yu et al., 2022). Parts made of this material are characterized by profound mechanical and tribological properties (Lammens et al., 20117; Razaviye et al., 2022).

Table 4
Plastic PA-12 material parameters

Parameter	Value	Unit
Density	21140	$kg \cdot m^{-3}$
Stretch strength	43	MPa
Elasticity module	2.2	GPa
Extension at breakdown	16-18	%
Hardness	75	Shore D

The results of the strength tests are shown in Figure 7. The maximum stress calculated according to von Misses' exhaust theory is 0,55 [MPa], which proves that the PA-12 material has mechanical properties (Tomanik et al., 2022) allowing for the manufacture of a fully functional prototype allowing the transfer of loads acting on the spoiler during operation of the vehicle throughout the available range of achieved speeds (Jurkowski, Janisz, 2019).

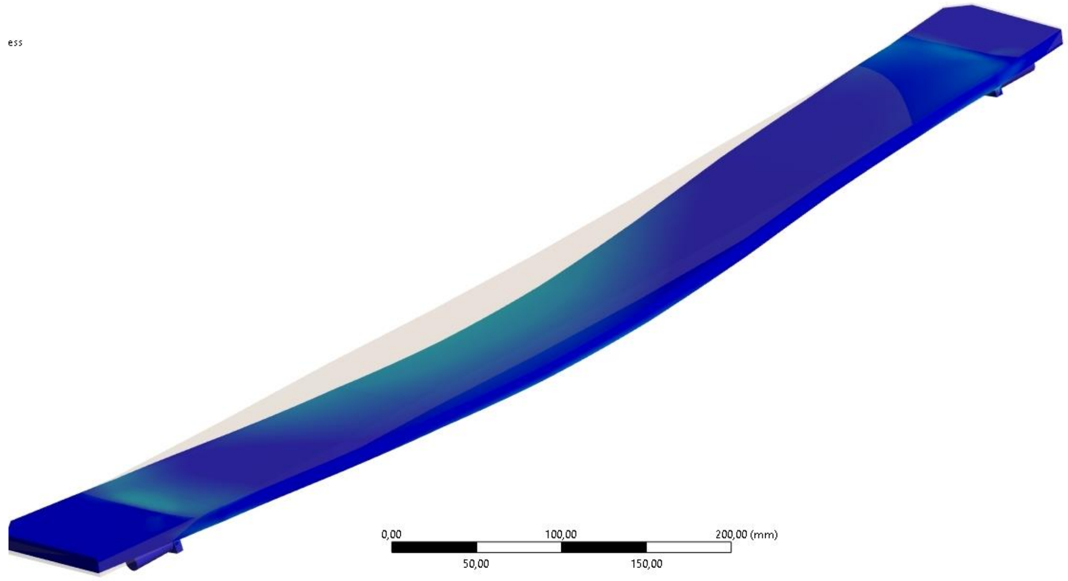

Figure 7. Stress map

The result differs significantly from the stretch strength of the material, which suggests the possibility of reducing the weight of the structure (material savings) while maintaining satisfactory strength properties. The Structural Optimisation module was used for this purpose, the software settings set the permissible weight reduction of the element to 50 [%] and the limit of computational iterations to 500. The results of the algorithm are shown in Figure 8. The resulting geometry forms the core of the structure (72,33 [%] of the output weight), carrying the loads, the remaining space can be supplemented with structures with empty spaces, e.g. with the structure of a honey plate, covered from the outside with a thin surface, preserving the aerodynamic and visual characteristics of the object.

Figure 8. Design with reduced volume

The results of the numerical tests confirm the validity of supplementing the vehicle’s body with a spoiler providing the aerodynamic pressure of the rear axle, the use of FEM calculation methods has also provided information confirming the possibility of using quick prototyping methods in constructing a fully functional device that can be mounted in the vehicle.

4. Further directions of research

Preliminary research has allowed to determine the working area of the active rear spoiler that can be mounted in the BMW E46. Further stages of work include:

- FEM analyses aim to adjust the spoiler's geometry to increase aerodynamic pressure, which includes selecting the optimal surface and determining the spoiler's output beyond the vehicle's outline while considering the driving speed.
- the design of the exit mechanism and the angle of the inclination of a spoiler are important considerations.
- the project involves the installation of control and execution systems.
- creation of a map that shows the settings of the spojler based on the vehicle's speed;
- we are performing a fatigue analysis of the spoiler structure under variable conditions of the loads recorded during the vehicle's operation, using a methodology similar to the fatigue analyses of machine parts (Bajerlein et al., 2020).

5. Conclusions

Numerical calculations in the range of vehicle speed 50-245 [km/h] are similar to cited articles. The procedures and settings adhere to the same principles as those in analogy research. The air flows flowing through the vehicle were analyzed. The engineered rear spoiler, dynamically changing its position in relation to the car's body, is positioned in three positions relative to the luggage compartment: 0°, 10°, and 20°. The analyzed speed range and angles of the spoiler setting allowed the determination of the force of aerodynamic pressure and the map of the control of the active spoiler, i.e., the push of the positioning mechanism and the setting of the angle of the system relative to the plane of the trunk depending on the speed of movement of the vehicle. The force of aerodynamic pressure ranged from 0.5 to 321 [N]. Based on the data obtained, it was determined that the factory geometry of the body provides an aerodynamic pressure ranging from 3 to 93 [N]. The use of a spoiler increases this value from 12 to 228 [N] with a decrease of the C_x factor from 1 to 3 [%]. The beneficial effect of using a spoiler is recorded above a speed of 50 [km/h], and the optimal angle of the spoiler's impact is 10°. The use of rapid prototyping methods allows using the market-available PA-12 material to produce a fully functional prototype of the active spoiler. The optimization module, available in the ANSYS package, reduces the mass of the material used to about 72 [%], while maintaining the strength and useful characteristics of the object.

References

Anderson, J.D. Jr. (2010). *Fundamentals of Aerodynamics*. Tata McGraw-Hill Education: New York.

Arrondeau, B., Rana, Z.A. (2020). Computational Aerodynamics Analysis of Non-Symmetric Multi-Element Wing in Ground Effect with Humpback Whale Flipper Tubercles. *Fluids, 10*(5), 247. DOI: https://doi.org/10.3390/fluids5040247.

Bajerlein, M., Bor, M., Karpiuk, W., Smolec, R., Spadlo, M. (2020). Strength analysis of critical components of high-pressure fuel pump with hypocycloid drive. *Bulletin of the Polish Academy of Sciences, Technical Sciences, 68*, 1341-1350. DOI: https://doi.org/10.24425/bpasts.2020.135380.

Bassett, K., Carriveau, R., Ting, D.S.K. (2015). 3D printed wind turbines part 1: Design considerations and rapid manufacture potential. *Sustain. Energy Technol. Asses, 10*(11), 186-193. DOI: https://doi.org/10.1016/j.seta.2015.01.002.
Choi, S.H., Samavedam, S. (2022). Modelling and optimisation of Rapid Prototyping. *Computers in Industry, 10*(47), 39-53. DOI: https://doi.org/10.1016/S0166-3615(01)00140-3.
Ciuła, J., Gaska, K., Iljuczonek, Ł., Generowicz, A., Koval, V. (2019). Energy efficiency economics of conversion of biogas from the fermentation of sewage sludge to biomethane as a fuel for automotive vehicles. *Architecture Civil Engineering Environment ACEE, 2*, 131-140.
Ciuła, J., Kowalski, S., Generowicz, A., Barbusiński, K., Matuszak, Z. Gaska, K. (2023). Analysis of Energy Generation Efficiency and Reliability of a Cogeneration Unit Powered by Biogas. *Energies, 10*(16), 2180. DOI: https://doi.org/10.3390/en16052180.
Confalone, C.G., Smith, J. Kinnare, T. (2023). 3D Scanning for Advanced Manufacturing, Design, and Construction Wiley Sons. DOI: https://doi.org/10.1002/9781119758532.
Cui, G. (2015). Shape Optimization Based on ANSYS. *Journal of Information and Computational Science, 12*(11), 4291-4297. DOI: https://doi.org/10.12733/jics20106234.
Czyż, Z., Karpiński, P., Gęca, M., Diaz, J.U. (2018). The air flow influence on the drag force of a sports car. *Advances in Science and Technology Research Journal, 12*(2), 121-127. DOI: https://doi.org/10.12913/22998624/86213.
Czyż, Z., Karpiński, P., Sevdim, T. (2018). Numerical analysis of the drag coefficient of a motorcycle helmet. *Applied Computer Science, I*(1), 16-26. DOI: https://doi.org/10.23743/acs-2018-02.
Dadbakhsh, S., Verbelen, L., Verkinderen, O., Strobbe, D., Van Puyvelde, P., Kruth, J.P. (2017). Effect of PA12 powder reuse on coalescence behaviour and microstructure of SLS parts. *Eur. Polym. J., 10*(92), 250-62. DOI: https://doi.org/10.1016/j.eurpolymj.2017.05.014.
Gao, W., Xin Xin, K. (2021). Review of state of the art in active aerodynamic control research for vehicles. *Journal of Physics Conference Series*. DOI: https://doi.org/10.1088/1742-6596/1985/1/012040.
Generowicz, A., Kowalski, Z., Kulczycka, J., Banach, M. (2011). Assessment of technological solutions of municipal waste management using technology quality indicators and multicriteria analysis. *Przemysł Chemiczny, 90*/5, 747-753.
Hyndhavi, D., Murthy, S.B. (2017). Rapid Prototyping Technology – Classification and Comparison. *Int. Res. J. Eng. Tech., 10*, 43107-3111.
Iljaszewicz, P., Łusiak, T., Pastuszak, A., Novak, A. (2020) Aerodynamic analysis of the aircraft model made with the 3D printing method Transp. *Res. Procedia., 10*(51), 118-133. DOI: https://doi.org/10.1016/j.trpro.2020.11.014.
Jurkowski, S., Janisz, K. (2019). Analiza wpływu parametrów siatki obliczeniowej na wynik symulacji przepływomierza. Autobusy. DOI: https://doi.org/10.24136/atest.2019.238.
Katz, J. (1985). *Calculation of the Aerodynamic Forces on Automotive Lifting Surfaces ASME J. Fluids Eng*. DOI: https://doi.org/10.1115/1.3242507.
Kochanek, A., Ciuła, J., Generowicz, A., Mitryasova, O., Jasińska, A., Jurkowski, S., Kwaśnicki P. (2024). The Analysis of Geospatial Factors Necessary for the Planning, Design, and Construction of Agricultural Biogas Plants in the Context of Sustainable Development. *Energies, 17*, 5619. DOI: https://doi.org/10.3390/en17225619.
Kochanek, A.J., Kobylarczyk, S. (2024). Analiza głównych czynników geoprzestrzennych z wykorzystaniem programów geoinformacyjnych niezbędnych do planowania, projektowania i budowy elektrowni fotowoltaicznej. *J. Ecol. Eng., 25*, 49-65.
Kowalski, S., Opoka, K., Ciuła, J. (2022). Analysis of the end-of-life the front suspension beam of a vehicle. *Eksploatacja i Niezawodność – Maintenance and Reliability, 10*(24), 446-454. DOI: https://doi.org/10.17531/ein.2022.3.6.
Kurec, K., Remer, M. (2019). Advanced Modeling and Simulation of Vehicle Active Aerodynamic Safety. *Journal of Advanced Transportation*. DOI: https://doi.org/10.1155/2019/7308590.

Lammens, N., Kersemans, M., De Baere, I. Van Paepegem, W. (2017). On the visco-elasto-plastic response of additively manufactured polyamide-12 (PA-12) through selective laser sintering. *Polym. Test, 10*(57), 149-55. DOI: https://doi.org/10.1016/j.polymertesting.2016.11.032.
Olejarczyk, M., Gruber, P., Ziólkowski, G. (2020). Capabilities and limitations of using Desktop 3D printers in the laser sintering process. *Appl. Sci, 10*(10) 6184. DOI: https://doi.org/10.3390/app10186184.
Park, T.S., Kwon, J.H. (1996). An improved multistage time stepping for second-order upwind TVD schemes Comput. *Fluids, 10*(25),629-645. DOI: https://doi.org/10.1016/0045-7930(96)00014-X.
Paszko, M., Łygas, K. (2016). Współczesne metody modelowania przepływów turbulentnych w otoczeniu poruszającego się autobusu miejskiego. *Autobusy, 17*(12), 1269-1272.
Pavan, M. (2017). On the influence of inter-layer time and energy density on selected critical--to-quality properties of PA12 parts produced via laser sintering. *Polym Test, 10*(61), 386-395. DOI: https://doi.org/10.1016/j.polymertesting.2017.05.027.
Pawłucki, M. (2015). Multiple objective shape optimization in Ansys Fluent Solver. *Mechanik, 10*(11), 893-895. DOI: https://doi.org/10.17814/mechanik.2015.11.587.
Piechna, J. (2012). *Podstawy aerodynamiki pojazdów*. Sulejówek: Wydawnictwo WKŁ.
Poole, S., Phillips, R. (2019). Pattern Recognition Association of South Africa and Robotics and Mechat Rapid prototyping of small wind turbine blades using additive manufacturingronics. *International Conference (PRASA-RobMech), 10*, 189-194.
Przydatek, G., Kochanek, A., Basta, M. (2017). Analysis of changes in municipal waste management at the county level. *Journal of Ecological Engineering, 18*(1), 72-80.
Razaviye, M.K., Tafti, R., Khajehmohammadi, A.M. (2022). An investigation on mechanical properties of PA12 parts produced by a SLS 3D printer: an experimental approach CIRP. *J. Manuf. Sci. Technol., 10*(38), 760-768. DOI: https://doi.org/10.1016/j.cirpj.2022.06.016.
Rohl, P.J., Mavris, D.N., Schrage, D.P. (1995). *Combined Aerodynamic and Structural Optimization of a High-Speed Civil Transport Wing*. American Institute of Aeronautics and Astronautics.
Rosso, S., Meneghello, R., Biasetto, L., Grigolato, L., Concheri, G., Savio, G. (2020). In-depth comparison of polyamide 12 parts manufactured by Multi Jet Fusion and Selective Laser Sintering. DOI: https://doi.org/10.1016/j.addma.2020.101713.
Sangeetha, C. (2015). Fluid structure interaction on AGARD 445.6 wing at transonic speeds. *J. Aircr., 10*(2), 28-34.
Somerfield, M. Retrieved from: https://www.motorsport.com/f1/news/analysis-is-f1-set-for-another-flexi-wing-war-777139/777139/2023.
Szczepaniak, R., Lamch, K., Smykla, I. (2015). *The analysis of the possibilities of using the finite element method to determine the impact of the winglet application on aerodynamic characteristics of the glider wing*. In: Proceedings of the Conference on Modelling Fluid Flow the 16th International Conference on Fluid Flow Technologies.
Tomanik, M., Zmudzinska, M., Wojtków, M. (2022). Mechanical and structural evaluation of the PA12 desktop selective laser sintering printed parts regarding printing strategy 3D Print. *Addit. Manuf., 10*(8), 271-280. DOI: https://doi.org/10.1089/3dp.2020.0111.
Tuliszka-Sznitko, E. (2011). *Wybrane zagadnienia z mechaniki płynów wirujących*. Poznań: WPP.
Vreman B., Geurts B., Kuerten, H. (1997). Large eddy simulation of turbulent mixing layer. *Journal of Fluid Mechanics*. DOI: https://doi.org/10.1017/S0022112097005429.
Yu, G., Ma, J., Li, J., Wu, J., Yu, J., Wang, X. (2022). Mechanical and tribological properties of 3D printed polyamide 12 and SiC/PA12 302 composite by selective laser sintering. *Polymers Basel, 10*(14), 2167. DOI: https://doi.org/10.1016/j.eurpolymj.2017.05.014.
Yurkovich, R., (2003). Status of unsteady aerodynamic prediction for flutter of high performance aircraft. *Autobusy – Buses, 10*(40), 832-842. DOI: https://doi.org/10.2514/2.6874.

Sławomir KOWALSKI[1], **Kacper MŁYNARCZYK**[2]

[1] University of Applied Sciences in Nowy Sącz, Faculty of Engineering Sciences, Zamenhofa 1a, 33-300 Nowy Sącz, e-mail: skowalski@ans-ns.edu.pl
[2] University of Applied Sciences in Nowy Sącz, Faculty of Engineering Sciences, Zamenhofa 1a, 33-300 Nowy Sącz, email: kmlynarczyk0509@gmail.com

Evaluation of the chemical composition of car exhaust gases based on selected parameters

Abstract

The aim of this work is to compare the concentration of chemical compounds found in the exhaust gases of cars supplied with different fuels, depending on the engine speed and vehicle mileage. Testing the exhaust gas composition of low and high mileage cars showed significant differences in emissions. High mileage cars demonstrate higher emissions of toxic exhaust gas components. However, those emissions do not exceed permissible standards and the vehicles may still be operated. A comparison of exhaust emissions from vehicles fueled with LPG and unleaded petrol confirmed the advantage of the gaseous fuel in terms of the emission of toxic components into the surroundings. Tests performed on cars with compression-ignition engines showed a negligible difference in the emission of particulates into the surroundings, despite the differences in exhaust gas treatment systems and the vehicle mileage.

Keywords: exhaust emissions, compression-ignition engine, spark-ignition engine, LPG system.

Ocena składu chemicznego spalin samochodowych na podstawie wybranych parametrów

Streszczenie

Celem niniejszej pracy jest porównanie stężenia związków chemicznych występujących w spalinach samochodów zasilanych różnymi rodzajami paliwa, w zależności od prędkości obrotowej silnika i przebiegu pojazdu. Badania składu spalin samochodów o niskim i wysokim przebiegu wykazały znaczące różnice w emisjach. Samochody o wysokim przebiegu wykazują wyższą emisję toksycznych składników spalin. Emisje te nie przekraczają jednak dopuszczalnych norm i pojazdy mogą nadal być eksploatowane. Porównanie emisji spalin z pojazdów zasilanych LPG i benzyną bezołowiową potwierdziło przewagę paliwa gazowego pod względem emisji toksycznych składników do otoczenia. Badania przeprowadzone na samochodach z silnikami wysokoprężnymi wykazały nieistotną różnicę w emisji cząstek stałych do otoczenia, mimo różnic w układach oczyszczania spalin i przebiegu pojazdów.

Słowa kluczowe: emisja spalin, silnik wysokoprężny, silnik benzynowy, instalacja LPG.

1. Introduction

Despite the dynamic development of electromobility, combustion engines as an energy source are, and will continue to be, a topical issue for many years to come, particularly in the context of the diagnostics of gas emissions and their impact on living organisms (Kęska, 2022). Road traffic can be counted as a significant sector in terms of energy consumption and greenhouse gas emissions. Meanwhile, air quality is deteriorating, which continues to be a key issue related to public health worldwide. Cars are one of the biggest emitters of CO_2 and account for up to 60.6 % of total emissions generated by road traffic (Šarkan, 2022).

Road transport has a significant impact on the economic and social development of every region of the world (Kuranc, 2021; Di, 2023). Road transport has always been a key element ensuring economic growth (Kuppili, 2021). Using a vehicle is very convenient for an individual, but society pays a very high price for that – especially in congested cities, where the number of cars is bigger than in towns. Motor vehicles are a source of air pollution in cities facing various environmental problems. Air pollution is becoming increasingly international.

During engine operation, vehicles produce a variety of gases and particles, called exhaust emissions (Tiwari, 2023). After emission, gaseous and particulate compounds undergo further changes as a result of various atmospheric processes, including oxidation and functionalization by hydroxyl (OH) and nitrate (NO3) radicals, ozone (O3) and photolysis. These oxidation processes lead to the formation of secondary PM (particulate matter) in the atmosphere, including secondary organic aerosol (SOA) and secondary inorganic aerosol (SIA) (Hartikainen, 2023).

Air pollution is one of the main causes of global health issues. Today, nine out of ten people breathe polluted air, which causes premature deaths of more than 4 million people every year. One of the causes of environmental degradation is the presence of an increasing number of cars on roads. In particular, old and run-down cars account for a significant proportion of vehicles and machinery equipped with combustion engines. Car exhaust gases are much more harmful to people than industrial exhaust gases, because the former spread in high concentrations at low altitudes in the immediate vicinity of people (Rymaniak, 2021).

Environmental protection is a top priority, which is why various institutions and vehicle designers strive to reduce the amount of noxious compounds emitted with car exhaust gases. It should therefore be emphasized that improving energy efficiency and reducing exhaust emissions are environmental goals of the highest importance in the transport and road traffic sectors (Mijailović, 2019).

Over the last decade, the European Union has sought to reduce greenhouse gas emissions from road traffic, which in the first phase has led to a significant increase in the proportion of more energy-efficient diesel vehicles in the fleet (Hakkarainen, 2020; Zimmer, 2017). However, as diesel oil-powered vehicles are the major emitters of nitrogen dioxide (NO2) and of greater mass emissions of particulate matter than petrol-fueled vehicles (Hakkarainen, 2020), newer and newer methods of vehicle fueling or other design details for vehicle exhaust systems continue to be sought.

In the transport sector, new renewable and alternative fuels are being introduced and engine cleaning and exhaust gas treatment technologies are being developed as emission standards become more and more rigorous. The Euro 6 emission standard was adopted in 2015 and several steps have been taken to control greenhouse gas emissions in Europe since then. In the evolving field of fuels, engines and emission control technologies, up-to-date and comparable data is needed on both the direct and indirect health and environmental impacts of these technologies. This is necessary to enable landmark decisions to be made to select the best low emission technologies and avoid investment in less efficient ones that could even lead to new emission-related issues (Aakko-Saksa, 2020).

The main NOx reducing technologies in modern diesel vehicles are exhaust gas recirculation (EGR) completed with exhaust gas treatment technologies such as the lean NOx trap (LNT) and/or selective catalytic reduction (SCR). Three-way catalytic converters (TWC) are widely used in petrol vehicles (Mera, 2021).

When investigating two experimental concepts of hydrogen combustion engines, the authors of (Sterlepper, 2021) found that in the case of the petrol engine-based concept, stoichiometric operation requires a three-way catalyst or a three-way NOX storage catalyst as the main exhaust gas treatment system. In the case of the concept based on the compression-ignition engine, state-of-the-art selective catalytic reduction (SCR) catalysts can be used to reduce NOx emissions provided that engine calibration ensures sufficient exhaust gas temperature levels.

The authors of (Shepelev, 2021) developed a generalized mathematical model of the changes in the exhaust gas composition as a function of changes in catalyst resistance, the spark plug gap and electromagnetic nozzle efficiency, and then conducted a technical and economic evaluation. The average return on investment in equipment enabling the implementation of that method was 3.5 months.

The authors of (Kadyrov, 2021) propose the use of ultrasonic radiation to remove particulate matter from the exhaust gases of combustion engines. Those authors proposed an experimental bench and conducted tests, the results of which confirm the feasibility and efficiency of using ultrasonic exhaust gas treatment a result of the particulate coagulation process. The experiment demonstrated the effectiveness of the ultrasound action on motor vehicle exhaust gases and thus proved to be a promising development towards the elimination of noxious pollutants from aerosols with the proposed method. The results of the experiment show that the concentration of hydrocarbons decreased by more than two times. The total weight of soot deposited in the experimental device under the influence of ultrasounds is more than 1.5 times greater than the weight of soot deposited without ultrasounds.

The aim of research presented in this article was to compare the concentration of chemical compounds in exhaust gases from cars fueled with different types of fuel as a function of engine speed and vehicle mileage.

2. Car exhaust gas components

Figure 1 presents the components of exhaust gases from cars equipped with both spark-ignition and compression-ignition engines. The breakdown of the components is presented from the point of view of their influence on the environment and human health.

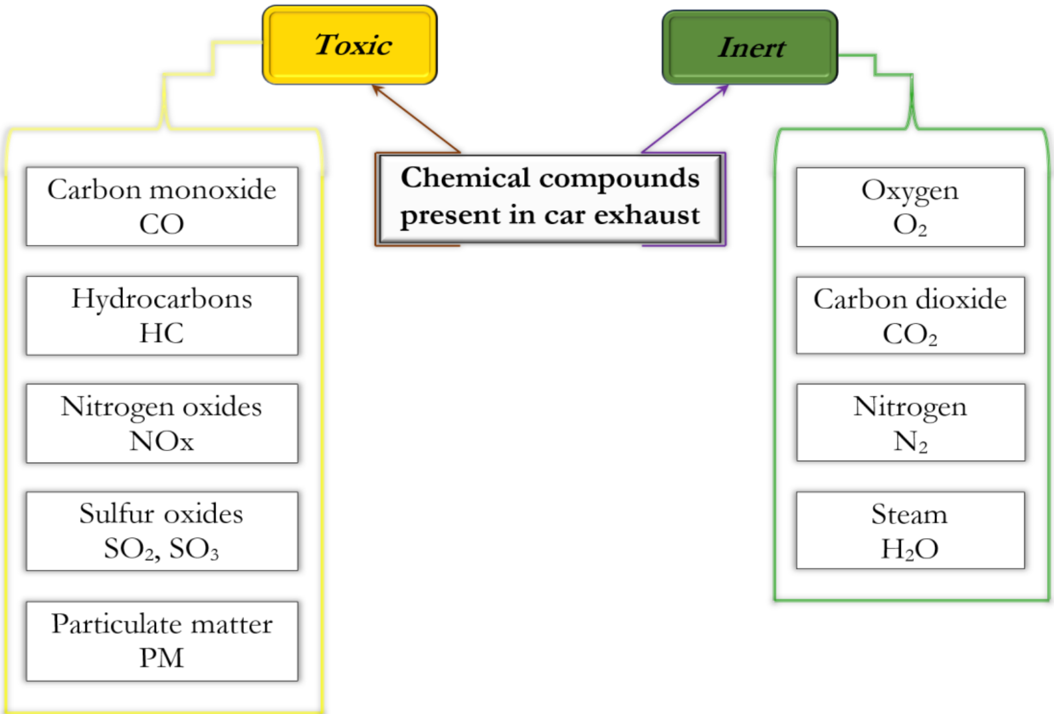

Figure 1. Chemical compounds in car exhaust gases

(source: own study)

In the first group, there are toxic compounds adversely affecting the environment. That group includes:

Carbon monoxide (CO), which is the product of the incomplete combustion of carbon as a result of the small amount of oxygen and the short time required for carbon to burn completely. Carbon monoxide is a colorless and odorless gas.

Hydrocarbons (HC) are unburned or partially burned fuel molecules and come into being in a similar way to carbon monoxide. The most dangerous group are single-ring aromatic hydrocarbons, which include benzene. These compounds are one of the causes of smog formation.

Nitrogen oxides (NO_x) include the following compounds: nitrogen oxide (NO) nitrogen dioxide (NO2) and dinitrogen monoxide (N2O). The volume of nitrogen oxide emissions depends on the combustion temperature and pressure in the engine chamber. Nitrogen oxides are a major cause of photochemical smog (Huang, 2022). NOX emissions directly contribute to a higher level of environmental pollutants such as nitrogen dioxide (NO2), while contributing to the formation of the ground-level ozone (O3) layer and fine particulate matter (Bernard, 2022).

Sulfur oxides (SO2 and SO3) are strongly irritant gases affecting mucous membranes. Sulfur oxides are involved in the formation of acid rain. Sulfur compounds in the exhaust gas can be partly stored in the exhaust gas treatment system at low temperatures and occasionally released at higher exhaust gas temperatures, which leads to the issue of short-term influence of sulfur content in fuel (Rönkkö, 2023).

Particulate matter (PM) is liquid or solid chemical compounds emitted by cars equipped with a compression-ignition engine. The quantity of particulate matter depends on the amount of free oxygen in such a way that the number of particles increases with the enrichment of the air-fuel mixture. Particulate matter contains a quantity of the chemical compounds discussed above. Air deficiency in the combustion chamber results in the formation of soot, which causes smoke. Particulate matter is very small in size, so it persists for a long time in the atmosphere thus affecting the human respiratory system (Lozhkin, 2018; Liu, 2021).

The second group of components in vehicle exhaust gases are chemical compounds that are neutral to the environment. Their excessive presence can cause damage to the environment, however. An example of such a compound is carbon dioxide (CO2). The excessive increase of that compound concentration contributes to the greenhouse effect causing climate change. The compound comes into being in the combustion chamber as a product of carbon combustion.

3. Research methodology

The analysis of exhaust gas chemical composition was made on the following vehicle group:

- cars with the maximum permissible weight of 3,500 kg, equipped with a spark-ignition engine (Group A);
- cars with the maximum permissible weight of 3,500 kg, equipped with a spark-ignition engine and, additionally, an LPG system (Group B);
- cars with the maximum permissible weight of 3,500 kg, equipped with a compression-ignition engine (Group C).

Twenty tests were performed in each vehicle group. The first half of the tested vehicles did low mileage (below 25,000 km) and the other half of the vehicles did high mileage (100,000-250,000 km).

The engines of the cars subjected to exhaust gas chemical composition tests were warmed up to an operating temperature, which is approximately 90oC for the coolant.

Tests for cars with spark-ignition engines were performed at the following engine speeds: 700 rpm (the idle value); 1,500 rpm; 2,000 rpm; 2,500 rpm and 3,000 rpm.

The basic technical parameters of the tested cars are presented in Tables 1-4.

Table 1

Basic technical data of the tested cars (Groups A and B) – low mileage

Year of manufacture	2023
Engine capacity	1498 cm^3
Engine power	150 HP
Torque	250 Nm
Emission standard	Euro 6d
Gearbox	Automatic DSG – 7 gears

(source: own study)

Table 2

Basic technical data of the cars tested (Groups A and B) – high mileage

Year of manufacture	2011
Engine capacity	1498 cm3
Engine power	115 HP
Torque	155 Nm
Emission standard	Euro 5
Gearbox	Manual – 5 gears

(source: own study)

Table 3
Basic technical data of the cars tested (Group C) – low mileage

Year of manufacture	2021
Engine capacity	1997 cm3
Engine power	177 HP
Torque	400 Nm
Emission standard	Euro 6d
Gearbox	Automatic EAT8 – 8 gears

(source: own study)

Table 4
Basic technical data of the cars tested (Group C) – low mileage

Year of manufacture	2003
Engine capacity	2453 cm3
Engine power	135 HP
Torque	310 Nm
Emission standard	Euro 4
Gearbox	Manual – 6 gears

(source: own study)

In the case of cars equipped with a compression-ignition engine, the measurements were performed in accordance with the conditions set out in the Regulation of the Minister of Infrastructure of 27 September 2022 on the scope and manner of the technical inspection of vehicles and on the specimens of documents used in these inspections.

The tests were conducted at a diagnostic station using an exhaust gas analyzer and opacimeter. The view of the measuring stand is presented in Figure 2.

Figure 2. The measuring stand for exhaust gas chemical composition tests

(source: own study)

The chemical composition of exhaust gases for Group A and B vehicles was evaluated with the use of a four gas analyzer.

The analyzer detects compounds such as carbon dioxide (CO2), hydrocarbons (HC), and carbon monoxide (CO). The measurement is based on the absorption of infrared radiation with a specific wavelength for each gas. The analyzer also detects the concentration of oxygen (O2), using the principle of an electrochemical cell, in which electrical voltage is generated with a value dependent on the amount of oxygen. The device also determines the excess air ratio λ, which is based on the oxygen content in exhaust gases. This measurement enables the determination whether the mixture burned by the engine is lean or rich.

Before the measurements, the leak-tightness of the exhaust system must be checked each time, which was also done. The result was successful, making it possible to perform the tests. In the event of a leak in the system, the vehicle would have been disqualified from the measurement until the defect was repaired.

During the tests, engine performance parameters should also be monitored. For that purpose, a measuring probe, installed in the place of the oil dipstick, was used to measure the engine oil temperature. The engine speed was monitored using an induction probe that reads parameters from the ignition cable.

To make the results more reliable, each measurement was repeated three times, and this article includes the averaging values.

Smoke evaluation for Group C vehicles was undertaken with the use of an opacimeter. The device enables the measurement of the range of light flux absorption by exhaust gases as they move along a chamber of a suitably selected length. That measurement permits the determination of the absorption coefficient (k) in the medium with the use of the BEER-LAMBERT law. The result may also be given in the form of the opacity index measured in percentages.

The opacimeter's operating principle is that during the measurement, exhaust gases pass through the measuring probe into the measuring chamber, where the temperature is approx. 100oC. A light source is placed on one side of the chamber, and the light flux passes through the chamber and into a detector on the other side. If there are exhaust gases in the chamber, part of the light flux reaches the detector and the absorption coefficient is calculated on that basis.

As is the case with the measurements done by means of the analyzer, a leak check of the exhaust system was conducted before the tests here, too. The engine was warmed up to an engine oil temperature of approximately 80oC. The sensor and attachments provided with the opacimeter were used to measure the engine speed and temperature.

Soot particles were also removed from the exhaust system by maintaining maximum engine speed for ten seconds. Once the system was cleaned, the measuring probe was placed in the tip of the exhaust system to a depth of three tip diameters.

To substantiate the results, three measurements were taken for each vehicle and the averaging values are included in this article.

4. Test results

The chapter presents the results of the exhaust gas chemical composition tests of cars equipped with a spark-ignition engine first. Next, the test results for cars with a spark-ignition and LPG system will be analyzed, and finally for cars equipped with a compression-ignition engine.

5. Cars with spark ignition engine

Figure 3 shows the results of measurements of environmentally and humanly harmful chemical compounds in exhaust gases depending on the engine speed of spark--ignition cars with high mileage. Table 5 summarizes the values obtained for carbon monoxide and non-toxic compounds in exhaust gases.

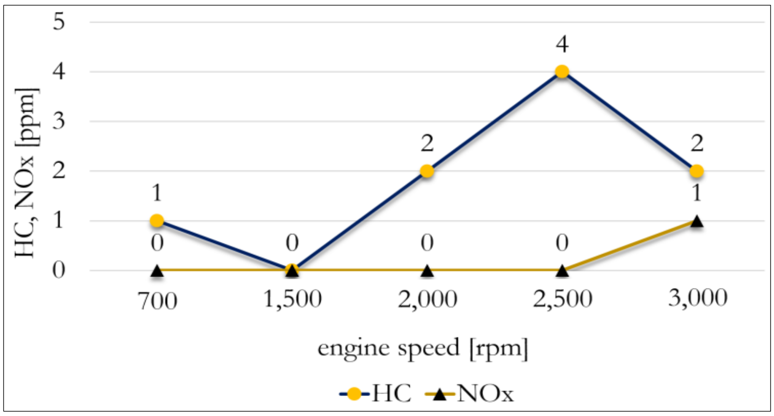

Figure 3. The values for toxic components of exhaust gases as a function of engine speed for a spark-ignition car with low mileage

(source: own study)

Table 5

Other measured components of exhaust gases for a car with a spark-ignition engine and low mileage

	Engine speed [rpm]				
	700	1,500	2,000	2,500	3,000
CO [% by volume]	0.00	0.00	0.00	0.00	0.00
CO_2 [% by volume]	14.5	14.6	14.8	14.9	14.7
O_2 [% by volume]	0.45	0.01	0.01	0.00	0.00
λ	1.021	0.999	0.999	0.998	0.999

(source: own study)

The analysis of the chemical composition of exhaust gases from the low mileage car showed the absence of nitrogen oxides at the engine speed range from idle to 2,500 rpm. At 3,000 rpm, a slight increase in the concentration of that chemical compound was noted. The increase by one unit is noted and the value is finally 1. That value should therefore be deemed to a measurement error and treated as insignificant.

One of the chemical compounds which is hazardous to people, namely carbon dioxide, was noted in the composition of exhaust gases.

The hydrocarbon content in exhaust gases varies with engine speed. The maximum content is 4 ppm. That value is insignificant in terms of standards recommended by Polish legislation. Pursuant to current legislation, the hydrocarbon content in exhaust gases from cars registered after 1 May 2004 must not exceed 100 ppm. The presence of hydrocarbons in the exhaust gases of new cars with low mileage may be caused by engine oil droplets penetrating into combustion chambers. In TSI engines, there is a considerable difference in operating temperature, it is therefore reasonable to increase the clearance of the piston ring locks, which is conducive to the penetration of small amounts of engine oil into combustion chambers. That phenomenon occurs particularly in the case of low viscosity synthetic oil.

Figure 4 shows the results of measurements of environmentally and humanly harmful chemical compounds in exhaust gases depending on the engine speed of spark--ignition cars with high mileage. Table 6 summarizes the values obtained for carbon monoxide and non-toxic compounds in exhaust gases.

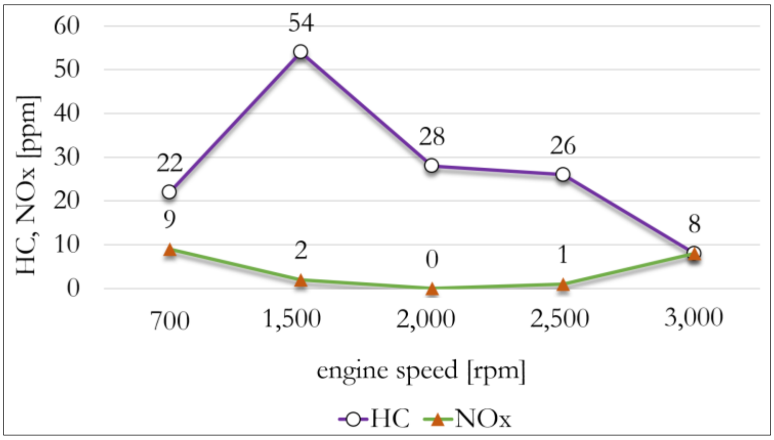

Figure 4. The values for the toxic components of exhaust gases as a function of engine speed for a spark-ignition car with high mileage

(source: own study)

The content of nitrogen oxides (NOx) in exhaust gases from high mileage cars varies from 0 to 9 ppm, which complies with the permitted values prescribed by Polish law.

The recorded nitrogen oxide values are indicative of the proper operation of systems responsible for the reduction of toxic emissions into the environment. NOx values above zero may be the result of the less efficient operation of the exhaust gas recirculation system or EGR valve due to them being heavily worn-out.

The hydrocarbon (HC) content in exhaust gases ranges from 8 to 54 ppm. As is the case with previously tested vehicles, those values are also within the range of the standards comprised by the Regulation of the Minister of Infrastructure, where the maximum HC value is set at 100 ppm.

Table 6

Other measured components of exhaust gases for a high mileage car with a spark-ignition engine

	Engine speed [rpm]				
	700	1,500	2,000	2,500	3,000
CO [% by volume]	0.06	0.30	0.27	0.30	0.19
CO_2 [% by volume]	14.5	14.5	14.6	14.5	14.6
O_2 [% by volume]	0.61	0.38	0.18	0.13	0.11
λ	1.026	1.055	0.999	0.990	0.997

(source: own study)

The varying amount of hydrocarbons depending on the engine speed may be indicative of the operational wear of the exhaust system components.

The highest hydrocarbons value was recorded at an engine speed of 1,500 rpm. This could be caused by engine leakage problems and engine oil penetrating into the combustion chamber.

At idle engine speed (700 rpm) engine oil may penetrate into the combustion chamber through leaking valve seals and then be combusted as the engine speed is increased.

The drop in hydrocarbon concentrations at higher engine speeds indicates that excess hydrocarbons that have penetrated into the combustion chambers have been combusted. In the case of high mileage cars, oil ingress can also be caused by wear on the piston rings resulting from vehicle operation, and the wear of the crankshaft venting system or so-called breather vents.

The increase in hydrocarbons may also be due to the incomplete combustion of the air-fuel mixture, which may result from the wear of the mixture ratio control components and the fuel supply system.

The diagnosed issues do not, however, exclude the tested vehicles from further operation, as they comply with the emission standards.

By analyzing the data in Table 6, it may be noted that the carbon monoxide (CO) content varies from 0.06 to 0.3 % by volume. Those values do not disqualify the cars from operation, as the values are within the limits set out by Polish law. It should be stressed, however, that those values fluctuate around the upper permissible limit. The standard for carbon monoxide as laid down in the Regulation of the Minister of Infrastructure is 0.3 % by volume at engine idle speed and 0.2 % by volume at 3,000 rpm.

The significant decrease in carbon monoxide values at 3,000 rpm may be related to combustion optimization at higher speeds. The increase, however, may result from the incomplete combustion of the air-fuel mixture due to a shortage of air.

That shortage may result from the wear of the components of the air-fuel ratio control system such as the flow meter or lambda probe. Mixture enrichment may also be affected by a very small leak in one of the injectors, so too much fuel enters the cylinder compared to air intake.

In the case of an increase in carbon monoxide in exhaust gases, mention should also be made of misfiring, which is a situation where the mixture is delivered to the cylinder, but not ignited. That phenomenon is due to the fact that misfiring is tolerated to a certain extent by the engine control system and not registered as an error by the EOBD system. Misfiring is usually caused by the wear of ignition system components such as coils and spark plugs.

An increase in carbon monoxide may also be caused by the wear of exhaust gas treatment system components resulting from vehicle mileage.

When comparing the two categories of spark-ignition cars being tested, it may be stated that low mileage vehicles emit toxic compounds at very low levels or not at all. This means that the systems responsible for the control of the mixture ratio and exhaust gas treatment operate faultlessly and meet the stringent quality control requirements to be satisfied by every new vehicle leaving the factory. High mileage vehicles emit more toxic compounds into the atmosphere, but the quantities do not exceed permissible standards and the vehicles may continue to be operated. However, the volume of emissions is a signal that the exhaust gas treatment and air-fuel mixture control issues in those vehicles should be looked at.

The remaining components of engine exhaust gases of both low and high mileage cars are at similar levels. Carbon dioxide (CO2) in all the tested vehicles oscillates between 14-15 % by volume. The situation is similar with the excess air ratio (λ), which varies between 0.997 and 1.026. The range indicates that the air-fuel mixture contains the correct amount of oxygen needed to burn the fuel.

6. Cars with a spark-ignition engine and LPG supply

Figures 5-7 shows the results of measurements of environmentally and humanly harmful chemical compounds in the exhaust gases depending on the engine speed of spark-ignition cars additionally fueled with LPG.

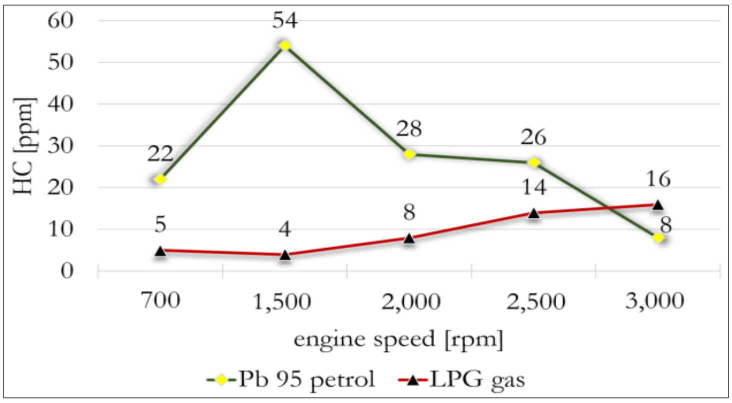

Figure 5. The hydrocarbon content in exhaust gases of spark-ignition cars additionally fueled with LPG

(source: own study)

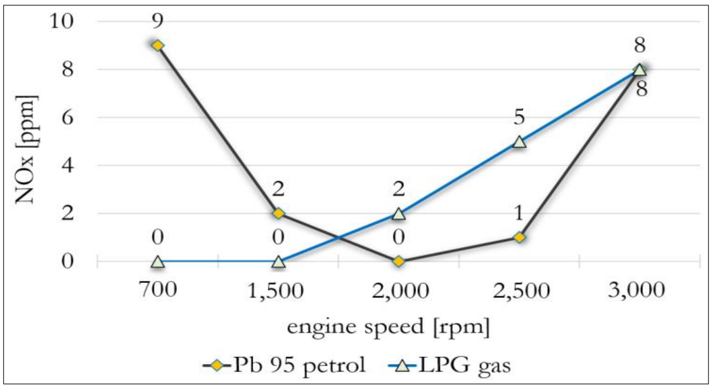

Figure 6. The nitrogen oxide content in exhaust gases of spark-ignition cars additionally fueled with LPG

(source: own study)

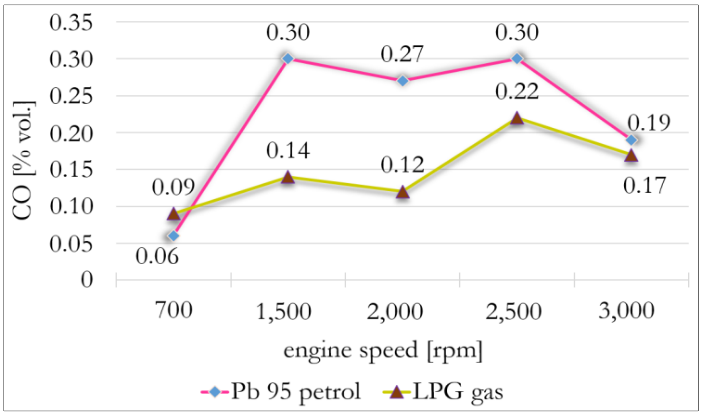

Figure 7. The carbon dioxide content in exhaust gases of spark-ignition cars additionally fueled with LPG

(source: own study)

Based on the diagrams above, it can be seen that both hydrocarbon and carbon monoxide contents are lower in almost the entire engine speed range in the exhaust gases from LPG fueling compared to the exhaust gases from unleaded Pb95 petrol combustion. The values are higher for hydrocarbons only at an engine speed of 3,000 rpm and for carbon monoxide at the idle speed (700 rpm). The difference of 0.03 % by volume is very small and may therefore be negligible. A similar situation occurs at an engine speed of 3,000 rpm, where the difference is 0.02 % by volume.

The lower hydrocarbon content in exhaust gases from LPG combustion is due to the fact that the mixture made with the use of propane-butane is more homogeneous. This improves combustion quality and, in the exhaust gases, there are fewer underburned particles, those being hydrocarbons. Hence, LPG is considered to be a more environmentally friendly fuel than unleaded petrol.

The difference in the carbon monoxide content in exhaust gases from LPG and unleaded petrol is due to the different combustion characteristics of the air-fuel mixture and the different fuel composition. LPG has a higher octane number and lower flash point, which may translate into lower emissions of carbon oxides into the atmosphere.

The content of nitrogen oxides found in the exhaust gases from an LPG-fueled engine is lower than that from an unleaded petrol-fueled engine for lower engine speeds. As engine speed increases, the nitrogen oxide content increases and at 3,000 rpm that content reaches the same value as in the case of exhaust gases from an engine running on unleaded petrol, i.e. 8 % by volume. LPG is free from fuel nitrogen and therefore the content of nitrogen oxides in the exhaust gases is significantly lower than in the case of petrol combustion. The opposite situation may be indicative of the incorrect installation of the LPG system or worn-out parts. In such cases, the system should be looked at and repaired if necessary.

Figure 8 shows the results of the carbon dioxide measurement in exhaust gases depending on the engine speed of spark-ignition cars additionally fueled with LPG.

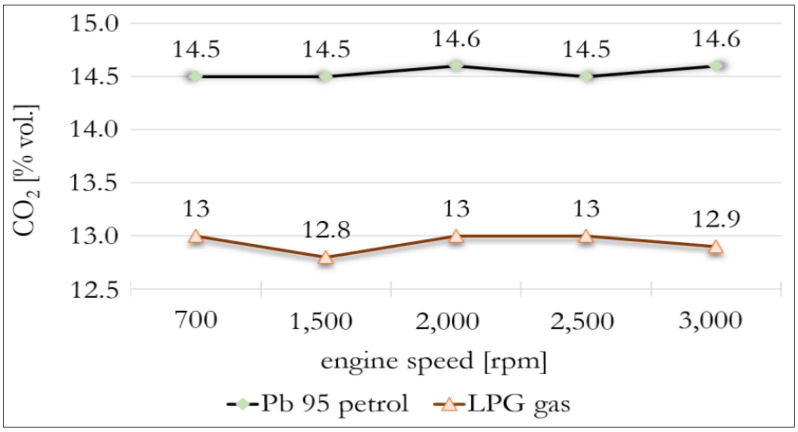

Figure 8. The carbon dioxide content in exhaust gases from spark-ignition cars additionally fueled with LPG

(source: own study)

The carbon dioxide content in exhaust gases when the engine is fueled with LPG is approximately 1.5 % by volume lower than in the case of unleaded petrol, and this follows from the properties of propane-butane. It may therefore be stated that that fuel is more environmentally friendly.

The issue of worldwide carbon dioxide emissions is currently one of the most frequently discussed environmental topics. Carbon dioxide is a gas which naturally occurs in the environment and also a product of complete combustion. The issue of carbon dioxide emissions relates to the current climate change as such emissions contribute to the greenhouse effect.

7. Cars equipped with a compression – ignition engine

Figure 9 shows the results of exhaust gas smoke measurements for low mileage cars equipped with a compression-ignition engine. The measurements were repeated three times for each acceleration. Acceleration 1 represents the measurement at idle speed, acceleration 2 shows the measurement at maximum engine speeds, and acceleration 3 represents the measurement at adjustable engine speeds. An average was taken from each measurement and presented in the diagram.

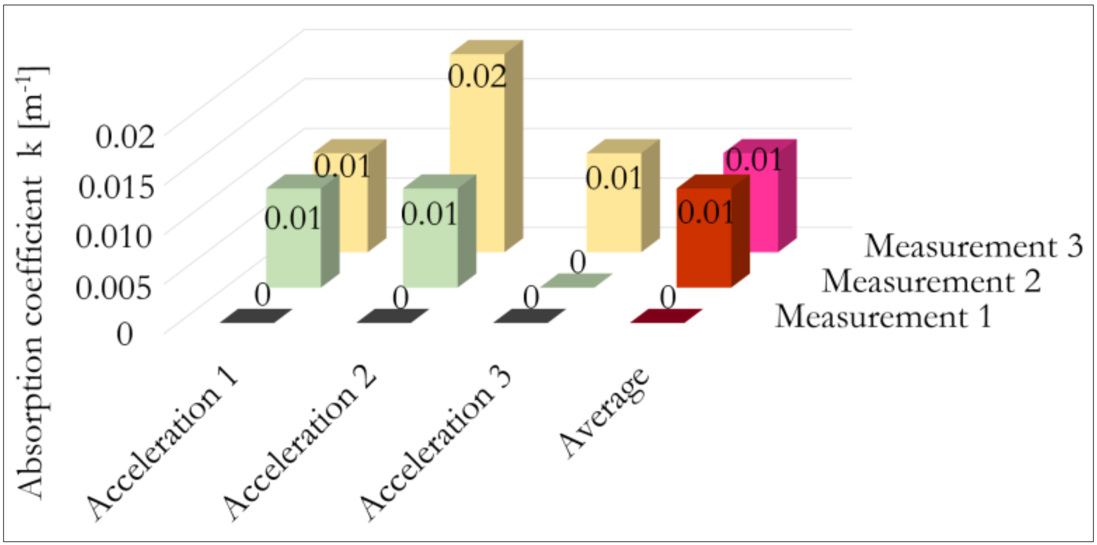

Figure 9. Exhaust gas smoke measurement for cars with compression ignition and low mileage (source: own study)

The mean values of the three exhaust gas smoke measurements indicate the correct operation of the components of the vehicle's exhaust gas treatment system. The mean values of the exhaust gas smoke measurements oscillate around 0.01 m-1.

In the regulations concerning vehicle technical inspection, the exhaust gas smoke standard for vehicles first registered after 30 April 2008 is k = 1.5 m-1. As regard those values, it should be stated that the exhaust gas treatment system of the tested vehicles fully eliminates the particulates emitted by the engine. The result of such low exhaust gas smoke content is also due to the faultless operation of the vehicle's fuel supply system components, the air-fuel ratio control and the exhaust gas recirculation system. The faultless operation of these components follows from the fact that the vehicle has done low mileage and the various components still operate like new, with no signs of wear.

Figure 10 shows the results of exhaust gas smoke measurements for high mileage cars equipped with a compression-ignition engine. The test procedure and presentation of the test results was analogous to the previously presented tests and results. Here too, three measurements were taken for each predetermined engine speed.

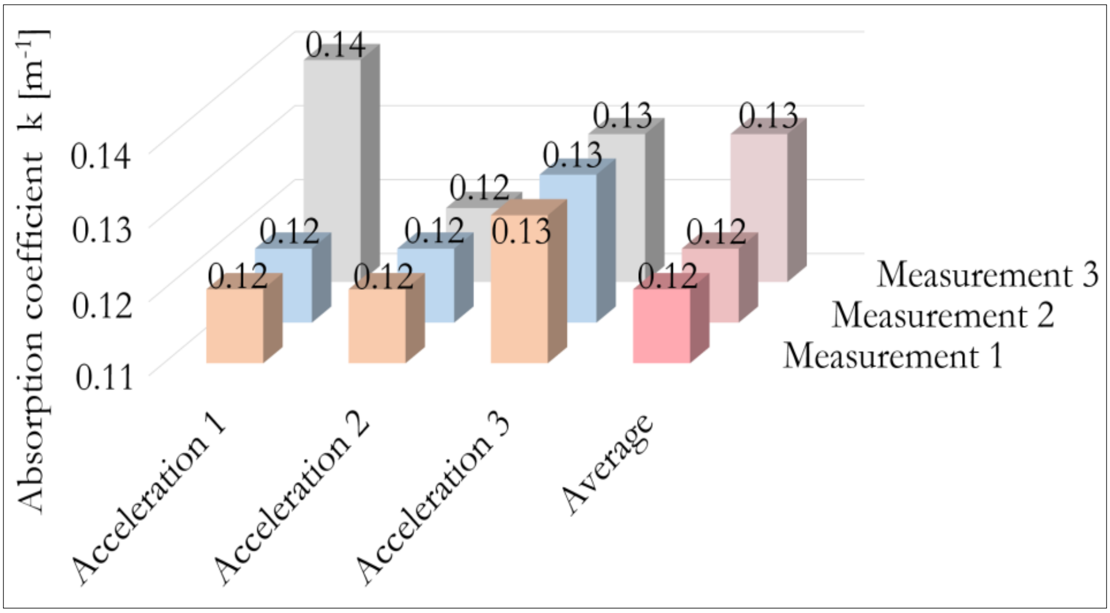

Figure 10. Exhaust gas smoke measurement for high mileage cars with compression ignition (source: own study)

The results of the exhaust gas smoke measurement indicate that the systems responsible for the reduction of particulate emissions operate properly. According to the values assumed in the standards, exhaust gas smoke content for vehicles registered for the first time before 30 April 2008 must not exceed k = 3.0 m-1. The average values of the various exhaust gas smoke measurements are k = 0.12-0.13 m-1. The tested cars, however, satisfy the more stringent standards applicable to vehicles registered after that date.

The results of the measurements authorize the conclusion that the various components of the exhaust gas treatment, fuel supply and air inlet, exhaust gas recirculation and air-fuel mixture control systems operate properly. The distribution of the results is far from the limit value for those vehicles. Such results may be influenced by the heavy repair of the components of the fuel supply system, including injectors, and the replacement of the exhaust gas recirculation valve, which was carried out not long before the test.

In summary, the measurement results for all the tested vehicles do not differ significantly from each other. The difference in the measurements between the low and high mileage cars is from 0.12 to 0.13 m-1. Those differences are most likely due to design differences in the exhaust gas treatment system of the various vehicles. Low mileage cars feature the latest design and technology relating to exhaust gas treatment systems. First of all, they are provided with particulate filters. High mileage cars are not equipped with such filters. It should therefore be concluded that the exhaust gas treatment system of high mileage vehicles operates properly and that the presence of untreated particulates is precisely the result of the absence of the particulate filter.

From the test results obtained, it can also be concluded that older, high mileage vehicles can also satisfy stringent exhaust emission standards applicable to newly manufactured vehicles provided that the former are properly used and serviced in accordance with the manufacturer's time schedule.

8. Conclusions

The aim of the tests presented in this article was to compare the concentrations of chemical compounds in the exhaust gases of cars fueled with various kinds of fuel in relation to the engine speed.

Based on the tests, the following conclusions can be drawn:

- Testing the exhaust gas composition of low and high mileage cars showed significant differences in emissions. High mileage cars demonstrate higher emissions of toxic exhaust gas components. However, those emissions do not exceed permissible standards and the vehicles may still be operated.
- The differences in the exhaust gas composition of low and high mileage vehicles are due to the mechanical wear of the exhaust and exhaust gas treatment system components. Repairs and appropriate maintenance can result in the reduction of the emissions of toxic components from run-down vehicles. Test results highlight the importance of regular diagnostics and repairs to minimize environmental impact.
- Increased emissions from high mileage vehicles may be due to differences in the design of exhaust gas treatment systems. New vehicles have more sophisticated systems designed to meet increasingly stringent emission standards.
- A comparison of exhaust emissions from vehicles fueled with LPG and unleaded petrol confirmed the advantage of the gaseous fuel in terms of the emission of toxic components into the surroundings. The tests have unambiguously confirmed lower emissions of these substances during the operation of an LPG-fueled vehicle, which is an important asset from the environmental point of view.
- An important aspect is lower carbon dioxide emission into the atmosphere when a car is fueled with LPG. Reducing that emission is crucial in the context of current environmental trends.
- The analysis of the test results suggests the need for a more in-depth consideration of the use of LPG as the main, or even only fuel for motor vehicles. Such a solution would bring tangible benefits not only for ecology, but also for drivers, in terms of reduced car operating costs.
- Tests performed on cars with compression-ignition engines showed a negligible difference in the emission of particulates into the surroundings, despite the differences in exhaust gas treatment systems and the vehicle mileage.

A common conclusion which arises for all analyzed scenarios is that vehicle age and mileage do not necessarily mean that a vehicle is excluded from operation due to emission standards being exceeded.

The way in which vehicles are operated and maintained plays an important role in their compliance with emission standards. Therefore, the authorities of cities in which access to the center is restricted should take into account the actual emissions of vehicles and not, as has been the case so far, the age of the vehicle and a note in the registration card stating that the vehicle satisfies emission standards.

The tests of the exhaust gas composition of vehicles with different parameters have provided important information that can be useful both for vehicle diagnostics and for the further development of environmentally friendly solutions in the automotive industry.

References

Aakko-Saksa, P., Koponen, P., Roslund, P., Laurikko, J., Nylund, N.-O., Karjalainen, P., Rönkkö, T., Timonen, H. (2020). *Comprehensive emission characterisation of exhaust from alternative fuelled cars*. *Atmospheric Environment, 236*, 117643. DOI: https://doi.org/10.1016/j.atmosenv.2020.117643.

Barwari, R.R.I. (2021). Study of air pollutions caused by exhaust gases emitted from gasoline vehicles in Erbil City. *IOP Conference Series: Materials Science and Engineering, 1105*, 012053. DOI: https://doi.org/10.1088/1757-899X/1105/1/012053.

Bernard, Y., Dornoff, J., Carslaw, D.C. (2022). Can accurate distance-specific emissions of nitrogen oxide emissions from cars be determined using remote sensing without measuring exhaust flowrate? *Science of the Total Environment, 816*, 151500. DOI: https://doi.org/10.1016/j.scitotenv.2021.151500.

Di, Z., Li, L., Li, M., Zhang, S., Yan, Y., Wang, M., Li, B. (2023). Research on the contribution of metro-based freight to reducing urban transportation exhaust emissions. *Computers & Industrial Engineering, 185*, 10622. DOI: https://doi.org/10.1016/j.cie.2023.109622.

Hakkarainen, H., Aakko-Saksa, P., Sainio, M., Ihantola, T., Rönkkö, T.J., Koponen, P., Rönkkö, T., Jalava, P.I. (2020). Toxicological evaluation of exhaust emissions from light-duty vehicles using different fuel alternatives in sub-freezing conditions. *Particle and Fibre Toxicology, 17*, 17. DOI: https://doi.org/10.1186/s12989-020-00348-0.

Hartikainen, A.H., Ihalainen, M., Yli-Pirilä, P., Hao, L., Kortelainen, M., Pieber, S.M., Sippula, O. (2023). Photochemical transformation and secondary aerosol formation potential of Euro 6 gasoline and diesel passenger car exhaust emissions. *Journal of Aerosol Science, 171*, 106159. DOI: https://doi.org/10.1016/j.jaerosci.2023.106159.

Hepelev, V., Gritsenko, A., Salimonenko, G. (2021). Control of hydrocarbon emissions when changing the technical condition of the exhaust system of modern cars. *FME Transactions, 49*, 749-755. DOI: https://doi.org/10.5937/fme2103749S.

Huang, J., Gao, J., Wang, Y., Chen, H., Laurikko, J., Pellikka, A.P., Yang, C., Ma, C. (2022). Insight into the penalty of exhaust emissions and fuel consumption by DPF regeneration of a diesel passenger car. *Chemosphere, 309*(1), 136629. DOI: https://doi.org/10.1016/j.chemosphere.2022.136629.

Kadyrov, A., Sarsembekov, B., Ganyukov, A., Zhunusbekova, Z., Alikarimov, K. (2021). Experimental research of the coagulation process of exhaust gases under the influence of ultrasound. *Communications, 23*(4), B288-B298. DOI: https://doi.org/10.26552/com.C.2021.4.B288-B298

Kęska, A. (2022). Analysis and evaluation of the composition of toxic groups of compounds emitted in the exhaust gases of vehicles compliant with the Euro 6 standard. *Przemysł Chemiczny, 101*(8), 606-610. DOI: https://doi.org/10.15199/62.2022.8.12.

Kuppili, S.K., Alshetty, V.D., Diya, M., Nagendra, S.M.S., Ramadurai, G., Ramesh, A., Gulia, S., Namdeo, A., Maji, K., Bell, M., Goodman, P., Hayes, E., Barnes, J., Longhurst, J., De Vito, J. (2021). Characteristics of real-world gaseous exhaust emissions from cars in heterogeneous traffic conditions. *Transportation Research Part D: Transport and Environment, 95*, 102855. DOI: https://doi.org/10.1016/j.trd.2021.102855.

Kuranc, A., Caban, J., Šarkan, B., Dudziak, A., Stoma, M. (2021). Emission of selected exhaust gas components and fuel consumption in different driving cycles. *Communications, 23*(4), B265-B277. DOI: https://doi.org/10.26552/com.C.2021.4.B265-B277.

Liu, Y., Chen, H., Li, Y., Gao, J., Dave, K., Chen, J., Li, T., Tu, R. (2022). Exhaust and non-exhaust emissions from conventional and electric vehicles: A comparison of monetary impact values. *Journal of Cleaner Production, 331*, 129965. DOI: https://doi.org/10.1016/j.jclepro.2021.129965.

Lozhkin, V., Lozhkina, O., Dobromirov, V. (2018). A study of air pollution by exhaust gases from cars in well courtyards of Saint Petersburg. *Transportation Research Procedia, 36*, 453-458. DOI: https://doi.org/10.1016/j.trpro.2018.12.124.

Mera, Z., Fonseca, M., Casanova, J., López, J.M. (2021). Influence of exhaust gas temperature and air-fuel ratio on NOx aftertreatment performance of five large passenger cars. *Atmospheric Environment, 244*, 117878. DOI: https://doi.org/10.1016/j.atmosenv.2020.117878.

Mijailović, R., Marković, N., Pešić, D., Vlajić, J.V. (2019). Evaluation of scenarios for improving energy efficiency and reducing exhaust emissions of a passenger car fleet: A methodology. *Transportation Research Part D: Transport and Environment, 73*, 352-366. DOI: https://doi.org/10.1016/j.trd.2019.07.005.

Rönkkö, T., Pirjolac, L., Karjalainen, P., Simonen, P., Teinilä, K., Bloss, M., Salo, L., Datta, A., Lal, B., Hooda, K., Saarikoski, S., Timonen, H. (2023). Exhaust particle number and composition for diesel and gasoline passenger cars under transient driving conditions: Real-world emissions down to 1.5 nm. *Environmental Pollution, 338*, 122645. DOI: https://doi.org/10.1016/j.envpol.2023.122645.

Rymaniak, Ł., Kamińska, M., Szymlet, N., Grzeszczyk, R. (2021). Analysis of harmful exhaust gas concentrations in cloud behind a vehicle with a spark ignition engine. *Energies, 14*(6), 1769. DOI: https://doi.org/10.3390/en14061769.

Šarkan, B., Loman, M., Synák, F., Skrúcaný, T., Hanzl, J. (2022). Emissions production by exhaust gases of a road vehicle’s starting depending on a road gradient. *Sensors, 22*(24), 9896. DOI: https://doi.org/10.3390/s22249896.

Sterlepper, S., Fischer, M., Claßen, J., Huth, V., Pischinger, S. (2021). Concepts for hydrogen internal combustion engines and their implications on the exhaust gas aftertreatment system. *Energies, 14*(23), 8166. DOI: https://doi.org/10.3390/en14238166.

Tchankova, L. (2002). Risk identification – basic stage in risk management. *Environmental Management and Health, 13*(3), 290-297.

Tiwari, K., Raghuwanshi, S.S., Sharma, S. (2023). Vehicle exhaust emissions: From peril to power. Materials *Today: Proceedings*. DOI: https://doi.org/10.1016/j.matpr.2023.10.055.

Zimmer, A., Koch, N. (2017). Fuel consumption dynamics in Europe: Tax reform implications for air pollution and carbon emissions. *Transportation Research Part A: Policy and Practice, 106*, 22-50. DOI: https://doi.org/10.1016/j.tra.2017.08.006.

Tomasz KĄDZIOŁKA[1]

[1] University of Applied Sciences in Nowy Sącz, Faculty of Engineering Sciences, Zamenhofa 1a, 33-300 Nowy Sącz, e-mail: tkadziolka@ans-ns.edu.pl

Transport and storage of selected industrial waste

Abstract

According to Statistics Poland (GUS), the amount of waste from industrial activities in Poland in 2021 exceeded 107 million tons. Waste poses a threat to the environment and human life and health, which is why it is so important to properly manage processes such as waste transportation and storage. The handling of industrial waste is covered by a number of regulations, which must be followed in order to protect the environment. Industrial companies are obliged to register and record a significant portion of their waste, and they must also submit reports regularly. Entrepreneurs acting in accordance with strict rules contribute to improving the quality of life of present and future generations.

Keywords: industrial waste, waste transport, food processing.

Transport i składowanie wybranych odpadów przemysłowych

Streszczenie

Według danych Głównego Urzędu Statystycznego (GUS) ilość odpadów pochodzących z działalności przemysłowej w Polsce w 2021 r. przekroczyła 107 mln ton. Odpady stanowią zagrożenie dla środowiska oraz życia i zdrowia ludzi, dlatego tak ważne jest właściwe zarządzanie procesami takimi jak transport i składowanie odpadów. Postępowanie z odpadami przemysłowymi reguluje szereg przepisów, których należy przestrzegać w celu ochrony środowiska. Przedsiębiorstwa przemysłowe są zobowiązane do rejestrowania i ewidencjonowania znacznej części swoich odpadów, a także do regularnego składania raportów. Przedsiębiorcy działający zgodnie z surowymi przepisami przyczyniają się do poprawy jakości życia obecnych i przyszłych pokoleń.

Słowa kluczowe: odpady przemysłowe, transport odpadów, przetwórstwo spożywcze.

1. Introduction

The primary piece of legislation dealing with waste is the Waste Act of December 14, 2012. It implements, within the scope of its regulations, European Union directives (Wieczorek, 2021). The act defines waste as "any substance or object which the owner disposes of, intends to dispose of, or is obligated to dispose of" (Act of Waste, 2013). The term "industrial waste" has not received a statutory definition.

The term is most often used to describe "waste generated as a result of various production processes" (Jakubowski, 2006). According to (Maciak, 2003), "Every economic activity of man is now inextricably linked with the production of waste. The ideal solution, impossible to apply on a larger scale neither now nor in the near future, is the use of waste-free technologies". Waste-free technology is based on full utilization of the raw material, thereby which waste is not generated. The development and implementation of such technology is generally difficult. It requires the involvement of, for example, many specialized scientific institutions and a significant financial contribution, which often goes beyond the capabilities of a single company (Rosik-Dulewska, 2015).

Industrial waste, generated in millions of tons per year, differs in composition and physicochemical properties, among other parameters. This depends on the branch of industry from which they originate. Waste can occur as relatively pure substances or as complex mixtures of varying composition, so industrial waste includes natural materials or such natural materials which were only anthropogenically transformed, as well as products hitherto unknown. They are generated in both liquid and solid form (Kozak, 2001; Maciak, 2003).

In the study, an attempt was made to analyze the regulations on the transport of pomace, two transport routes were selected from the Fruit Processing Plant in Nowy Sacz to the Mládežnícka waste disposal site in Slovakia The transport cost estimate was determined and the optimal transport route was selected, both in terms of regulations on the transport of hazardous materials, traffic regulations, relief, operation of motor vehicles and ecology. These issues are not addressed by the authors of the works (Ciuła, 2023; Kądziołka, 2021; Kowalski, 2021) no less, they can complement the present study especially in terms of the durability of motor vehicle assemblies and their impact on road safety.

2. Waste classification

The basis of any classification is provided by appropriately selected criteria. In the case of waste, a division reflecting the source of waste generation, waste properties, environmental harmfulness, usefulness and mass production is necessary (Rosik-Dulewska, 2015). There are many classifications of waste and one of them is the division according to the share of the organic fraction in the composition of waste.

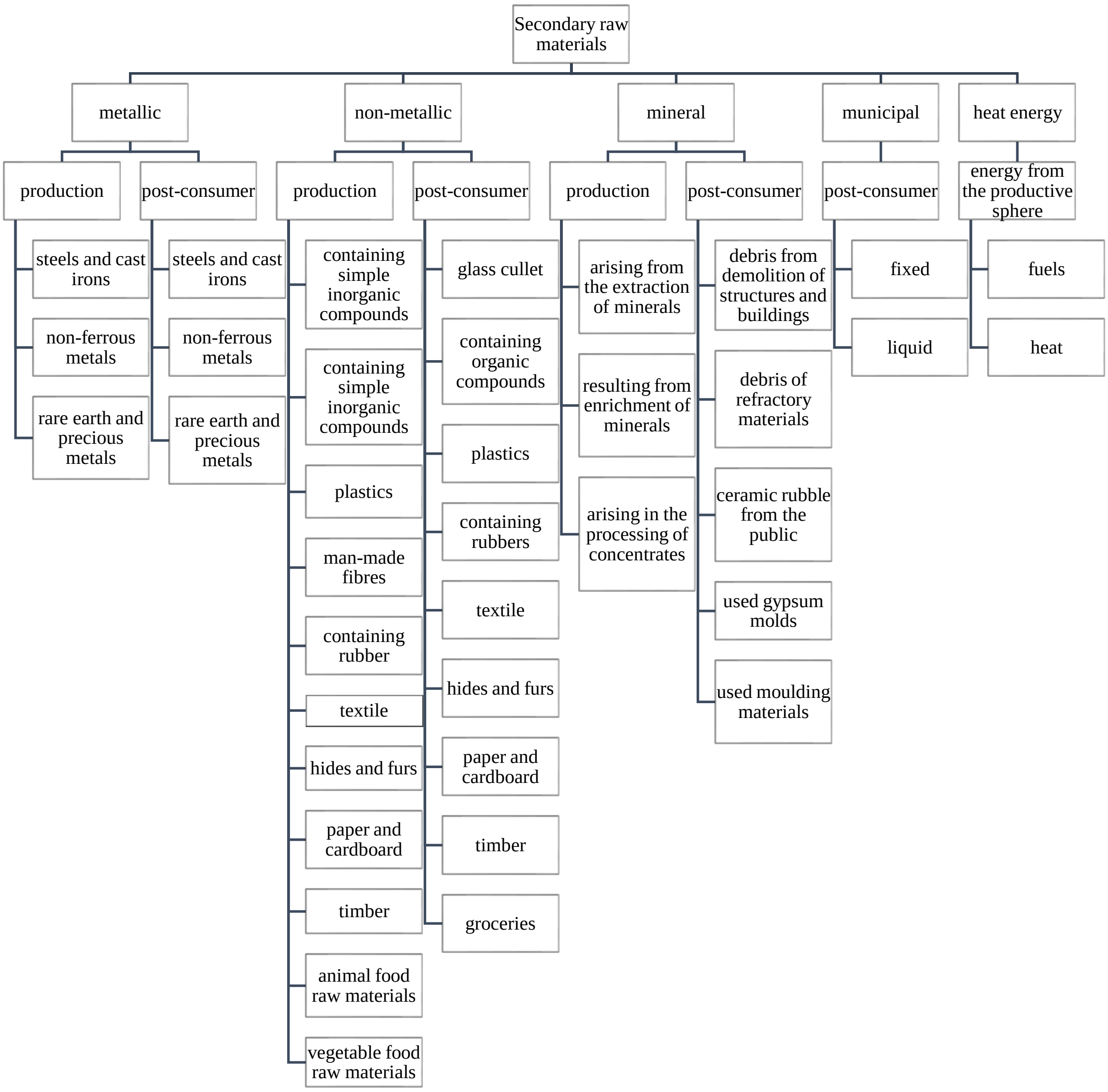

Figure 1. Division of secondary raw materials

(source: own study based on Rosik-Dulewska, 2015)

This division distinguishes the following waste (Figure 1):
- mineral (up to 1% of organic matter);
- organic – mineral (5-50% of organic matter);
- organic (the share of organic matter is more than 50%).

The sources of organic waste, containing more than 50% of organic matter (on a dry weight basis), include the agro-food and timber industries. Figure one shows the classification which has been in use since 1976.

It treats waste as secondary raw materials. This classification, based on a multilevel structure, using different criteria for the division of waste, distinguished 5 basic groups of waste:
- metallic;
- non-metallic;
- mineral;
- municipal;
- thermal energy.

The basis for the further division of waste is the place where waste comes into being. In the next stage, non-uniform criteria were adopted, for example the state of aggregation for municipal waste. This classification can be used as an overview in economic practice (Peng, 2023; Rosik-Dulewska, 2015).

3. Industrial waste in Poland

The largest share, that being 59%, in the amount of waste generated in 2020, was waste generated in the exploration, extraction and processing of ores and other minerals, which is called mining waste. In second place came waste from thermal processes with a share of 17%. Taking these data into account, the regions where the largest amount of industrial waste is generated are the Śląskie (Silesia) and Dolnośląskie (Lower Silesia) regions, since the mining industry is located there. The smallest amount is generated in Lubuskie and Podkarpackie regions. The share of each of these regions in the total amount of industrial waste generated is only 1% (Figure 2).

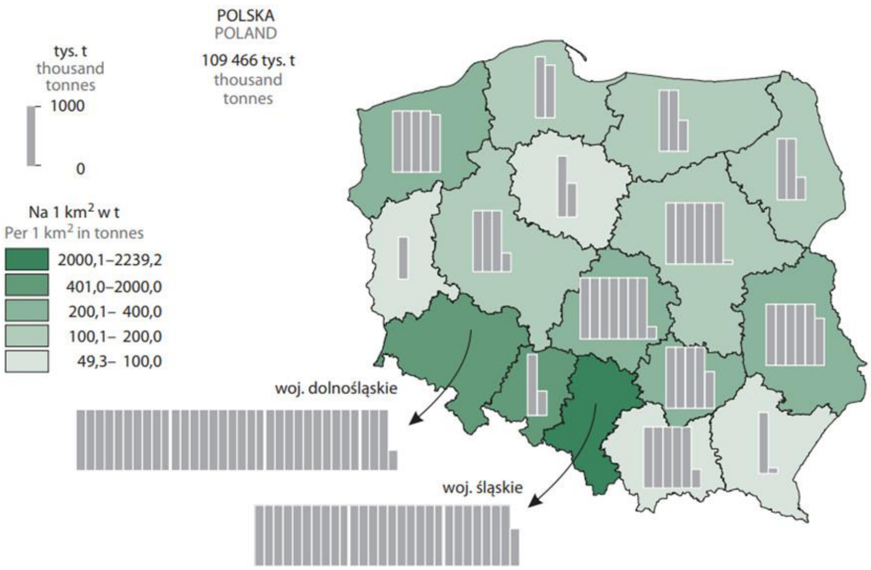

Figure 2. Waste generated (excluding municipal waste) by region in 2020

4. Waste treatment methods

Waste should be treated as a potential raw material after first being subjected to various recovery methods. Recovery is any process that aims to bring waste to such a state that it can replace a specific raw material for use in a particular production process. The disposal process can be treated as a manifestation of economic inefficiency, since it is a process that does not lead to the recovery of the waste (Ciuła, 2023). Disposal processes, in addition to landfilling, include treatment in soil and ground or post-landfill retention (accumulation of waste in lagoons or sediment plots) (Central Statistical Office Environmental Protection, 2022). A breakdown of recovery and disposal processes is shown in Figure 3.

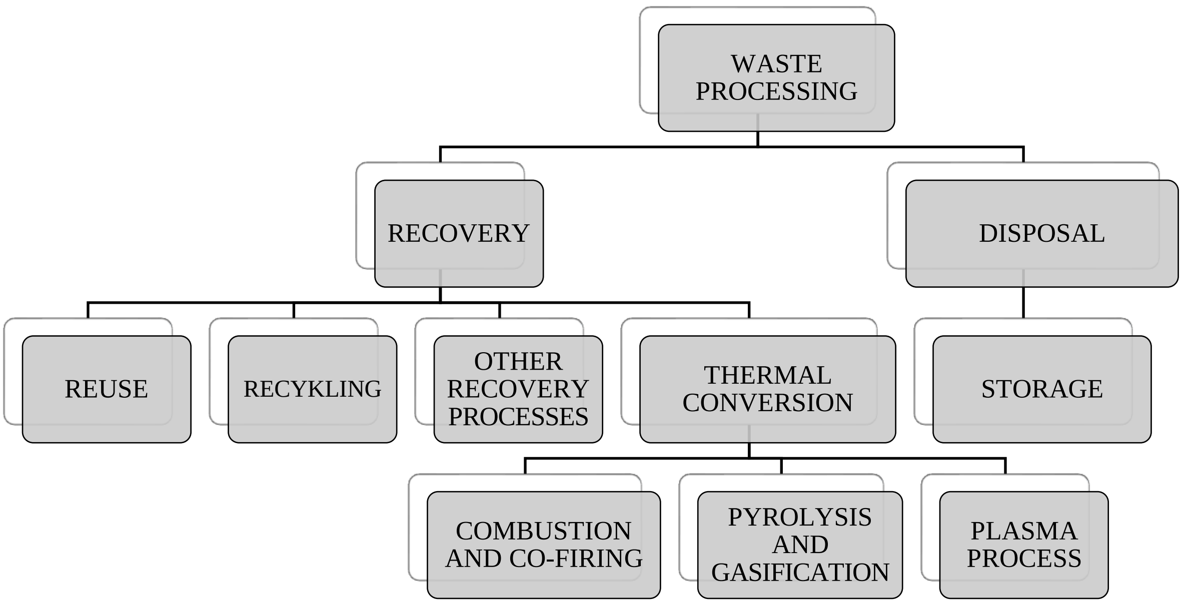

Figure 3. Waste management – the breakdown of waste processing

(source: own study based on Wieczorek, 2022)

In 2020, industrial processing contributed approximately 23 thousand Mg of waste. More than one half of that volume, some 16.5 thousand Mg, was recycled (one of the recovery processes). Almost 6 thousand Mg of waste generated in this industry sector was disposed of. The exact figures are shown in Table 1.

Table 1

Waste generated by industrial processing and its handling

	Waste generated during the year [Mg]					
			inactivated			
	total	recycled	total	of which the amount stored	temporarily stored	waste previously stored
Industrial processing	**23 123**	**16 418**	**5 909**	**3 332**	**517**	**282 500**

(source: own study based on Central Statistical Office Environmental Protection, 2022)

According to the principle of proximity of waste treatment, "...Waste, taking into account the hierarchy of waste treatment methods, shall first be treated at the place of its origin. Waste that cannot be processed at its place of origin shall be transferred, taking into account the hierarchy of the ways of handling waste and the best available technology referred to in Article 207 of the Environmental Protection Law Act of April 27, 2001, or the technology referred to in Article 143 of that Act, to the closest places where such waste can be processed..." (Act of Waste, 2013).

5. Waste storage

Waste storage refers to the temporary storage of waste. This storage includes:

- pre-storage by the waste generator;
- temporary storage by the waste collector;
- storage by the waste processor.

Under Article 25(1) of the Waste Act, "Storage of waste shall be carried out in accordance with the requirements for protection of the environment and safety of human life and health, in particular, in a manner that takes into account the chemical and physical properties of the waste, including its state of aggregation, and the hazards that the waste may cause, including in accordance with the requirements set forth in the regulations issued pursuant to paragraph 7" (Act of Waste, 2013). The basic principles of storage include:

1. The waste holder has legal title to the land where the waste is stored.
2. The storage of waste is carried out as part of waste generation, collection or processing – only in connection with these processes.
3. The storage of waste is allowed if the need for storage arises from organizational or technological processes, but may not exceed 3 years, and may not apply to waste intended for storage, which may be stored for a maximum of 1 year in order to collect a sufficient amount for transport to a landfill. The aforementioned storage periods are counted together, for each subsequent holder of such waste.
4. In some cases, a visual system of inspection of the waste storage or disposal site must be carried out (Act of Waste, 2013).

The requirements set forth in the regulations issued under paragraph 7 of Article 25 of the Waste Act are contained in the Regulation of the Minister of Climate, dated September 11, 2020. This regulation "specifies detailed requirements for waste storage, covering initial storage of waste by a waste generator, the temporary storage of waste by a waste collector, and the storage of waste by a waste processor" (Regulation on specific requirements for waste storage, 2020).

5.1. Specific requirements for the place and manner of waste storage

The place and method of storage depend primarily on the chemical and physical properties of waste, including the state of aggregation. The place where waste is kept should have a surface area adapted to the amount of waste generated in a certain period of time and the frequency at which the waste is received, while the method of storage is selected in such a way as to prevent the spread of waste beyond the designated storage area. In the storage process, special consideration should be given to the use of:

– packaging;
– bins;
– bags;
– tanks;
– containers.

Storage in piles and prisms is permitted, provided that it does not cause the pollution of surface and groundwater, soil and the ground (this applies, in particular, to waste generated from weather-resistant products).

More stringent regulations require that waste be stored on a surface paved with construction products, and that protection against unauthorized entry and the adverse effects of the weather should be used.

In the case of waste that may cause leaks or leachate escape from storage areas, protection in the form of sealed packaging, containers, tanks, etc., impermeable substrate with a drainage system for leaks and seals is used. Spills and wastewater generated at the storage site should be treated, for example, in oil separators (Regulation on specific requirements for waste storage, 2020).

5.2. Storage of hazardous waste

Hazardous waste shall be stored in a separate zone, where the storage of non--hazardous waste is also allowed. In the case of hazardous waste, the rules cited above shall apply, along with additional regulations concerning, for example, the marking of the storage zone for such waste. A sign with the words "HAZARDOUS WASTE" should be displayed at a conspicuous place. This sign should be weatherproof, durable and legible (Naeem, 2024; Regulation on specific requirements for waste storage, 2020).

Hazardous waste shall be placed in packages, containers, bins, tanks or bags. If their capacity exceeds 5 liters, each shall be marked with a label (Regulation on specific requirements for waste storage, 2020).

6. Pomace as industrial waste

The generation of pomace is related to the increase in the consumption of fruits and vegetables, and in particular the processed products extracted from them, i.e. purees, juices or jams. The food sector is the fifth largest generator of waste in Europe. After the processed fruit or vegetable production process based on the raw material, approximately 20% of the fruit and vegetable mass remains, which receives the status of waste and is called pomace. Fruit and vegetable processing begins at the time of delivery. Upon receipt, the raw material should be pre-washed and separated from rotten and defective fruits and vegetables and from other contaminants. This is followed by crushing, pressing, pasteurization, depectinization and filtration. The final stage is packaging of the finished product and pasteurization. During these processes, waste such as the following is generated:

– post-production wastewater;
– rotten and defective fruits;
– pomace (Jakubowski, 2006; Kozak, 2001, Magiera, 2006).

According to statistics kept by the Statistics Poland, more than 3 thousand tons of apples were allocated to the production of concentrated juice in Poland in the 2018/2019 season. Assuming that 20% of the raw material consumed was pomace, about 630 thousand Mg of it was generated. Depending on the processing method and variety of raw material, pomace may include fruit and vegetable peels, seeds or pulp residues. This is a material characterized primarily by low durability and stability. In addition, pomace is distinguished by high water content, which exposes the material to rapid growth of contamination (Pietrzyk-Sokulska, 2018; Tran, 2024).

Pomace belongs to perishable wastes, which can lead to the microbiological contamination of the enterprise and hinder the production process. Pomace should be utilized as soon as it is obtained and as long as it is fresh because its quality deteriorates over time and this leads to a change in the physical and chemical composition and to the reduction of pomace value and usefulness (Jakubowski, 2006; Zhang, 2023).

6.1. Example of pomace utilization

Pomace is waste because it is not used in a technological process. However, pomace can be properly utilized elsewhere (Jakubowski, 2006). Waste generated in fruit processing contains many valuable components, so it should be treated as a secondary raw material (Ciuła, 2023). Pomace as a secondary raw material is used in the food industry as an ingredient of confectionery products or as an additive to fruit infusions. Pomace can also be used to obtain dyes, oils and aromatic substances (Pietrzyk-Sokulska, 2018), which are used in many other industries, e.g. in the cosmetics industry various extracts obtained from pomace are used as cosmetic ingredients. In the textile industry, pomace is an alternative to animal skin (Wieczorek, 2022). In addition, pomace is among the types of waste that individuals or non-business entities can recover for their own use. The recovery process R1 or R3 is involved – pomace used as a fuel (Ciuła, 2023) or soil fertilizer. The acceptable maximum quantity to be received is the amount that can be utilized (Regulation on waste recovery by non-entrepreneurs, 2015; Tran, 2024).

6.2. Assigning the correct waste code to pomace

The waste code is an important part of the waste handling process. In order to assign the code correctly, it is first necessary to select the appropriate group from among 20 possible ones, taking into account the source of waste being classified (Dobroselskyi, 2019). Pomace is a waste generated during food processing, so it belongs to group 02 of the waste catalog – waste from agriculture, horticulture, hydroponics, fishing, forestry, hunting and food processing. In group 02 of the waste catalog, there are 7 subgroups including: waste from agriculture, horticulture, hydroponics, forestry, hunting and fishing (the subgroup code: 02 01); waste from preparation and processing of food products of animal origin (the subgroup code: 02 02); waste from the preparation, processing of food products and stimulants and waste of vegetable origin, including waste from fruit, vegetables, grain products, edible oils, cocoa, coffee, tea and tobacco preparation and processing, yeast and yeast extract production, molasses preparation and fermentation (the subgroup code: 02 03); wastes from the sugar industry (subgroup code: 02 04); waste from the dairy industry (the subgroup code: 02 05); waste from the baking and confectionery industry (the subgroup code: 02 06); waste from the production of alcoholic and non-alcoholic beverages (the subgroup code: 02 07). The subgroup to which pomace belongs is subgroup

02 03 – waste from preparation, processing of food products and stimulants, and waste of vegetable origin, including waste from fruit, vegetables, cereal products, edible oils, cocoa, coffee, tea, and preparation and processing of tobacco, yeast and production of yeast extracts, preparation and fermentation of molasses. The relevant group and subgroup enables the designation of final six-digit code 02 03 80 to pomace. The group comprises pomace, sludge and other waste from the processing of plant products (excluding waste from the production of plant feed).

7. Pomace storage

7.1. Characteristics of a food processing enterprise

The food processing company from which pomace will be transported is engaged in the production of jams, juices, purees, etc. from more than 30 kinds of fruits and vegetables. The company operates in Nowy Sącz in the Małopolska region, Poland. The company supplies products to local stores and confectionery plants located both throughout Poland and in other countries. Unfortunately, the production process generates a significant amount of waste in the form of pomace, and its utilization is no less important (Dobroselskyi, 2019).

The estimated amount of raw materials received daily on the production line is approximately 10 tons. For the purpose of the analysis, it was assumed that pomace accounts for 30% of the weight of the raw material, so approximately 3 Mg of pomace is generated daily. The waste transporter collects the waste once a week (Friday).

7.2. Pre-storage of pomace by its generator

Waste storage is regulated by the Waste Act of December 14, 2012 and the Regulation of the Minister of Climate of September 11, 2020 on detailed requirements for waste storage. A person who conducts waste storage must have the relevant permit. However, an exception is made for the initial storage of waste by the waste generator (Act of Waste, 2013). The company under analysis only stores pomace on a preliminary basis. Pomace is a biologically unstable plant matter. It is characterized by a high content of water and, for example, sugars, which promotes decay processes. The prolonged storage of fresh pomace is dangerous, as it poses the risk of biological contamination. The methods of preserving pomace include pickling and drying. These processes inhibit disadvantageous changes that reduce pomace quality. The food processing company presented in the article has a specially designated area where pomace is pre-stored until it is collected by a collection service provider. The area is a cold store, where low temperature is maintained to keep pomace in good condition until it is transported so that it does not rot or become moldy. Pomace is pre-stored in plastic bins with a capacity of 1 ton of the raw material.

8. General principles of waste transportation

Pursuant to Article 24 of the Waste Act of December 14, 2012, "The transportation of waste shall be carried out in accordance with the requirements for the protection of the environment and the safety of human life and health, in particular, in a manner that takes into account the chemical and physical properties of waste, including the state of aggregation, and the hazards that waste may cause, including in accordance with the requirements set forth in the regulations issued pursuant to paragraph 7" (Act of Waste, 2013). The requirements specified in the regulations issued pursuant to paragraph 7 of Article 24 of the Waste Act are contained in the Regulation of the Minister of the Environment of October 7, 2016 (Regulation on specific requirements for waste transport, 2016). The Regulation contains basic information on the means of transportation, including their correct marking and the method of waste transport. First of all, attention should be paid to:

1. Preventing the mixing of different types of waste;
   a. Care should be taken to ensure that the means of transport does not contain residues of previously transported waste.
   b. The exception is a situation where the mixed types of waste are dispatched in their entirety to be processed in the same process.
2. Preventing the spread of waste beyond the means of transportation;
   a. Reducing odor nuisance and waste spillage, dusting and leaks.
3. Preventing atmospheric factors from affecting the waste which, under the influence of those factors, can cause a hazard;
4. Preventing waste bins or bags from tipping over, by stacking or securing them properly in the means of transport, unless waste is transported in tanks or in bulk.

9. Transport of pomace

Transport of pomace will be described on the example of a local transport company based in Podrzecze, the commune of Podegrodzie. The company provides services in the field of truck transport by specialized vehicles. The company has been in business for almost 30 years. It is a partnership founded by two brothers. It also holds a permit for the collection of certain types of waste (Appendix 1) including waste with code 02 03 80 – pomace, sludge and other waste from the processing of plant products (excluding waste from the production of plant feed). The permit allows for the collection of waste from a given enterprise and allows for temporary waste storage (according to the guidelines specified in the permit) and subsequent waste transport to the place of processing. As of 2018, the company has operated the mandatory BDO (Waste Database) system, in which every activity of the company in relation to waste management is electronically documented. Currently, any entrepreneur transporting waste or carrying out waste transportation on behalf of another company is only registered in section VII of BDO – "VII Waste Transporters". It is not necessary to have a "paper permit" as is the case with the waste collection permit.

Waste transport is regulated by the Waste Act of December 14, 2012 and the Regulation of the Minister of the Environment of October 7, 2016 on detailed requirements for waste transport. If waste is dangerous, it is additionally subject to the Transportation of Dangerous Goods Act of August 19, 2011. However, it should be noted that not all hazardous waste will be a dangerous cargo.

The place for the processing of pomace collected from the food processing company is a biogas plant located in Slovakia (Kądziołka, 2021; Kowalski, 2021). Transportation will be carried out by the following means of transport Figure 4:

- MAN truck tractor (year of manufacture 2010, the EURO 5 standard),
- Semi-trailer – the ZASŁAW D-653 tipper truck (year of manufacture 2011, the open load-carrying body made of aluminum, sealed with continuous welding, and equipped with a tarpaulin. The permissible load capacity is 28,260 kg).

Figure 4. The pomace transport vehicle

The next step in preparing the means of transport is proper marking. The article outlines the cross-border shipment of waste, so a plate with the capital "A" in a prominent place is attached to the vehicle. The plate must be durable and weatherproof (Kądziołka, 2021; Kowalski, 2022, Wojnarowski, 2019).

The waste transfer process is presented in Table 2. The stages of the procedure in the BDO system are shown in Figure 5. The waste transfer card, or KPO for short, can be prepared in the system in advance, but not yet approved. The card will not be visible to other entities then. It should be kept in mind that before issuing the KPO by the holder/generator, the latter should communicate with the transporter/collector beforehand, since the information needed for issuing the KPO includes the registration number of the means of transport or the date and time of the start of the transport. At the time of approval, the-entities mentioned in the card, as well as state institutions such as the Department of Environmental Protection Inspection, have access to the card.

The approved waste transfer card permits the generation of the confirmation of the issuance of the waste transfer card, a document needed during transportation. The confirmation does not have to be printed, and holding an electronic version only is possible. Both the transferee (processor) of waste and the transporter must confirm the completion of processes in the BDO system. In this article, the recipient is a foreign company, so actions based on the waste transfer card will be taken only during the transfer of waste to the collector or during the transfer to the transferee using the services of a transport company (Jakubowski, 2009).

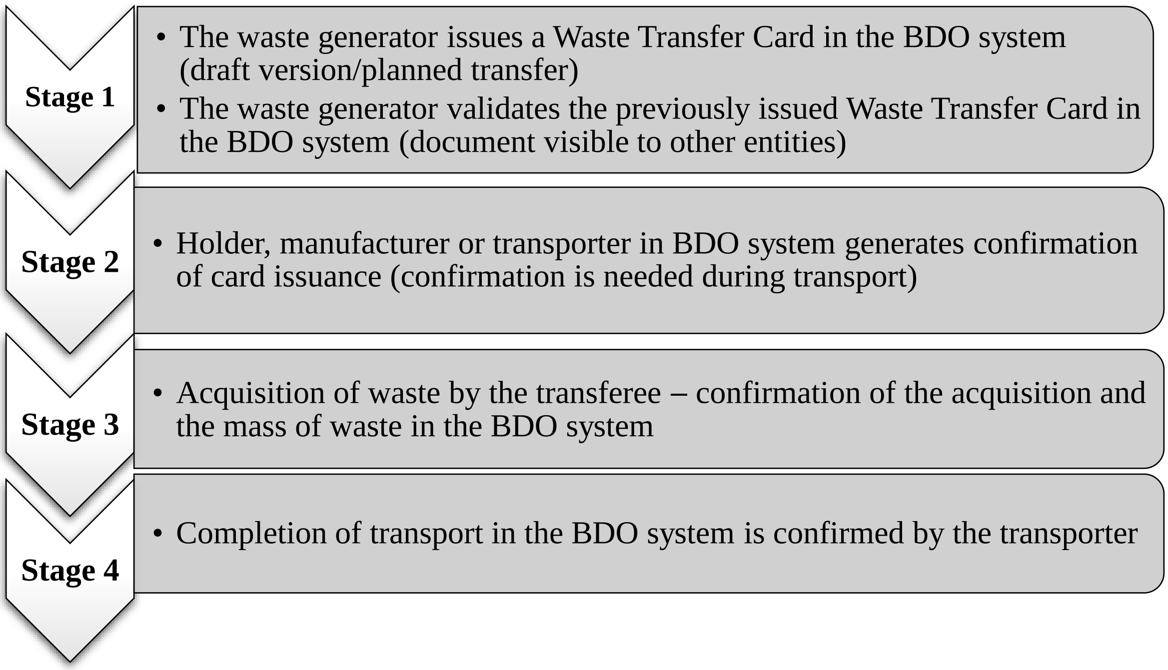

Figure 5. Steps in the waste transfer process

Table 2
Methods and conditions of waste transfer

	Method I **Transfer of waste by the transporter Company "Y"**	**Method II** **Transfer of waste by collector Company "X"**
Waste generator	Company "X" (POLAND)	
Quantity of waste	approx. 20 Mg of pomace	
Waste processor	Company "Z" (SLOVAKIA)	
Type of transport	**ROAD TRANSPORT – INTERNATIONAL**	
Responsibilities of the parties	**The party ordering the transportation** service is obliged to indicate the destination of the waste and the holder to whom waste is to be delivered. That party ceases to be the holder of the waste only at the moment of handing it over to the processor. **The transporter** is obliged to deliver the waste to its destination, but never becomes the holder of the waste. The transporter only keeps simplified records.	**The waste generator** transfers waste on the basis of the waste transfer card to the waste collector. The waste generator keeps records on the basis of the waste transfer card. **The collector of waste** becomes the waste holder and bears full responsibility and records waste. Based on the international bill of lading and Annex VII, the collector transfers waste to the processor
Waste transfer documentation prepared in the BDO system	NONE	**(Generator – Collector)** Waste Transfer Card
Waste transfer documentation prepared outside the BDO system	**(Generator – Processor)** International bill of lading Annex VII	**(Collector – Processor)** International bill of lading (Annex 2) Annex VII
Records	The generator keeps records only on the basis of the waste record card – general rules apply.	The generator keeps full records. The collector only on the basis of the waste record card.

10. Alternative pomace transport routes

10.1. Alternative 1 – Transport from Nowy Sacz to the waste processing site in Slovakia

When analyzing the route determined with the help of Google Maps, it should be concluded that the fastest transport route will be the shortest route of approximately 275 km (Figure 6). The transport time, depending on the traffic volume, will be approximately 4 to 5 hours. Assuming that the average fuel consumption of a MAN truck tractor is 45 l/100 km and the price of 1 liter of diesel fuel is PLN 6.50, the cost of the fuel consumed by the pomace transport vehicle was determined, which in the analyzed alternative amounted to PLN 805 (Kowalski, 2022; Zhang, 2023).

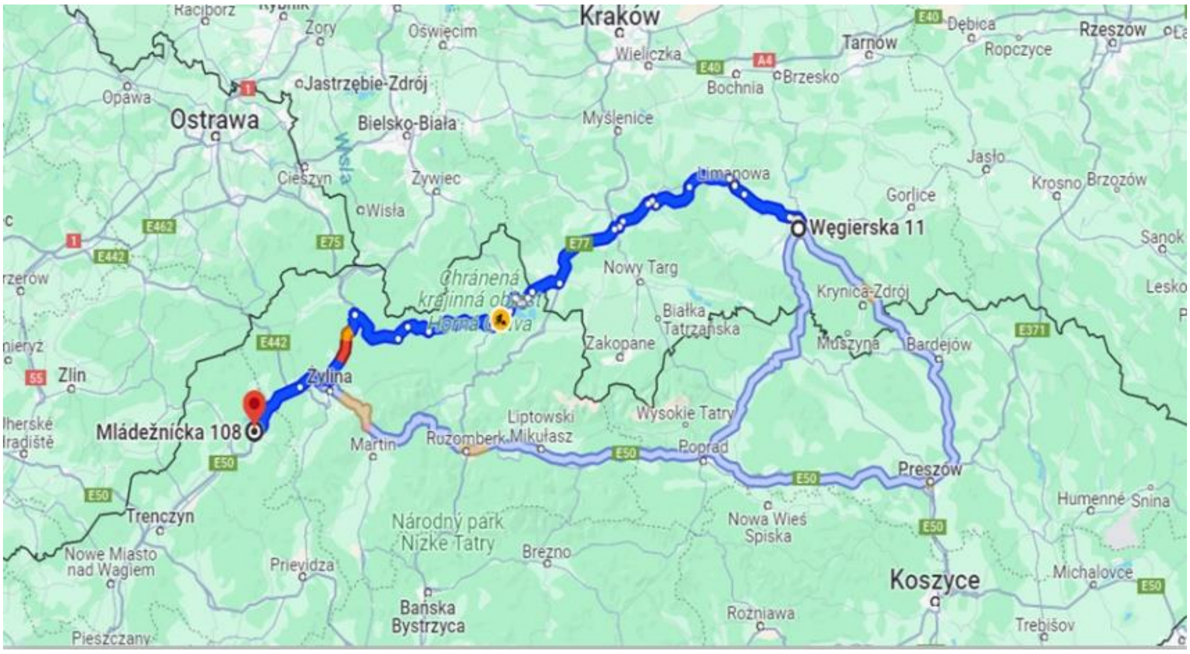

Figure 6. The waste transport route from the food processing company in Nowy Sącz to the waste processing site in Slovakia

10.2. Alternative 2 – Transport from Nowy Sącz to Podrzecze (waste receipt at the collector's warehouse), then transport from Podrzecze to the waste processing site in Slovakia

In alternative 2, pomace will be transported from the Fruit and Vegetable Production Company of Nowy Sącz to Podrzecze by smaller vehicles (in smaller transport batches), where pomace will be received into the carrier's warehouse. Once pomace has been collected in an amount that ensures the optimal use of the cargo space, pomace will be transported from Podrzecze to Slovakia for processing (Figure 7).

In this alternative, the distance is approximately 300 km, while the transport time will depend on traffic and will be, as in alternative 1, from 4 to 5 hours. The cost of fuel for alternative 2 was also determined, which amounted to PLN 880. An important aspect for the transportation of dangerous goods is the effect of road surface condition on the wear and tear of vehicle components. This problem, the aspect of protecting vehicle components from damage, and ways to increase the durability of automotive vehicle assemblies are discussed in detail in the articles (Kądziołka, 2021; Kowalski, 2021; Kowalski, 2022; Wojnarowski, 2019).

The disadvantage of this solution is the need for the carrier to have a warehouse in which waste can be stored. There will also be the cost of fuel and the salary of the driver, who, with a smaller vehicle, will collect pomace from the producer and transport that waste to the transport company's warehouse (WANG, 2023).

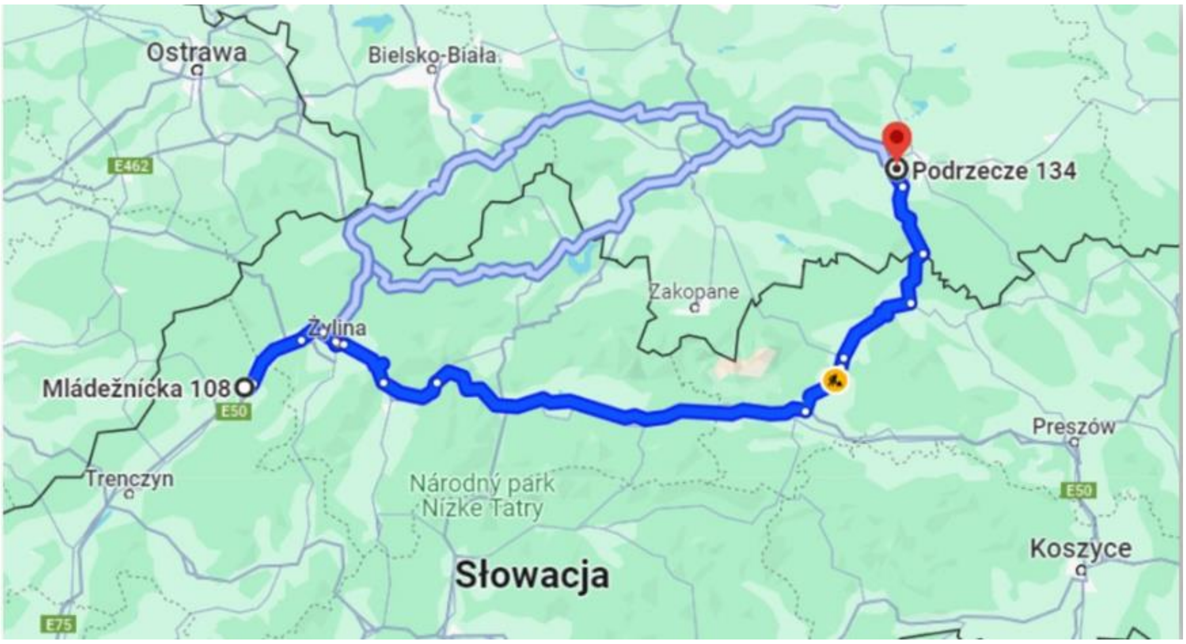

Figure 7. The waste transport route from the waste collection company in Podrzecze to the waste processing site in Slovakia

11. Conclusions

In the present study, the waste transporter carries waste from the place of its generation to the place of processing, i.e. from Nowy Sącz (Poland) to Mládežnicka (Slovakia). As the place of pomace processing is the biogas plant located in Slovakia, international transport is involved. The transport company must be registered in Section VII of the Waste Database (BDO) in order to transport non-hazardous waste. The entity responsible for the waste during transport is the waste holder, in this case the waste generator.

The documents required for transport are the confirmation of the generation of the waste transfer card (the paper version of the document is not necessary), Annex VII and the international waybill. In order for a company to be a waste collector i.e. also to receive waste into the company’s warehouse, the company must hold a decision on waste collection. If pomace is received by the waste collector, the responsibility for waste management passes to the collector and rests on it until waste is transferred to the processor.

The waste transfer process in the BDO system is fast and efficient. Documentation prepared in the system can have a working version, which is needed at a later stage and can be approved, which means that the physical transfer of waste, the start or end of waste transport also takes place. The records are visible to the relevant services, including the Environmental Inspection Department. The waste records maintained in the system make it possible to compile the relevant static data of the enterprise, both for the entity itself and the state. As the obligations of the waste generator, collector, transporter and processor, are specified in the laws and regulations on waste management, these entities perform those obligations taking into account the safety of the environment as well as human health and life. Waste has more or less harmful properties, and its proper identification and classification are key elements in waste management. If any doubts arise as to whether the activities pose a hazard, documentation made at each stage of waste management, allows the relevant services to react (Tran, 2024; Wang, 2023; Zhang, 2023).

Analyzing the route variants in question, it should be noted that the choice of their variant depends on the driver. Although route 2 is longer than route 1 by about 25 kilometers, nevertheless, this does not represent a drastic increase in fuel costs – PLN 75. It is worthwhile before setting out on the road for the driver to assess traffic congestion using Google Maps and choose an appropriate route. This can save time and fuel.

References

Act of 14 December 2012 on waste. *(The Journal of Laws of the Republic of Poland 2013, item 21).*

Act of 29 June 2007 on international shipments of waste. *(The Journal of Laws of the Republic of Poland 2007, no. 124, item 859).*

Akram, H., Butt, T.E. (2022). WET nexus between the three sectors – waste to energy for transport. *Journal of Cleaner Production, 339,* 130545. DOI: https://doi.org/10.1016/j.jclepro.2022.130545.

Anser, M.K., Yousaf, Z., Hishan, S.S., Nassani, A.A., Sheikh, A.Z., Vo, X.V., Zaman, K., Abro, M.M.Q. (2020). Dynamic linkages between transportation, waste management, and carbon pricing: Evidence from the Arab World. *Journal of Cleaner Production, 269*. DOI: https://doi.org/10.1016/j.jclepro.2020.122151.

Central Statistical Office. (2022). *Environmental Protection*.

Ciuła, J., Kowalski, S., Wiewiórska, I. (2023). Pollution Indicator of a Megawatt Hour Produced in Cogeneration – the Efficiency of Biogas Purification Process as an Energy Source for Wastewater Treatment Plants. *Journal of Ecological Engineering, 24*(3), 232-245. DOI: https://doi.org/10.12911/22998993/158562.

Dobroselskyi, M., Madleňák, R. (2019). Model of waste transportation management in the conditions of a production company. *Transportation Research Procedia, 40,* 1023-1029. DOI: https://doi.org/10.1016/j.trpro.2019.07.143.

Feng, J., Xu, S. X., Xu, G., Cheng, H. (2022). An integrated decision-making method for locating parking centers of recyclable waste transportation vehicles. *Transportation Research Part E: Logistics and Transportation Review,* 157, 102569. DOI: https://doi.org/10.1016/j.tre.2021.102569.

Jakubowski, T. (2006). Waste management at the fruit product manufacturing plant. *Inżynieria Rolnicza, 11,* 147-156.

Jia, D., Shen, Z., Li, X., Lv, X. (2023). Bi-level scheduling model for a novel virtual power plant incorporating waste incineration power plant and electric waste truck considering waste transportation strategy. *Energy Conversion and Management, 298,* 117773. DOI: https://doi.org/10.1016/j.enconman.2023.117773.

Kądziołka, T., Opoka, K. (2021). Forecasting the number of failures of the steering system components with the use of the grey system theory method. *Scientific Journal of Silesian University of Technology. Series Transport, 112,* 85-97. DOI: https://doi.org/10.20858/sjsutst.2021.112.7.

Kowalski, S. (2021). Influence of diamond-like carbon coatings on the wear of the press joint components. *Wear, 486-487,* 204076. DOI: https://doi.org/10.1016/j.wear.2021.204076.

Kowalski, S., Opoka, K., Ciuła, J. (2022). Analysis of the end-of-life the front suspension beam of a vehicle. *Eksploatacja i Niezawodność, 24*(3), 446-454. DOI: https://doi.org/10.17531/ein.2022.3.6.

Kozak, D., Chmiel, B., Niećko, J. (2001). *Environmental protection. Textbook for field exercises. Chemical aspects of environmental protection*. Lublin: Wydawnictwo Uniwersytetu Marii Curie-Skłodowskiej.

Maciak, F. (2003). *Environmental protection and remediation*. Warszawa: Wydawnictwo Szkoły Głównej Gospodarstwa Wiejskiego.

Magiera, J. (2006). *Re-refining of used oils*. Warszawa: Wydawnictwa Naukowo-Techniczne.

Naeem, M., Asam, Z.Z. (2024). Contaminant transport from solid waste dumps: Implications for environmental degradation with a focus on capital territory regions. *Environmental Research, 247*, 118152. DOI: https://doi.org/10.1016/j.envres.2024.118152.

Peng, H., An, C., Ng, K.T.W., Hao, J., Tian, X. (2023). Advancing cleaner municipal waste transport through carbon accounting in the cap-and-trade system. *Transportation Research Part D: Transport and Environment, 114,* 103560. DOI: https://doi.org/10.1016/j.trd.2022.103560.

Pietrzyk-Sokulska, E., Radwanek-Bąk, B., Kulczycka, J. (2018). Secondary mineral resources – problems of nomenclature and classification in connection with the implementation of the circular economy. *Przegląd Geologiczny, 66*(3), 160-165.

Regulation (EC) No 1013/2006 of the European Parliament and of the Council of 14 June 2006 on shipments of waste. *(OJ L 190, 12.7.2006).*

Regulation of the Minister of Climate of 2 January 2020 on the catalogue of waste. *(Journal of Laws 2020, item 10).*

Regulation of the Minister of Climate of 11 September 2020 on specific requirements for waste storage. *(Journal of Laws 2020, item 1742).*

Regulation of the Minister of the Environment of 7 October 2016 on specific requirements for waste transport. *(Journal of Laws 2016, item 1742).*

Regulation of the Minister of the Environment of 10 November 2015 on the list of types of waste that natural persons or organisational units that are not entrepreneurs may subject to recovery for their own purposes, and the permissible methods of their recovery. *(Journal of Laws 2016, item 93).*

Rosik-Dulewska, C. (2015). *Fundamentals of waste management*. Warszawa: Wydawnictwo Naukowe PWN.

Tran, T.H., Ngyuen, T.B.T., Le, H.S.T., Phung, D.C. (2024). Formulation and solution technique for agricultural waste collection and transport network design. *European Journal of Operational Research, 313*(3), 1152-1169. DOI: https://doi.org/10.1016/j.ejor.2023.08.052.

Wang, H., Yi, W. (2023). *A Stackelberg game model for construction waste transportation. Advanced Engineering Informatics, 56*, 101991. DOI: https://doi.org/10.1016/j.aei.2023.101991.

Wieczorek, A., Siekierski, M. (2022). Waste management. Medical Waste. *Mazowsze Studia Regionalne, 40,* 9-26. DOI: https://doi.org/10.21858/msr.40.01.

Wieczorek, A., Siekierski, M. (2021). Waste Management. Waste processing installations and facilities. *Mazowsze Studia Regionalne, 36,* 31-44. https://doi.org/10.21858/MSR.36.02.

Wojnarowski, J., Drewniak, J., Kądziołka, T., Kopeć, J., Stańco, K., Zawiślak, S. (2019). Application of Contour Equations to Kinematic Analysis of Complex and Compound Planetary Gears. *Mechanisms and Machine Science, 73,* 987-996. DOI: https://doi.org/10.1007/978-3-030-20131-9_98.

Zhang, L., Liu, Z., Shan, W., Yu, B. (2023). A stabilized branch-and-price-and-cut algorithm for the waste transportation problem with split transportation. *Computers & Industrial Engineering, 178*, 109143. DOI: https://doi.org/10.1016/j.cie.2023.109143.

Andrzej RYNIEWICZ[1]

[1] University of Applied Sciences in Nowy Sącz, Faculty of Engineering Sciences, Zamenhofa 1a, 33-300 Nowy Sącz, e-mail: aryniewicz@ans-ns.edu.pl

Assessment of shape reproduction in computed tomography using reference spheres

Abstract

The aim of this study was to evaluate the accuracy of shape reproduction in computed tomography using reference spheres. Measurements were carried out with Siemens Somatom Sensation 64 and Werth Tomo Scope Compact scanners, with data analyzed in the Amira system. The workflow included segmentation, interpolation, surface smoothing, and tetrahedral mesh generation. Diameter measurements revealed the influence of imaging parameters and object positioning on accuracy. The results confirm the usefulness of computed tomography as a control and measurement tool in both medicine and industry, enabling non-invasive assessment of complex geometries and comparison with CAD models.

Keywords: computed tomography, shape reproduction, reference spheres, 3D metrology, geometric analysis.

Ocena odwzorowania kształtu w tomografii komputerowej z zastosowaniem kul wzorcowych

Streszczenie

Celem pracy była ocena dokładności odwzorowania kształtu w tomografii komputerowej z wykorzystaniem kul wzorcowych. Badania przeprowadzono na skanerach Siemens Somatom Sensation 64 oraz Werth Tomo Scope Compact, a dane analizowano w systemie Amira. Proces obejmował segmentację, interpolację, wygładzanie powierzchni i generowanie siatek tetrahedralnych. Pomiary średnic kul wykazały wpływ parametrów obrazowania i pozycjonowania obiektu na uzyskiwaną dokładność. Uzyskane wyniki potwierdzają przydatność tomografii komputerowej jako narzędzia kontrolno-pomiarowego w medycynie i przemyśle, umożliwiającego nieinwazyjną ocenę geometrii złożonych elementów i porównanie ich z modelami CAD.

Słowa kluczowe: tomografia komputerowa, odwzorowanie kształtu, kule wzorcowe, metrologia 3D, analiza geometryczna.

1. Introduction

A Computed tomography (CT) scanner is different from standard measuring devices in that, in addition to the external dimensions and shape of the object being examined, it allows for analysis of the object's internal structure (Ketcham, Mote, 2019). Tomographs can be used both in industry to assess the quality of examined objects – their geometry or internal structures – without destroying them, and in medicine to analyze internal organs (Liu et al., 2024).

The problem of assessing the accuracy of element mapping is extremely important and has fascinated scientists in various fields for years (Busch, Hausotte, 2024; Blažek et al., 2019). The latest spiral computed tomography (SCT) imaging techniques partially solve this problem, but determining 3D geometry still poses many challenges (Zemek et al., 2025). STC techniques do not allow for the simultaneous determination of the geometry of the structures of the objects under examination throughout the entire examination space with a certain degree of uncertainty (Bircher et al., 2021).

Ensuring that the shape of the examined surfaces is reproduced with sufficient accuracy (on a macro and micro scale) will allow for the assessment of the quality of parts in industry or medicine, the assessment of the condition of the examined organ, and a sufficiently rapid response to any changes that have occurred, which will contribute to the introduction of appropriate changes in the technological process or the making of an appropriate diagnosis (Stolfi, De Chiffre, Carmignato, 2016; Scherberich et al., 2025).

Figure 1. Ball patterns

(source: own study)

The first stage involved testing reference spheres (Figure 1) using Siemens Somatom Sensation 64 and Werth Messtechnik Tomo Scope Compact computed tomography scanners. The next step was to generate the surfaces of these elements in a 3D system and measure the dimensions of the spheres using Amira software.

Amira is a system used for 3D modeling and visualization. It allows for the visualization of scientific applications in various fields such as engineering, medicine, biology, chemistry, physics, and others. 3D objects can be represented as a mesh used for numerical simulations.

Using tomographs and analysis software, the diameters of the reference spheres were imaged and measured in two perpendicular planes (10 times each) for the following elements:

- reference sphere marked as Phantom 1 with a nominal diameter of Ø = 25.7 [mm];
- reference ball marked as Phantom 2 with a nominal diameter of Ø = 25.0 [mm];
- reference ball marked as Phantom 3 with a nominal diameter of Ø = 26.4 [mm].

2. Launch the Amira application

After launching the application, the main program window appears (Figure 2).

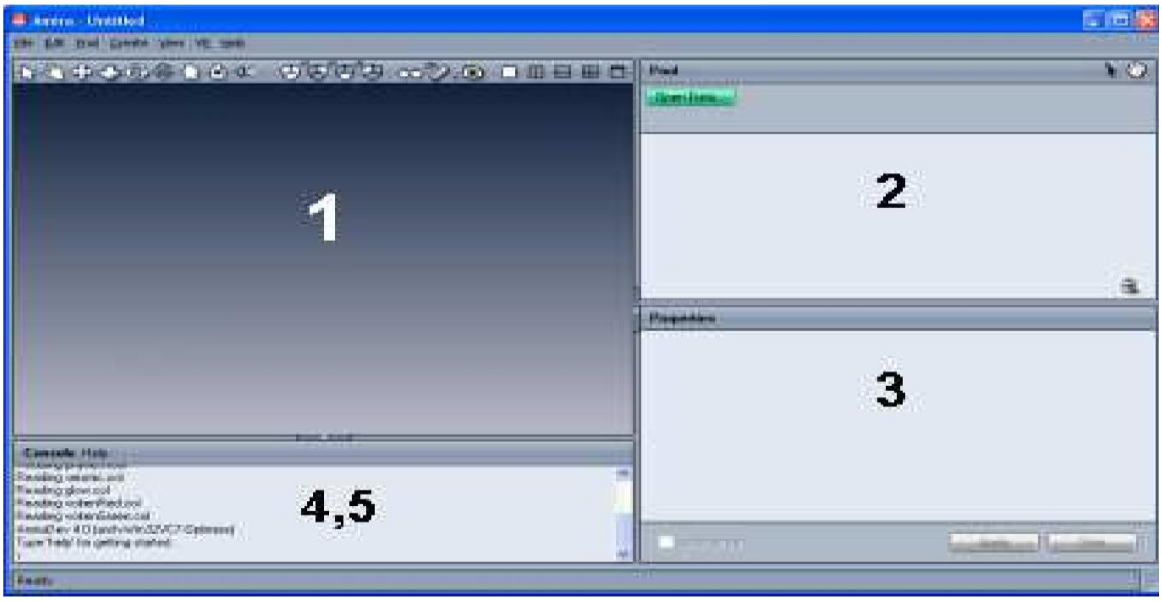

Figure 2. The application interface is divided into four-dimensional windows for visualization: (1) modular window, properties window (2), operations window (3), console window (4), and help window (5).

(source: own study)

3. Loading data received from computed tomography scanners

Data can be loaded in several ways (e.g., from File) and then on Open Data. After searching for the appropriate files obtained from tomographic diagnosis, they were loaded into the program.

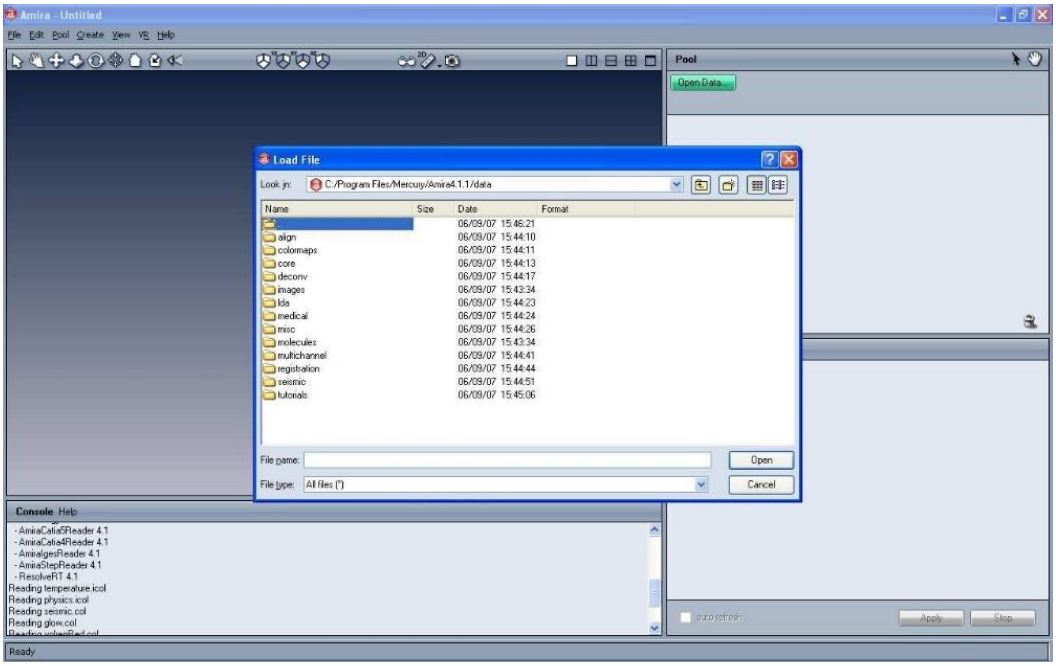

Figure 3. Loading data

(source: own study)

The loaded data appears in the module window as green icons with the .am extension (Figure 3). Each icon is a collection of related data from the tomograph. Clicking on an icon displays information in its properties window, such as the size or coordinates of the data (Figure 4).

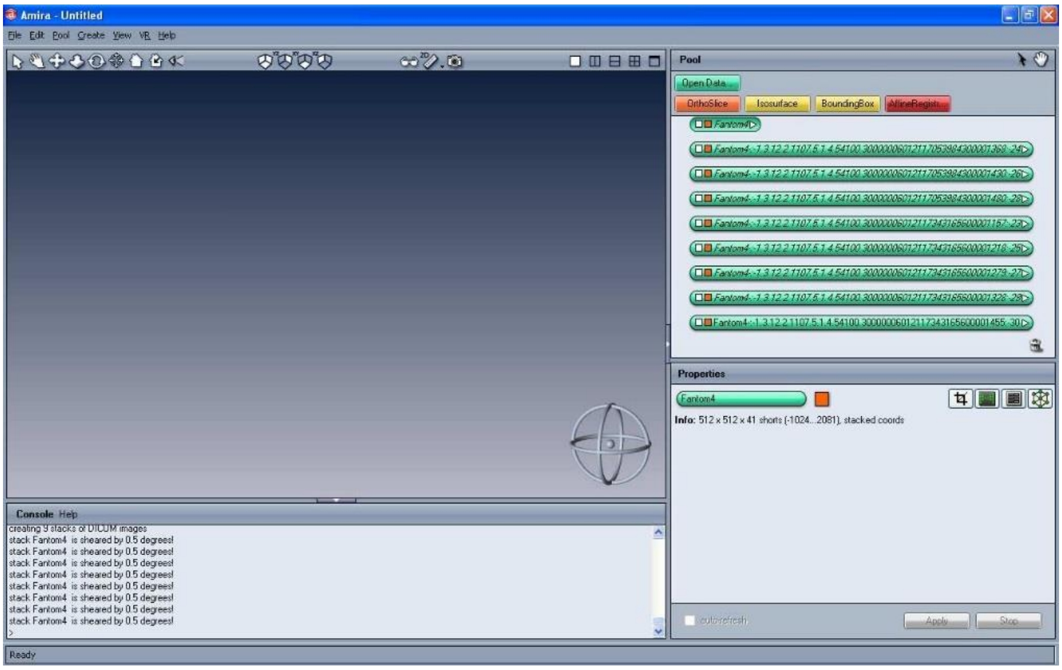

Figure 4. The data is represented as green icons

(source: own study)

4. Data visualization

Object data can be visualized by attaching display modules represented by the color yellow. Clicking on the icon displays a menu from which we can choose several visualization methods, e.g., displaying isosurfaces.

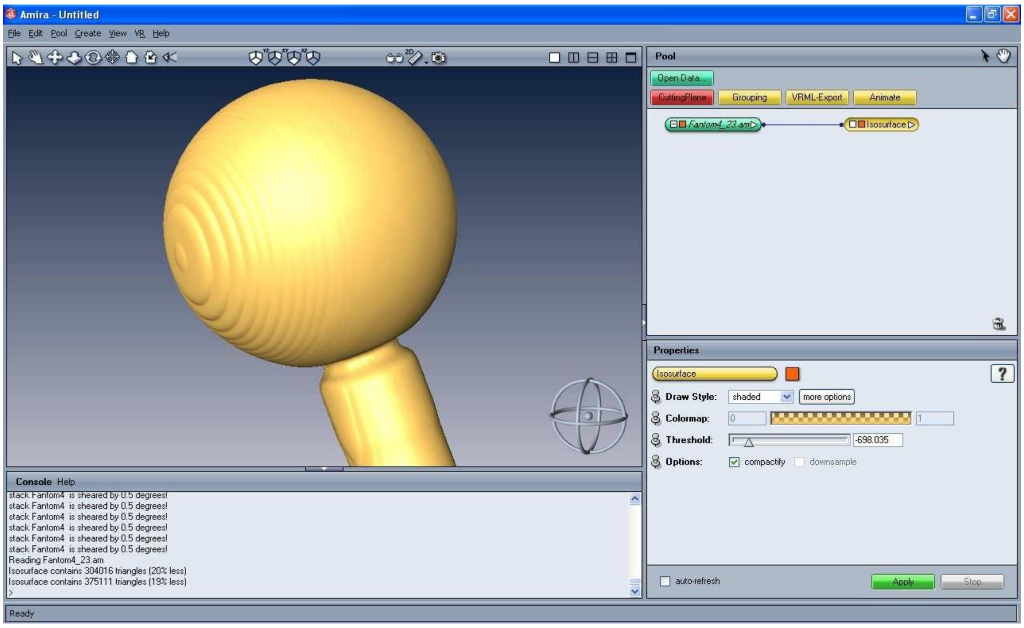

Figure 5. Isosurface generated for a sample Fantom 3 reference sphere

(source: own study)

As can be seen in Figure 5, the generated surface is not perfectly spherical. Methods for smoothing the surface will be presented later, but such actions should always be analyzed.

In the window displaying the surface, we can view the object from every side using, for example, the navigation compass located in the lower right corner of the window.

The first step to fully reflect the object under study is to perform 3D image segmentation. Segmentation assigns each pixel of the image a layer describing which area or material the pixel belongs to. This can be done with the Labelling function and then LabelField or LabelVoxel. The LabelField module allows us to perform manual segmentation using various types of tools, while the LabelVoxel module performs automatic segmentation using information stored in the tomograph data. Figure 6 shows the effect of automatic segmentation.

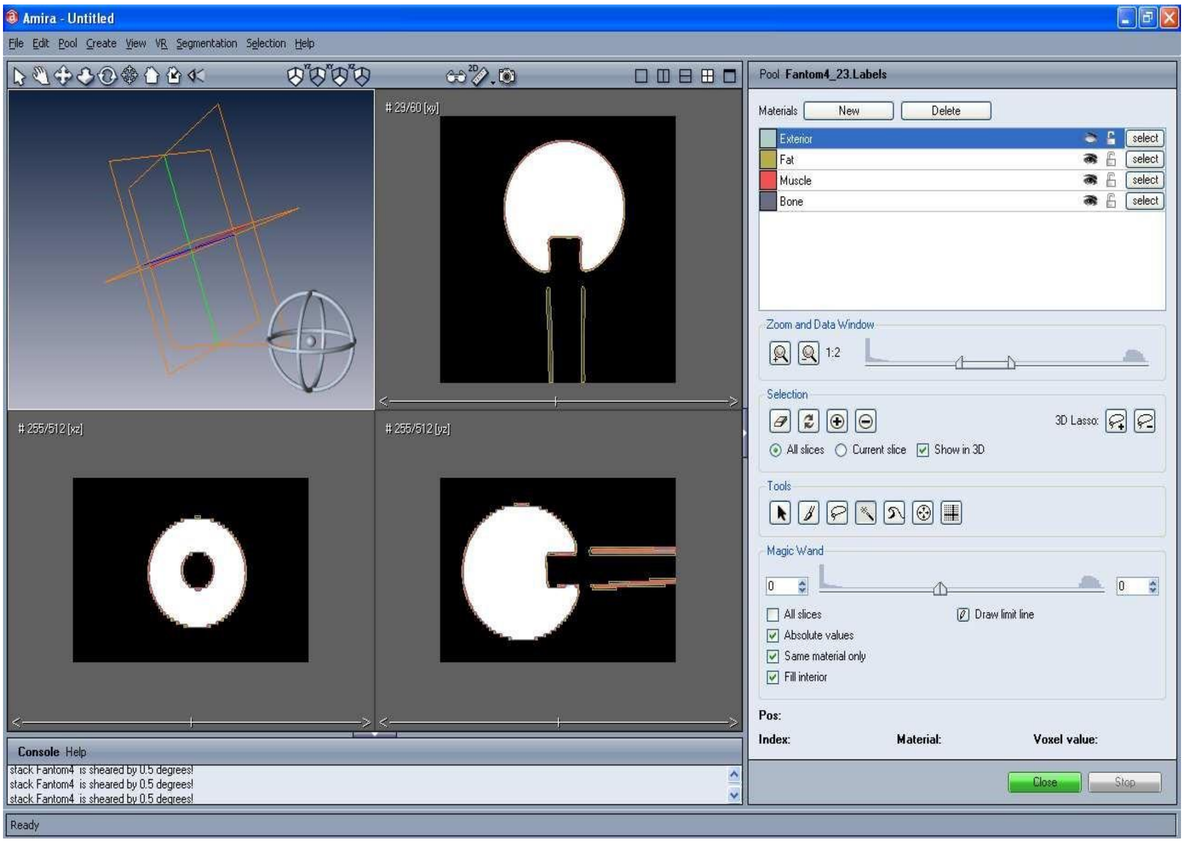

Figure 6. Result of automatic segmentation

(source: own study)

During segmentation, we can clean up the image, e.g., by removing pixels not assigned to layers, known as islands (Remove Island option), and smoothing layers (Figure 6).

It is possible to reduce the so-called staircase effect occurring on the surface of an element. We perform this operation by attaching the InterpolateLabels calculation module to the icon created after segmentation. This module inserts additional "slices" between the base "slices". The program sets the recommended distance between the "slices" and allows you to select the layer for which the interpolation is to be performed (Figure 7).

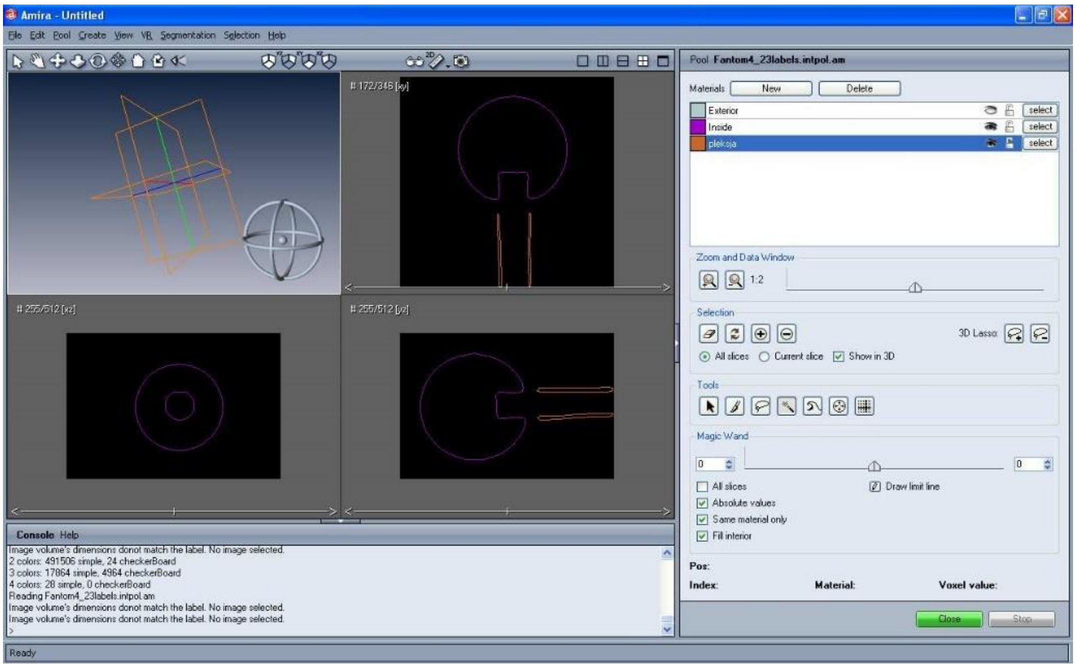

Figure 7. View of layers after interpolation

(source: own study)

The next step is to generate a surface using the SurfaceGen module connected to the icon created after interpolation. After launching, the program performs calculations and creates a surface from the layers created during segmentation. Figure 8 shows the created surface displayed thanks to the connected SurfaceView module.

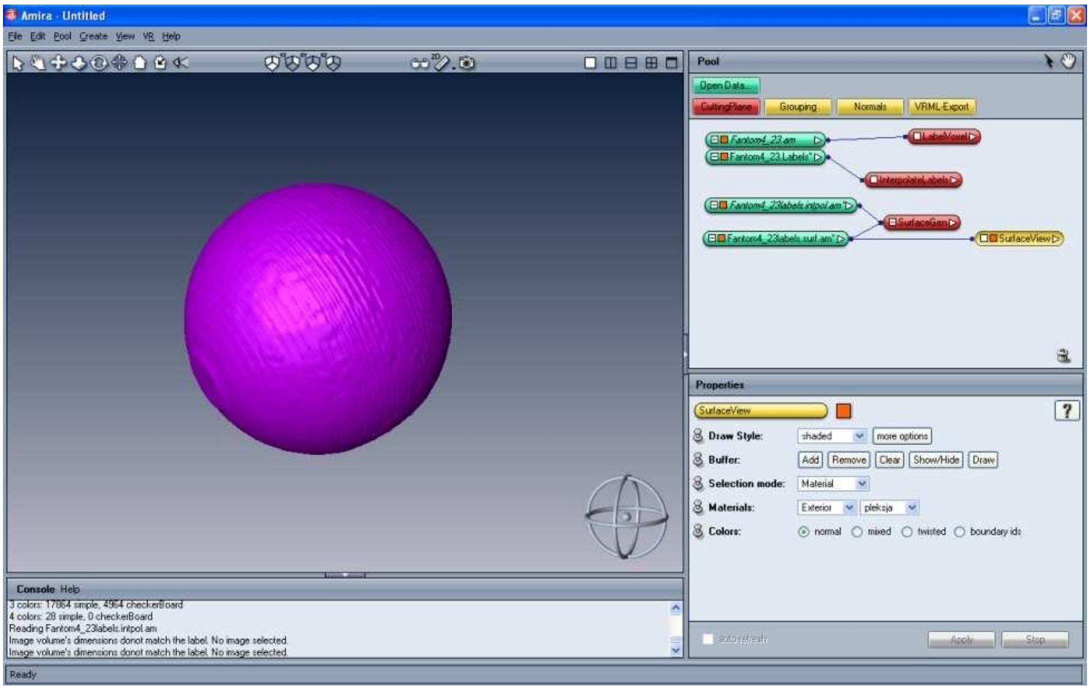

Figure 8. Generated surface after segmentation and interpolation

(source: own study)

In the SurfaceView properties, we can specify what surface is to be displayed and how, e.g., a point cloud or a transparent view.

Figure 8 shows that the surface of the sphere is not yet smooth. To change this, we can use the SmoothSurface module, but first we can simplify the surface, as the created surface may have too many triangles for further operations. The Simplifier editor in the Properties window is used for simplification. After setting the number of triangles, click the Simplify now button and wait for the program to finish simplifying. Figure 9 shows the effect of modifying the surface with a visible triangle mesh.

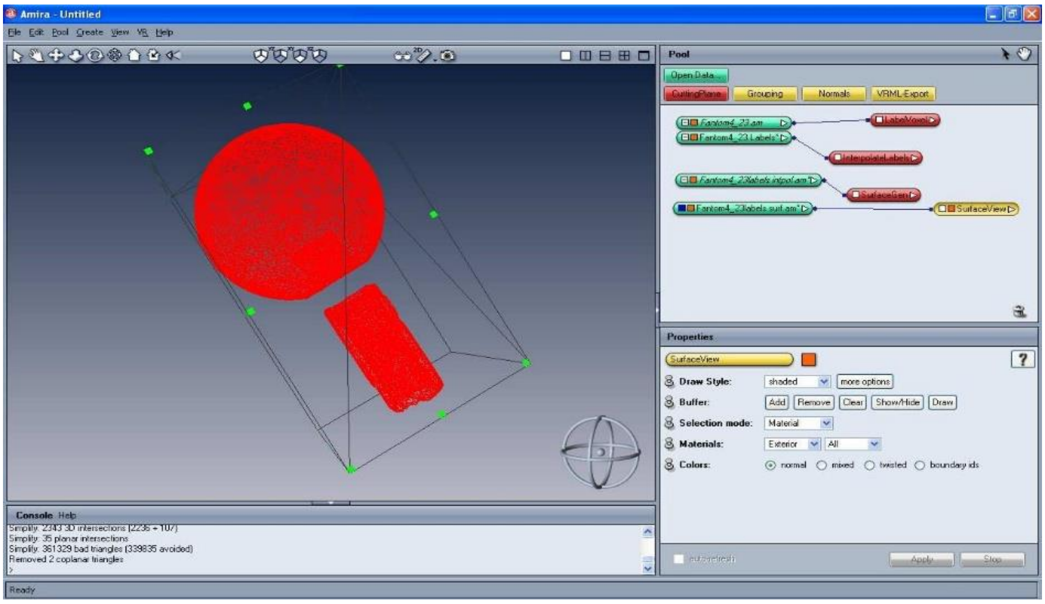

Figure 9. A mesh composed of triangles after simplifying the surface

(source: own study)

After this transformation, we can smooth the surface if necessary. In the SmoothSurface module properties, we set the number of iterations. Figure 10 shows the result of the algorithm.

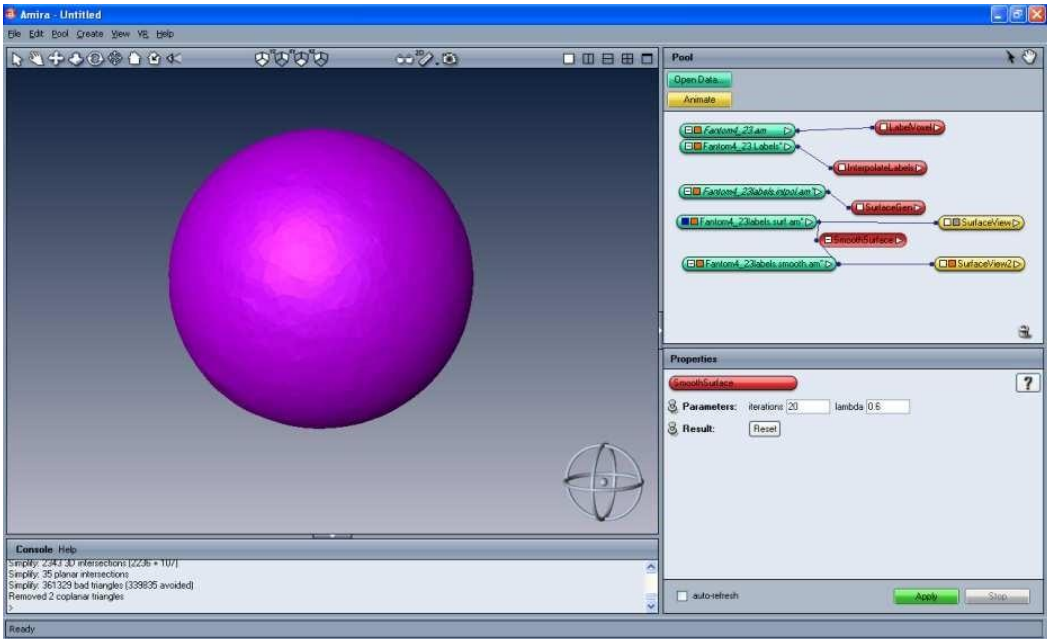

Figure 8. View of the generated surface of the reference sphere after smoothing

(source: own study)

Computer operations that modify the shape of the object under examination introduce specific geometric changes and may also introduce dimensional changes in relation to the actual object. The magnitude of these changes should be analyzed, especially in relation to metrological activities.

5. Generating a tetrahedral mesh

To begin working on creating a tetrahedral mesh, you need a surface composed of triangles. This surface is the result of a previous reconstruction. In this example, it is Fantom3labels.smooth.surf. The surface to be converted into a tetrahedral mesh must meet several requirements, e.g., it must be a closed surface. To check this, we use the Surface Editor located in the properties window. The menu of this editor allows you to perform six tests useful for preparing a tetrahedral mesh. In this work, three tests were used: the Intersection test, the Closedness test, and the Orientation test.

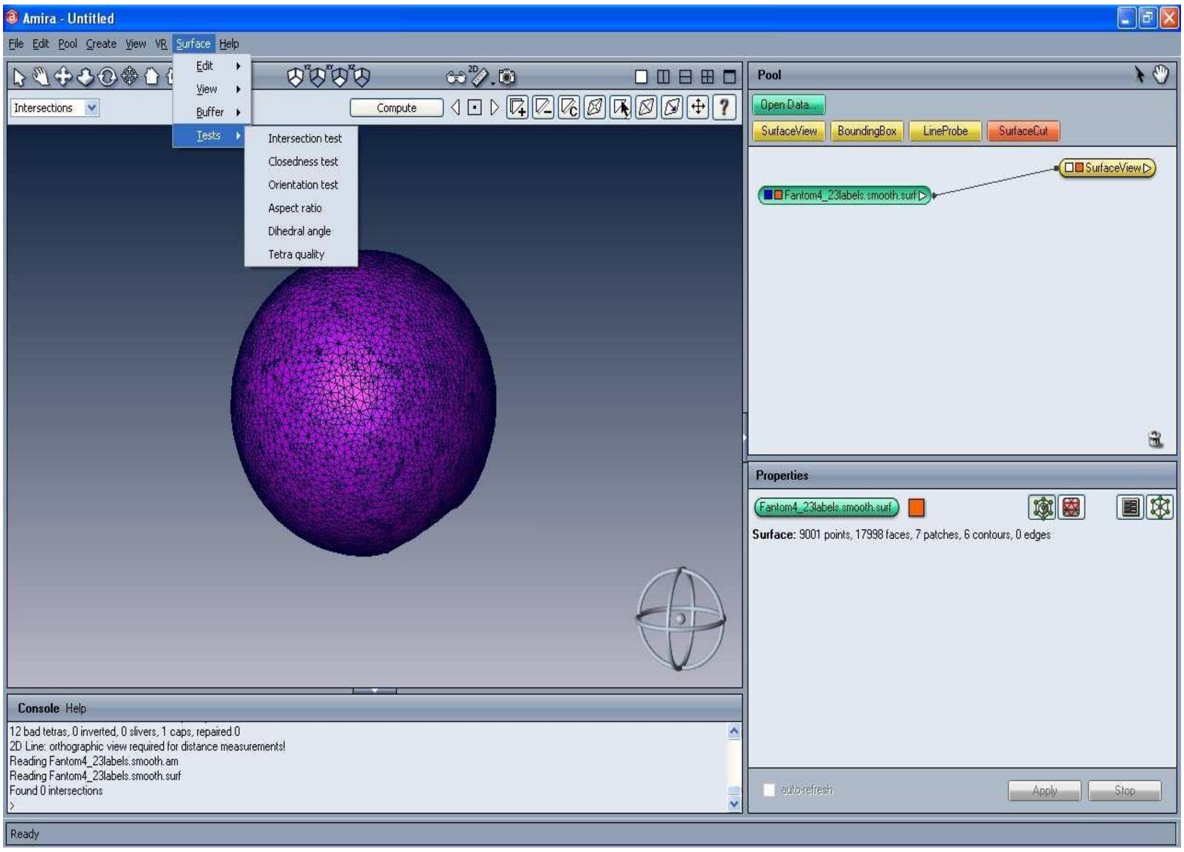

Figure 11. Editing surfaces before generating a tetrahedron mesh

(source: own study)

After successfully passing the verification tests, we proceeded to generate a tetrahedral mesh. We attached the TetraGen module, selected the surface we wanted to convert into a tetrahedral mesh in the properties window, and clicked Run now. After the calculations were completed, a view of a solid composed of a tetrahedral mesh was displayed, which is the basis for creating various views of the internal parts of the object, e.g., cross-sections, and for numerical simulations in finite element analysis (Figure 12).

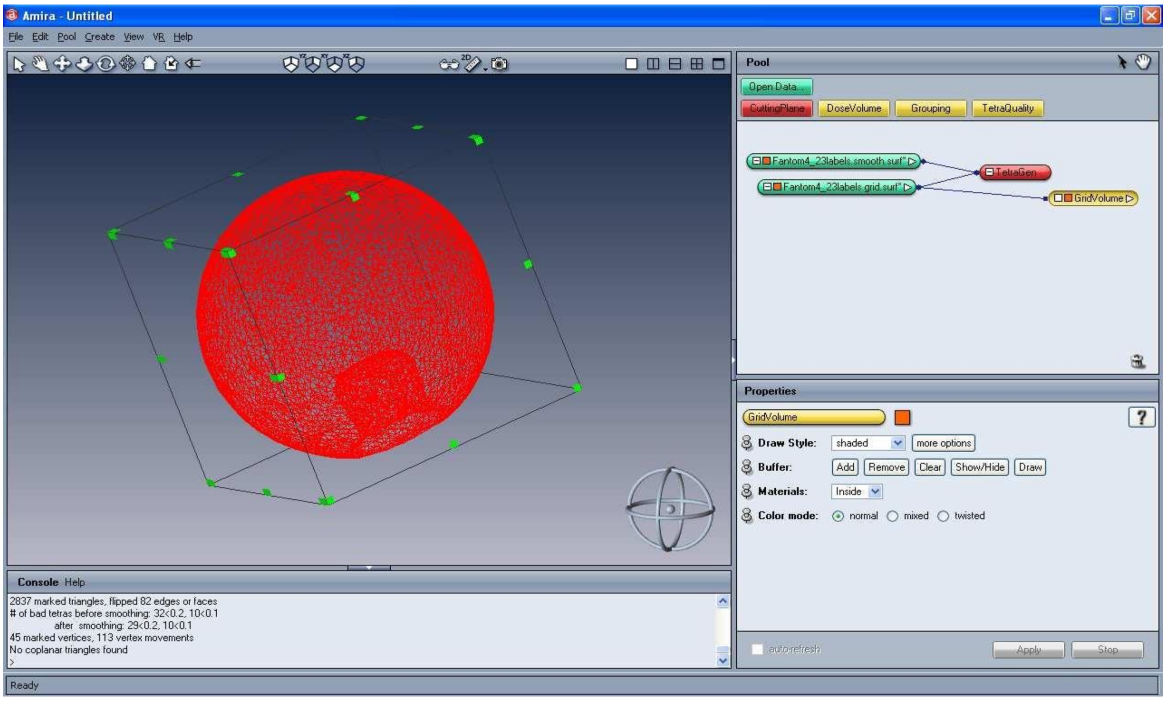

Figure 12. View of a tetrahedral mesh

(source: own study)

6. Measurement of reference balls

The Measuring module available from the View menu was used for the measurements. The diameter and radius of each reference sphere were measured ten times in the XY and YZ planes. The standard deviation was then calculated for each measurement.

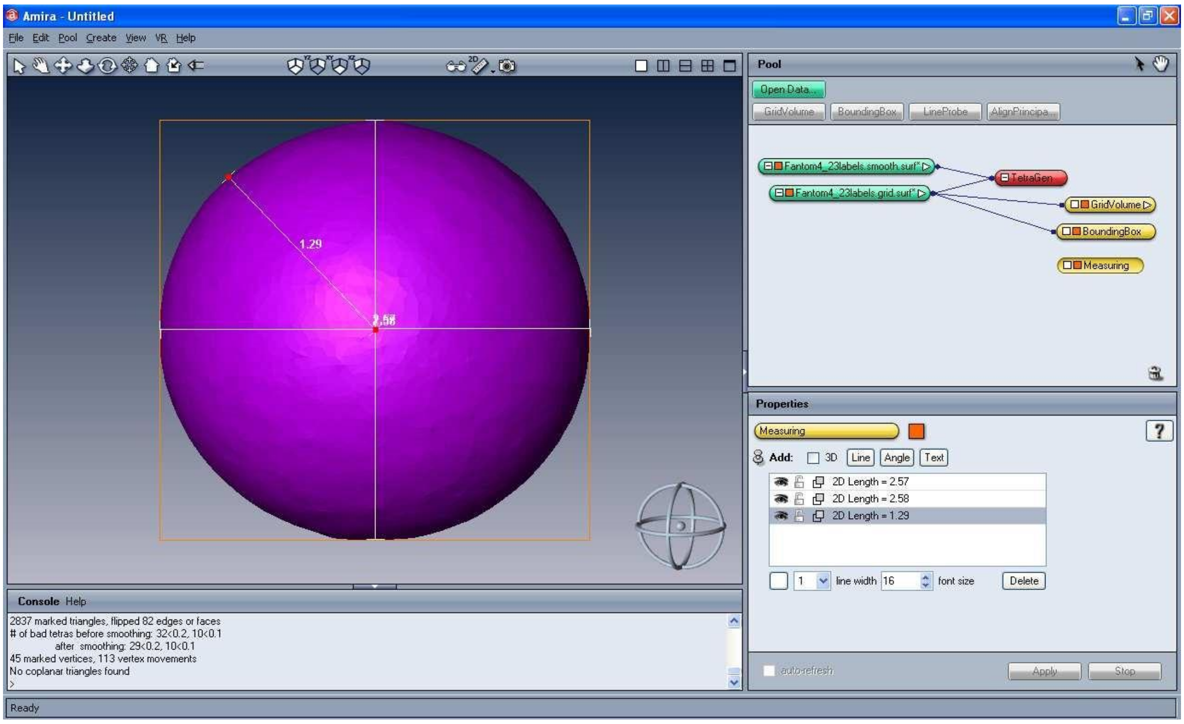

Figure 13. Measurement of a ball marked Fantom 1 with a nominal diameter of Ø = 25.7

(source: own study)

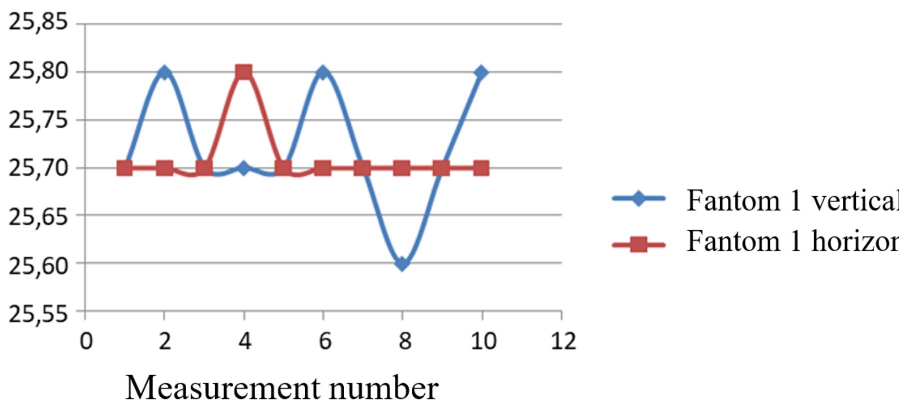

Figure 14. Chart of measurement results Fantom1

(source: own study)

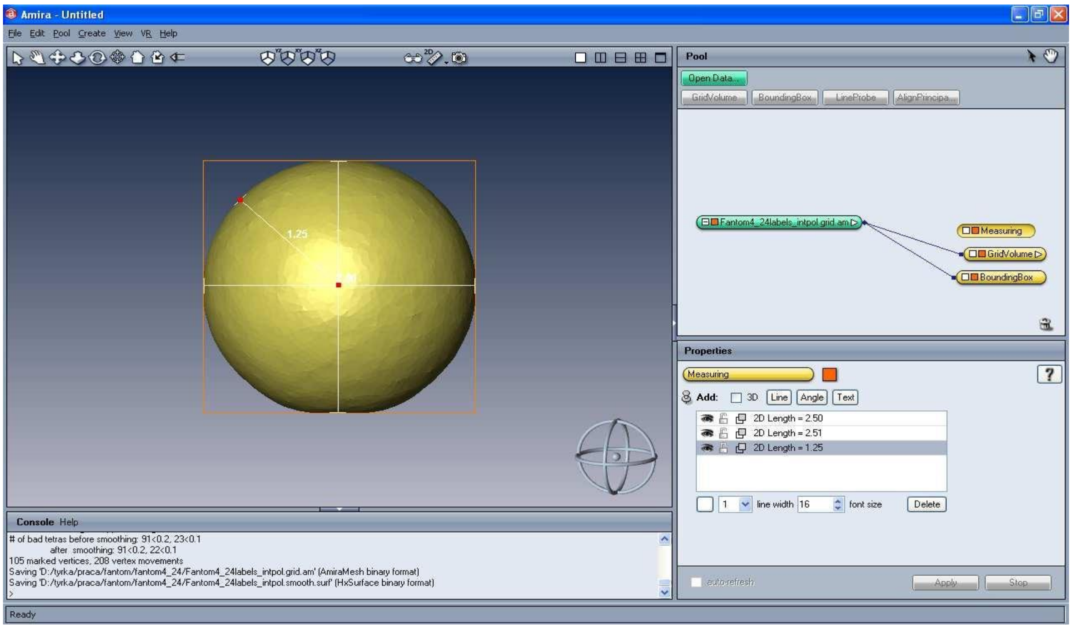

Figure 15. Measurement of a ball marked Fantom 2 with a nominal diameter of Ø = 25.7 [mm]

(source: own study)

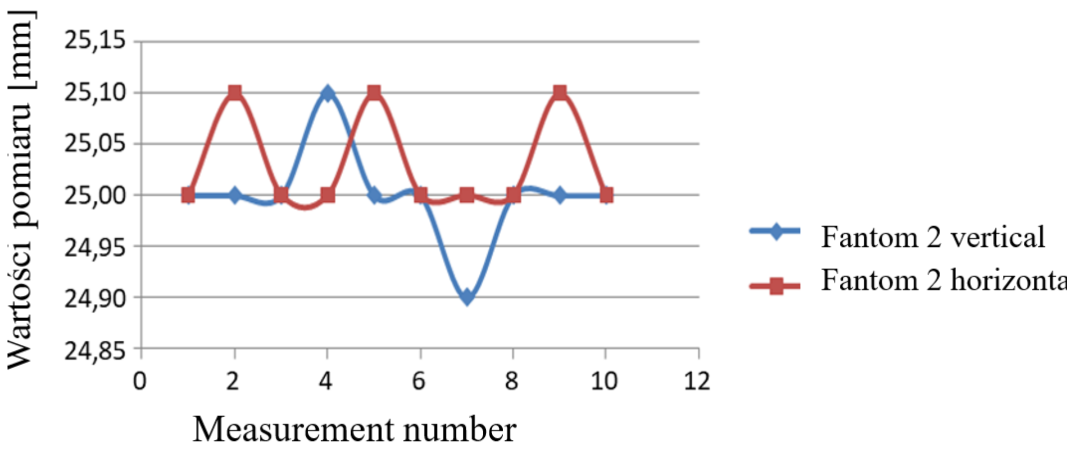

Figure 16. Chart of Fantom2 diameter measurement results

(source: own study)

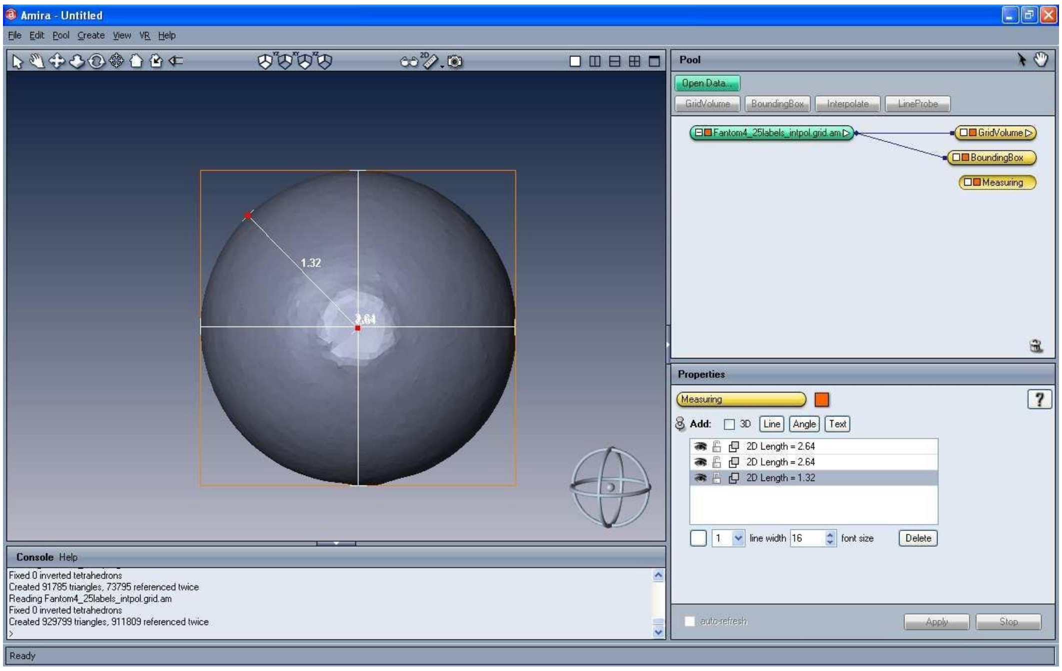

Figure 17. Measurement of a ball marked as Fantom3 with a nominal diameter of Ø = 26.4 [mm]

(source: own study)

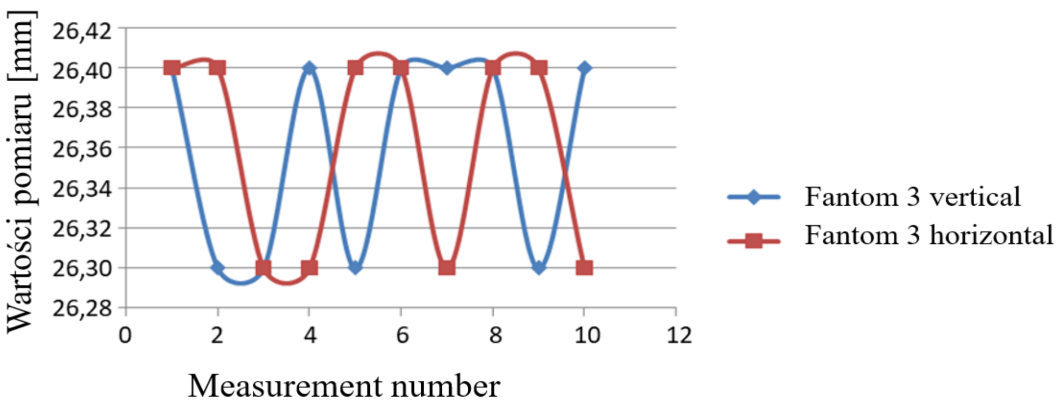

Figure 18. Chart of Fantom3 diameter measurement results

(source: own study)

Analyzing the results obtained, it can be concluded that in computer imaging, an important issue is the correct selection of diagnostic parameters and the positioning of the diagnosed products in the adopted reference system of the computed tomography scanner.

7. Conclusions

In recent years, the use of computed tomography as a control and measurement device has become increasingly popular (Bartscher et al., 2017). The process of three--dimensional visualization can be useful not only in medicine, but also in industry for assessing the quality of products or technological devices (De Chiffre, Carmignato, Kruth, Schmitt, Weckenmann, 2014).

The non-invasive technique of taking measurements using a tomograph is increasingly being used for digital imaging (Thompson et al., 2018).

The use of tomography in industry creates new opportunities for quality control. X-rays allow complex shapes to be examined without the need to dismantle them or create new cross-sections. Devices using X-ray computed tomography allow for the measurement of parts with complex shapes and their internal structure, as well as for the comparison of the obtained metrological results with CAD models.

Modern three-dimensional optical methods have many advantages: they are fast, non-contact, and can be integrated into the production process, e.g., the Metrotom-scatter Control diagnostic system from Zeiss (Kruth et al., 2011).

References

Bartscher, M., Hilpert, U., Goebbels, J., Weidemann, G. (2007). Enhancement and proof of accuracy of industrial computed tomography (CT) measurements. *CIRP Annals – Manufacturing Technology, 56,* 495-498.

Bircher, B., Meli, F., Küng, A., Thalmann, R. (2019). CT geometry determination using individual radiographs of calibrated multi-sphere standards. *e-Journal of Nondestructive Testing, 24*(3). DOI: https://doi.org/10.58286/23677.

Blažek, P., Šrámek, J., Zikmund, T., Kalasová, D., Hortvík, V., Klapetek, P. (2019). *Voxel size and calibration for CT measurements with a small field of view. Proceedings of iCT 2019.*

Busch, M., Hausotte, T. (2024). Practical Approaches for Determining the Structural Resolution Capability of X-ray Computed Tomography Measurement Tasks. *Metrology, 4*(3), 457-468. DOI: https://doi.org/10.3390/metrology4030028.

De Chiffre, L., Carmignato, S., Kruth, J.P., Schmitt, R., Weckenmann, A. (2014). Industrial applications of computed tomography. *CIRP Annals, 63*(2), 655-677.

Ketcham, R.A., Mote, A.S. (2019). Accurate measurement of small features in X-ray CT data volumes, demonstrated using gold grains. *Journal of Geophysical Research: Solid Earth, 124,* 3508-3529. DOI: https://doi.org/10.1029/2018JB017083.

Kruth, J.P., Bartscher, M., Carmignato, S., Schmitt, R., De Chiffre, L., Weckenmann, A. (2011). Computed tomography for dimensional metrology. *CIRP Annals – Manufacturing Technology, 60*(2), 821-842. DOI: https://doi.org/10.1016/j.cirp.2011.05.006.

Liu, W., Chen, X., Zeng, W., Sun, W., Gorman, D., Wilson, A., Qi, Q., Scott, P., Jiang, J., Lou, S. (2024). Comparison of X-ray computed tomography and coordinate-measuring system dimensional measurement for additive manufacturing parts using physical and simulation methods. *Measurement, 229,* 114414. DOI: https://doi.org/10.1016/j.measurement.2024.114414.

Ryniewicz, A. (2009). The analysis of the geometry of osseous tissue of the biological bearings interaction zone in the aspect of accuracy of shape mapping. In: *XIX IMEKO World Congress – Fundamental and Applied Metrology*. Lisbon.

Scherberich, J., Windfelder, A.G., Steinbart, J., Krombach, G.A. (2025). Measurement accuracy of CT systems: The importance of calibration phantoms. *PLoS ONE, 20*(9). DOI: https://doi.org/10.1371/journal.pone.0332263.

Stolfi, A., De Chiffre, L., Carmignato, S. (2016). 3D artefact for concurrent scale calibration in Computed Tomography. *CIRP Annals, 65*(1), 499-502.

Thompson, A., Maskery, I., Leach, R. (2016). X-ray computed tomography for additive manufacturing: A review of metrological challenges. *Measurement Science and Technology, 27*(7), 072001. DOI: https://doi.org/10.1088/0957-0233/27/7/072001.

Zemek, M., Blažek, P., Salplachta, J., Zikmund, T. et al. (2025). Scale Correction in Submicron Computed Tomography with a Submillimeter Field of View. *Tomography of Materials and Structures, 7,* 100054. DOI: https://doi.org/10.1016/j.tmater.2025.100054.

Sławomir KOWALSKI[1], Mateusz MENDRYGAŁ[2], Zbigniew MATUSZAK[3], Dalibor BARTA[4], Ján DIŽO[5], Aleš DITTRICH[6]

[1] University of Applied Sciences in Nowy Sącz, Faculty of Engineering Sciences, Zamenhofa 1a, 33-300 Nowy Sącz, e-mail: skowalski@ans-ns.edu.pl
[2] University of Applied Sciences in Nowy Sącz, Faculty of Engineering Sciences, Zamenhofa 1a, 33-300 Nowy Sącz
[3] Faculty of Marine Engineering, Department of Mechanics, Maritime University of Szczecin, Willowa 71, 70-500 Szczecin
[4] University of Zilina, Faculty of Mechanical Engineering, Department of Transport and Handling Machines, Univerzitná 1, 010 26 Žilina
[5] University of Zilina, Faculty of Mechanical Engineering, Department of Transport and Handling Machines, Univerzitná 1, 010 26 Žilina
[6] Technical University of Liberec, Faculty of Mechanical Engineering – Department of Vehicles and Engines, Studentská 1402, 46117 Liberec

A proposal to use selected mechatronic devices in bicycles to improve travel safety

Abstract

The conceptual design of the smart bike was developed to implement new technologies to the constantly developing bicycle market. The electronic systems described and presented are focused on the issue of safety when using a bicycle in public space. The implemented safety systems consist of lighting elements, such as front and rear position lights, direction indicators and brake light, as well as an obstacle detection system, twilight sensor, speed and mileage measurement. All electronic components are integrated into the spatial model of the illustrative design, the outline of which is included in the content of the project. The presented concept has great potential for further development and work focused on creating a complete, ecological and safe means of transport for the twenty-first century.

Keywords: bike, mechatronics, transport.

Propozycja wykorzystania wybranych urządzeń mechatronicznych w rowerach w celu poprawy bezpieczeństwa podróży

Streszczenie

Projekt koncepcyjny inteligentnego roweru został opracowany w celu wdrożenia nowych technologii na stale rozwijającym się rynku rowerowym. Opisane i przedstawione systemy elektroniczne koncentrują się na kwestii bezpieczeństwa podczas korzystania z roweru w przestrzeni publicznej. Zaimplementowane systemy bezpieczeństwa składają się z elementów oświetleniowych, takich jak przednie i tylne światła pozycyjne, kierunkowskazy i światło hamowania, a także system wykrywania przeszkód, czujnik zmierzchu, pomiar prędkości i przebiegu. Wszystkie elementy elektroniczne są zintegrowane z modelem przestrzennym projektu ilustracyjnego, którego zarys jest zawarty w treści projektu. Przedstawiona koncepcja ma duży potencjał do dalszego rozwoju i prac ukierunkowanych na stworzenie kompletnego, ekologicznego i bezpiecznego środka transportu na miarę XXI wieku.

Słowa kluczowe: rower, mechatronika, transport.

1. Introduction

An analysis of various types of bicycles commonly found around the world shows the need to implement new, personalized accessories and parts for even the smallest group of customers (Kapousizis et al., 2023; Novak, 2016). Bicycles are used in many areas of everyday life, and their versatility, comfort, ease of use, and safety are indisputable (Boot et al., 2024). Users of such equipment can be as young as three years old, and the upper limit is late old age, so each of them will need a set of accessories and technologies tailored to their needs in order to fully exploit the potential of their skills and abilities (Avina-Bravo et al., 2022).

This work was motivated by the desire to design and find appropriate solutions in the world of cycling, adapted to the realities of our fast-paced world. The project is based on proposing an electronic system that controls the vehicle's lighting, provides additional safety support, and monitors and collects data on the current status of the bicycle (Omri et al., 2024; Gómez-Suárez et al., 2022). For this purpose, an appropriate programming platform that meets the design requirements and reliable and compatible electronic components will be used (Henao et al., 2021).

The topic will be complemented by a comprehensive bicycle design, with particular attention paid to the individual components of the electronic system and their location (Novak, 2016). A visualization of the finished product will be presented using a spatial modeling environment.

A bicycle is clearly defined in traffic regulations. It is a vehicle with a maximum width of 0.9 m, powered by the muscular strength of the person riding it. Additionally, it may be equipped with an auxiliary electric drive, activated by pressing the pedals; the supply voltage must not exceed 48 V. The continuous rated power may be a maximum of 250 W, which gradually decreases when the speed exceeds 25 km/h (Jannah et al., 2025).

The electronic system is an indispensable part of the smart bike design. It allows the use of various types of sensors and actuators to improve the functionality and safety of the vehicle (Luo et al., 2024; Eisenman et al., 2007). The systems installed in cars are connected to an on-board computer patented by the respective brand. Pioneering solutions, security measures, and individual programming effectively prevent unauthorized users from making any changes outside of an authorized service center (Fischer et al., 2024).

The automotive industry has a huge budget and staff, and also mass-produces the technologies it develops. The bicycle market needs simpler, widely available, and affordable solutions (Reggiani et al., 2022; Beeking et al., 2024; Lee et al., 2025). At the same time, it has significant limitations that must be met by the control unit.

The Arduino programming platform seems to be the right solution in this case. Arduino is an open-source project, where both the hardware and software are made available by the copyright owner to users for further research, modification, improvement, and distribution of their own solutions (Kumar, Motupalli, 2020; Luo et al., 2024). Arduino is a miniature computer system with the ability to program and operate on input and output data using appropriate instructions (Henao et al., 2021).

2. Purpose and scope

The project was developed with the aim of presenting the design of a modern, smart bicycle equipped with systems supporting cyclists in everyday use. The main objective of the project is to create an electronic system that sends signals to the user and receives information from the environment in order to improve safety and ergonomics when using the bicycle.

The basis of the electronic system is a control unit. The microcontroller of such a unit must be able to handle all installed input and output devices, so it is necessary to adjust it in terms of the number of inputs and outputs, both digital and analog. Required number of inputs/outputs: digital – 12, analog – 2 using the I2C bus. The following are also required: easy and quick access to modify the software, compact dimensions in relation to the bicycle frame, a lightweight and miniature power source, and high compatibility with accessory devices.

The current system for detecting objects in front of the vehicle should inform the cyclist of a possible hazard on the road with sufficient advance warning of approximately three seconds. This is sufficient time to perform a maneuver to prevent an unexpected collision. The distance sensor should therefore be adjusted in terms of measurement range so that it is effective at both low and high speeds. An equally important parameter is the frequency of measurements, so as not to cause too much delay – at least 30 measurements per second. Compact dimensions and low weight will be additional advantages.

The lighting included in the construction of the bicycle must meet the basic functionality of accessory lights intended for use in traffic. A front headlight that produces bright white light that does not dazzle other road users, with two lighting modes – flashing warning light and continuous light illuminating the area in front of the vehicle. The rear light is red and has at least one flashing signal mode. An integrated brake light is also required, with continuous illumination and greater intensity than the position light. In addition to the standard light control button, the lighting system reacts to changes in the intensity of ambient light. This means that the lights are automatically switched on or off from dusk to dawn and when entering tunnels and overpasses. The measuring range of such a photocell must be at least 0 to 250 lux and read the measurement 10 times per second.

Turn signals are not legally required as necessary equipment for the use of a bicycle, but they have a very significant impact on safety while riding. Signaling maneuvers is crucial for good communication between road users and pedestrians. Taking your hands off the handlebars is not safe, especially when turning, so the use of turn signals is justified. For simple and uniform communication, orange LED lights with intermittent operation should be used at both the front and rear of the vehicle.

Measuring the speed of a vehicle is very important for other electronic subsystems. They rely on its correct reading: the obstacle detection system, the functioning of the brake lights, the display of the current speed and the distance traveled. The main criterion for selecting a sensor is its measurement frequency, which must be at least 7 measurements per second.

3. Smart bike components

The Arduino Uno R3 board was selected for the project, as it meets the design requirements in terms of available inputs and outputs, offers compact dimensions and high peripheral device compatibility, and has an open programming environment, allowing users with knowledge of electronics and C programming languages to modify the software.

An alphanumeric LCD display with a working area arranged in two rows of 16 characters was used to display the basic current parameters of the vehicle. To facilitate operation and reduce the number of microcontroller pins required, the screen is equipped with an I2C converter module soldered to the connector, making it possible to control the display using the SDL and SDA lines of the I2C bus. The content is displayed in black against a green backlight, and the contrast can be adjusted using a built-in potentiometer.

The first line shows the current vehicle speed in the center and the battery charge level on the right edge. The second line shows the distance traveled, and on the left side, the current mileage, which is reset when the central unit is turned off, while on the right side of the display, the total mileage calculated and recorded during all trips is shown.

The display is mounted in an ergonomic position for user comfort and ease of use, as well as in a low-collision location, as the housing containing the display and other electronic components is mounted in the steering bridge Figure 1. The housing itself has transparent plexiglass to prevent dirt and moisture from getting inside the display, while remaining unnoticeable for comfort of use. The screen wiring runs through the inside of the bridge, going directly to the bicycle frame, where the Arduino board is mounted.

Reading the current speed in various types of vehicles is standard practice. For the user, this is a simple message informing them whether the speed achieved is satisfactory in relation to the planned travel time or compliance with traffic rules. However, the correlations that arise between different electronic systems are invisible – only the effects of the correct functioning of such a system are visible.

The first of the dependencies involving speed measurement is cooperation with an obstacle detector. The aim is to make the speed of the vehicle dependent on the distance to the obstacle, thus enabling the creation of an intelligent system that will alert the cyclist early enough about an approaching obstacle, regardless of the speed reached. When using a proximity sensor alone, it is only possible to determine the distance from which the alarm is triggered. This is a very imprecise method due to the frequent and large differences in bicycle speed.

Figure 1. Location of the LCD display on the bicycle handlebars

(source: own study)

The second connection is the functioning of the brake light system, which activates when the speed is reduced. This solution avoids the use of additional equipment in the form of a limit switch, which, like any mechanical component, has limitations such as declared service life, weight and size, and the use of an additional digital microcontroller input.

Speed is measured using a Waveshare module equipped with an AH49E Hall sensor with adjustable sensitivity. The integrated circuit is characterized by low output noise, which eliminates the need for external filtering. It also contains precision resistors that ensure increased temperature stability and measurement accuracy. The output voltage depends on the supply voltage, which should be between 2.3 and 5.3 V, and varies in proportion to the magnetic field strength. The module has 4 pins: VCC – power supply (2.3-5.3 V), GND – power supply ground, AOUT – analog output, DOUT – digital output.

The Hall effect sensor module connected to the D8 digital input of the Arduino board counts the frequency of occurrence within the measurement range of a magnet attached to the rim of a bicycle wheel. If the magnetic element is detected by the sensor, a short high signal is sent to the microcontroller, which starts measuring time until the next high state appears. In order to calculate the speed, it is necessary to enter the circumference of the wheel mounted on the vehicle into the controller – this will allow the creation of a relationship between the occurrence of one high signal and the distance traveled at that time.

Assuming that the bicycle will be equipped with 700x35C wheels and 35-622 tires, the approximate circumference of the entire wheel is 2.168 meters, which means that this distance is covered in the time between two high states of digital input D8.

The resulting bicycle speed v [m/s] is used to operate the obstacle detector and brake light. The information provided to the user via the LCD display is additionally converted into speed V in km/h.

An important issue when deciding to use and ensure the efficient functioning of a sensor utilizing the Hall effect is its proper placement. The sensor itself detects the presence of a magnetic field at a maximum distance of 12 mm. The magnet mounted in the holder and attached to the spokes of the bicycle wheel is 3 mm away from the Hall sensor when it passes it, so no reading should be missed and its effectiveness should remain at a satisfactory level. The sensor module is built into a housing with a clamp, and the whole unit is enclosed, leaving only a small opening for the measuring element to protrude towards the rotating wheel. The connection cable is ultimately routed in the armor, close to the front shock absorber, and then passes through a hole with a seal to enter the interior of the bicycle frame Figure 2.

Figure 2. Location of the speed measurement system

(source: own study)

The obstacle detector is designed to improve user safety when moving among other vehicles and traffic participants. It is a support system for the often-imperfect sense of sight. The distance sensor must therefore have sufficient sensitivity and maximum measurement distance to effectively inform the user of a possible hazard in advance.

The speed measurements used to select the appropriate distance sensor were made using a GPS satellite system and the Strava mobile app. The speed graphs for each route are shown in Figure 3.

Route 1 (Trasa 1) with a total distance of 20.6 km, was covered in favorable conditions with a lot of elevation changes, completed alone and focused on achieving a specific goal. The graph shows an average speed of 19.5 km/h. The maximum speed achieved was 48.1 km/h, but it is not repeatable, while a regularly occurring value of around 40 km/h can be read.

Route 2 (Trasa 2) took much longer to complete, with a result of 38.9 km. The trip consisted of a group of two people and was focused solely on recreation. The average speed achieved fluctuates around 12.7 km/h, and the highest speed achieved is 41.4 km/h. Again, the repeatable high speed is slightly lower than the maximum and is around 30 km/h.

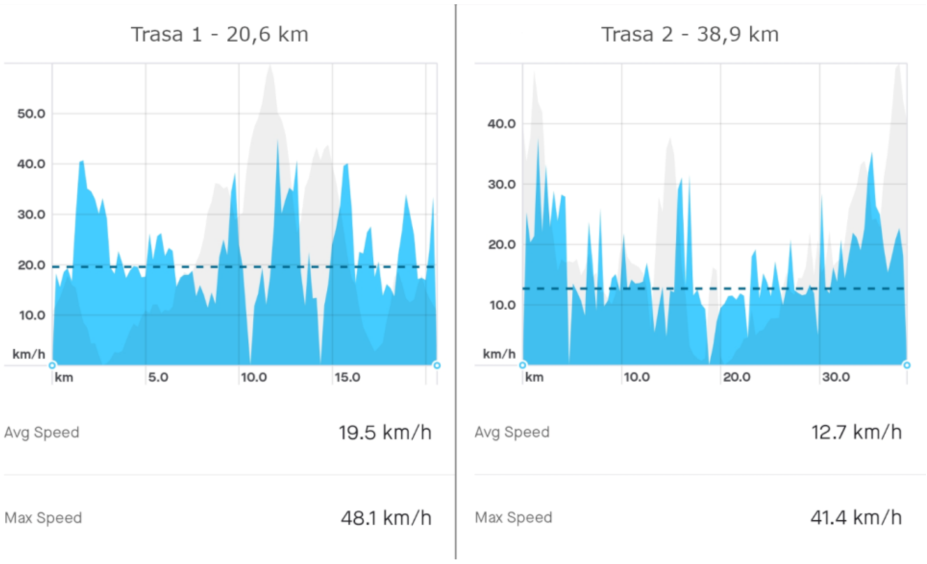

Figure 3. Speed measurement using a GPS system

(source: own study)

For the purposes of the project, the maximum speed was set at 50 km/h. Using Figure 3, it can be seen that for the assumed speed, the vehicle travels 41.67 meters in 3 seconds. To ensure optimal system performance and utilize the full measurement range, a sensor with a maximum range of 40 meters should be used.

A laser sensor compatible with and dedicated to many open-source programming platforms was used for the obstacle detection system. The TeraRanger Evo 40m is a versatile, long-range Time-of-Flight (ToF) distance sensor designed for navigation and obstacle avoidance in robotics Figure 4. It offers the ability to detect objects up to 40 meters away, with a refresh rate of up to 240 Hz. The sensor is very lightweight, weighing only 12 grams, and has compact dimensions. The set includes one selected, replaceable stand for mounting on a surface, which also serves as a connection interface for I2C/UART projects.

The system operates primarily by maintaining an appropriate relationship between the speed of the bicycle and the distance to the detected obstacle. Speed should be interpreted as the time needed to approach an object that poses a threat to the user. The project assumes that the time needed for the cyclist to react appropriately is 3 seconds from the moment an undesirable object appears on the vehicle's path. The system adjusts the distance read from the U2 sensor depending on the current speed indicated by the U1 sensor and interprets whether to send a warning signal to the user and in what form.

Calculated on the basis of the assumed speed v = 25 km/h and the corresponding distance value vm = 20.83 m/3s, the coefficient k is approximately 1.2. For the obstacle detection system, each speed measurement v is divided by the coefficient k to obtain the variable x. This variable is compared with the distance value s read from the Terabee laser distance sensor. The result of the comparison is considered in terms of four possible situations.

The first situation occurs when, for a given calculated variable x, the time needed to approach the obstacle is greater than 3 seconds. This means that the optical and acoustic alarm signals remain inactive – digital outputs D12 and D13 are in a low state.

The second situation occurs when the time it takes for the cyclist to approach the object is less than or equal to 3 seconds, but greater than 2 seconds for the calculated variable x. An optical alarm signal is triggered in the form of a flashing red LED located on the housing next to the main display. The digital output of controller D12, responsible for controlling LED7, is triggered by a signal corresponding to a flashing frequency of 2.5 Hz with a period of 0.4 s. Both the high and low states last for 0.2 s.

The third situation is possible when the time needed to reach the obstacle is less than or equal to 2 seconds, while at the same time it is greater than 1 second for the variable value x. An optical alarm signal is triggered in the form of a flashing LED7 and an intermittent, loud audible signal generated by the BUZ1 buzzer connected to the D13 digital output. Digital outputs D12 and D13 are triggered by signals with the same time parameters – frequency 2.5 Hz, period 0.4 s.

Situation four describes the behavior of the alarm system when, for a given variable x, the time remaining to contact the object is less than or equal to 1 second. This is a critical situation, so the warning LED continues to flash as in the previous situations, while the acoustic alarm changes to a continuous, loud buzzer sound.

In an ideal laboratory experiment, where a bicycle with an intelligent obstacle detection system is traveling at a constant speed toward a stationary obstacle, each situation involving an active alarm signal should last one second and cyclically go through successive alarm stages.

In order to fulfill its task, the obstacle detector was mounted at the front of the bicycle, perpendicular to the ground, so that the laser beam would maintain the correct angle, even at long distances. Placing the sensor on the frame, i.e., on the head of the bicycle frame, instead of on the handlebars, allows for greater stability of readings, as the movement of the handlebars is more chaotic than the road on which the vehicle is traveling. The distance sensor is located in a housing that prevents foreign objects from entering the structure. The connection cables run directly through the inside of the bicycle frame to the microcontroller connectors.

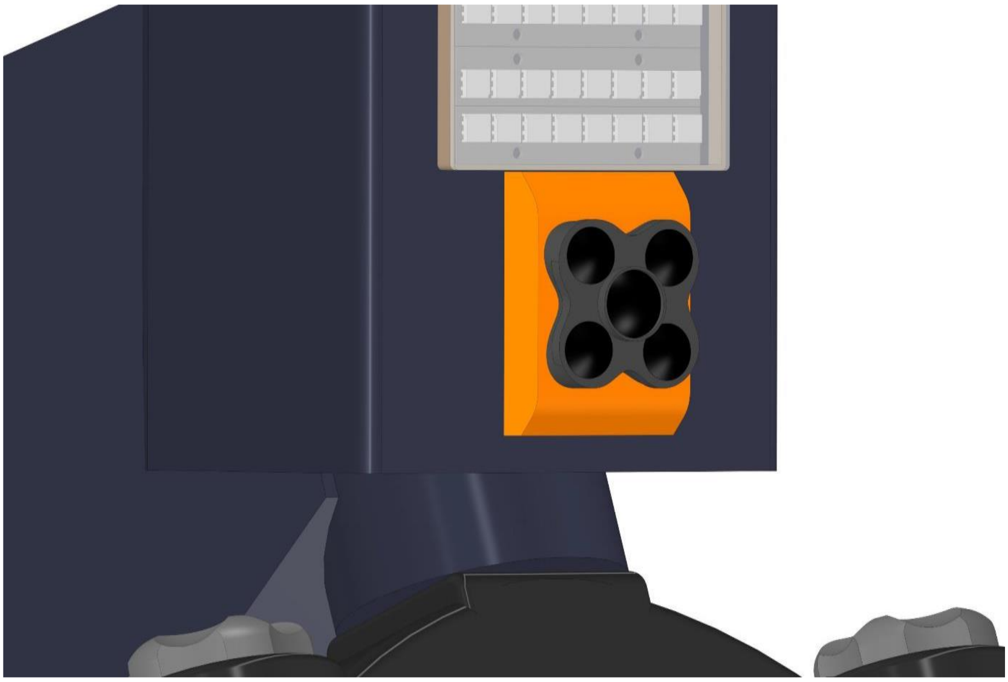

Figure 4. Obstacle detector mounting location

(source: own study)

The lighting system used in the project consists of:

- Integrated, intelligent LED modules;
- Light intensity sensor;
- Buttons and switches.

Modules equipped with individually addressed WS2812B RGB LEDs are an intelligent LED light source. The integrated single LED controller allows for addressing of modules connected in series in such a way that the color of each LED can be set separately. The LEDs used are manufactured in the SMD5050 standard – the size of the LED is 5 x 5 mm. Each of them consists of three basic colors: red, green, and blue, which can achieve up to 256 brightness values, i.e., over 16.7 million color combinations.

The communication protocol consists of a single signal line, so it is a serial protocol, also known as non-return-to-zero (NRZ). It is a simple code in which logical 0 and logical 1 are encoded by different durations. Data is sent in 24-bit frames containing GRB components in descending order. For Arduino clocked at 16 MHz, the acceptable tolerance is 150 ns – this is a few clock cycles. In reality, the WS2812B controller allows for greater flexibility, but the most important thing is to maintain a minimum duration of 1250 ns. The appropriate libraries available for download and initialization in the microcontroller have encoded timing characteristics for the operation of the modules.

The main switch, used to cut off the power supply connected to the Arduino board, is based on the MRS-101 rocker switch, with the following specifications:

- Switching mode: OFF – ON;
- Switch type: bistable;
- Contact arrangement: SPST (NO-C);
- Contact rating: 3 A at 250 VAC;
- Service life: 10,000 cycles.

The switch controlling the operation of the turn signals is a small Canal MR3-H rocker switch. A rectangular type with the following parameters was used for the project:

– Switching mode: ON-OFF-ON;
– Switch type: bistable;
– Contact rating: 10 A at 250 VAC;
– Initial contact resistance: max. 20 mΩ;
– Dielectric strength: 1000 VAC for 1 minute;
– Temperature range: from -20° to +85° C;
– Service life: 10,000 cycles.

Control button for front and rear lighting – model PBS-33B. Technical parameters:

– Switching mode: OFF – ON;
– Initial state: normally open;
– Switch type: normally open, monostable with automatic return;
– Contact load capacity: 1 A at 250 VAC;
– Initial contact resistance: max. 20 mΩ;
– Dielectric strength: 1000 VAC for 1 minute;
– Temperature range: from -20° to +85° C;
– Service life: 50,000 cycles.

The main switch for the entire electronic system is built into a panel located on the steering bridge, providing easy access for activating or deactivating the system, as shown in Figure 1. The lighting controls, both for the turn signals and the main lights, are located on the handlebar, close to the left handle and brake lever, in an ergonomic position for the thumb Figure 5.

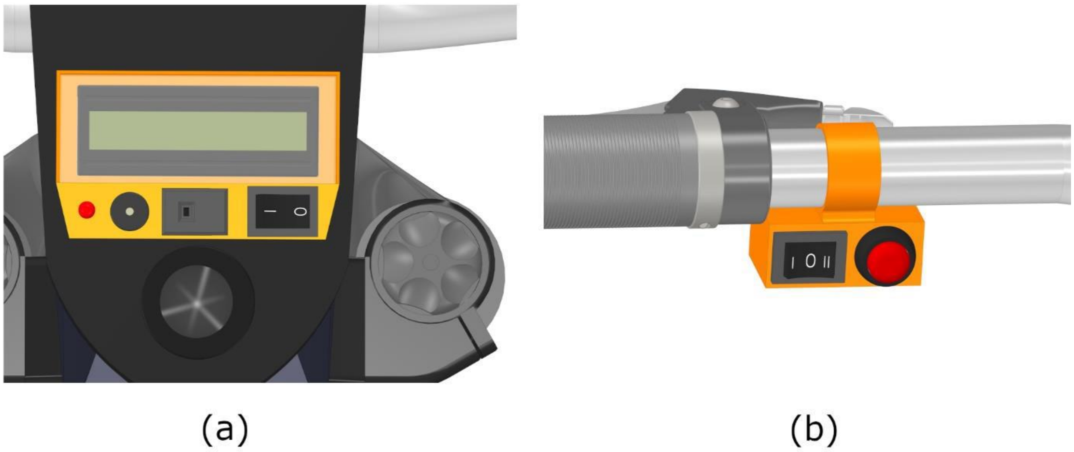

Figure 5. Buttons and switches: a) main switch, b) lighting control

(source: own study)

The rear light consists of a NeoPixel Stick 8 strip equipped with 8 WS2812B modules. The ready-made LED assembly saves a lot of space, as the length of the set is about 3 times shorter than individual modules placed in series.

One lighting strip performs two basic functions:

– position light;
– brake light.

The position light uses half of the available LEDs, arranged every other one in the set. This saves energy, but also emphasizes the brake light, which uses all LEDs.

The brake light functions independently and takes precedence over the position light. This means that all LEDs on the strip light continuously when the appropriate condition is met.

The NeoPixel Stick 8 strip requires a single 5 V power source, the GND pin must be connected to ground, and for communication with the microcontroller, the DIN pin must be connected to the D3 digital output.

The rear light is built into a housing on a long arm attached to the seat tube instead of the seat post to avoid changing the position of the rear light when the saddle height is changed, thus reducing the frequency of movement of the power cables. The position light is located vertically in the center of the bracket, between the turn signals, and has a red plexiglass lens with a high light transmission coefficient Figure 6.

The front lighting of the bicycle mainly serves to illuminate the road ahead of the vehicle, so in order to create an effective light source, the LED6 front headlight module consists of 4 NeoPixel Stick 8 strips connected in series, placed in a housing with a transparent lens that focuses the light beam. The front headlight can also serve as a signal for other road users when there is no need to illuminate the road ahead of the vehicle. The front lighting operates in two modes and is controlled manually using the same button as the rear light. The color of the light can be freely adjusted thanks to the use of three-color LEDs, but for the clearest and most ergonomic effect, it is programmed to a cool white color.

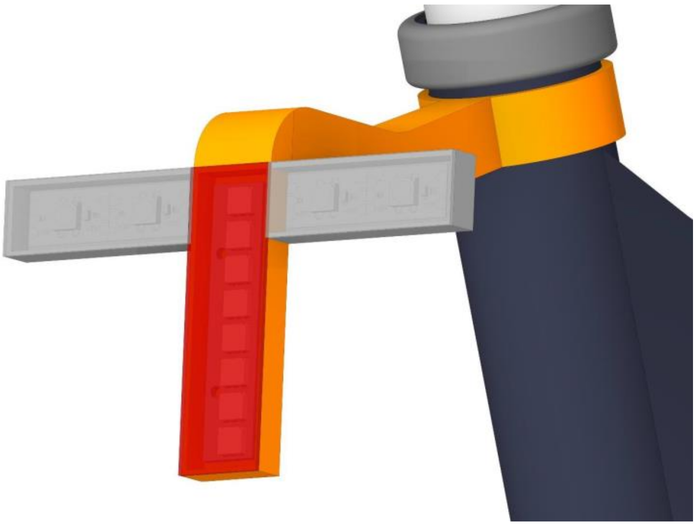

Figure 6. Installation of position lights

(source: own study)

The front lighting is located in a housing with a glass lens that focuses the light, creating a more orderly beam of light rays, affecting the intensity and efficiency of the headlight. The front light is directed slightly towards the ground to minimize the risk of dazzling oncoming traffic and to maximize the lighting potential. The headlight is mounted on the head of the bicycle frame, between the handlebar stem and the obstacle detector Figure 7, so that the cables remain hidden inside the frame along their entire length.

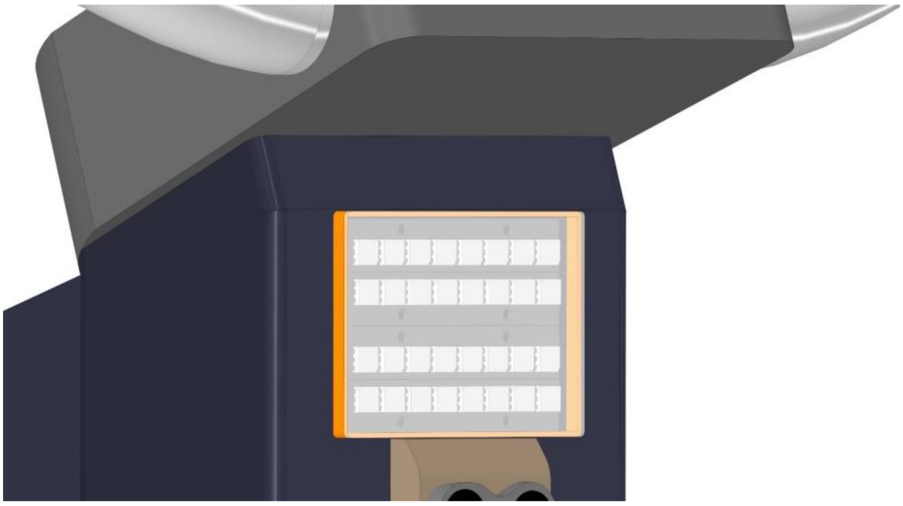

Figure 7. Location of the headlight

(source: own study)

The WS2812B LED modules responsible for the turn signals are divided into two sections:

- front section;
- rear section.

The front section contains two segments – left and right, each consisting of two LED modules. The left segment, marked LED1, contains LED1-1 and LED1-2 modules connected in series. They are connected to Arduino on digital output D7. The right element, marked LED2, uses two LED2-1 and LED2-2 modules connected in series, connected to digital output D6.

The rear section is also divided into two parts – left and right. The left part, marked LED3, consists of two LED3-1 and LED3-2 modules connected in series to digital output D5. The right part, marked LED4, contains two LED4-1 and LED4-2 modules connected to output D4.

Switch S1 is responsible for controlling the turn signals. When the switch is set to the extreme left position, contact 1 is closed, causing a signal to be sent to digital input D9. Turn signals LED1 and LED3 start working. The flashing occurs at a frequency of 1.25 Hz, with a period of 0.8 s, assuming that the high and low states occur equally at 0.4 s. When switch S1 returns to the middle position and none of its contacts are closed, the operation of turn signals LED1 and LED3 is interrupted.

When switch S1 is moved to the far right position, contact 2 is closed and a signal is sent to digital input D10. At this point, the LED2 and LED4 turn signals begin to flash at a frequency of 1.25 Hz and a period of 0.8 s. The high and low states last 0.4 s each. If switch S1 returns to the middle position, LED2 and LED4 stop working.

The rear turn signals are located in a common housing with the rear position light, which separates the two turn signals from each other, creating a clear gap between them and thus better informing the traffic participant behind the bicycle in which direction the maneuver will be performed. The wires are routed through narrow channels. The front turn signals have their own housing, with an additional white reflective element in the center. The whole assembly is attached to the highest point, the front shock absorber bridge Figure 8b. The wiring, with a reserve length, is routed through sealing grommets to the inside of the support frame via the shortest route.

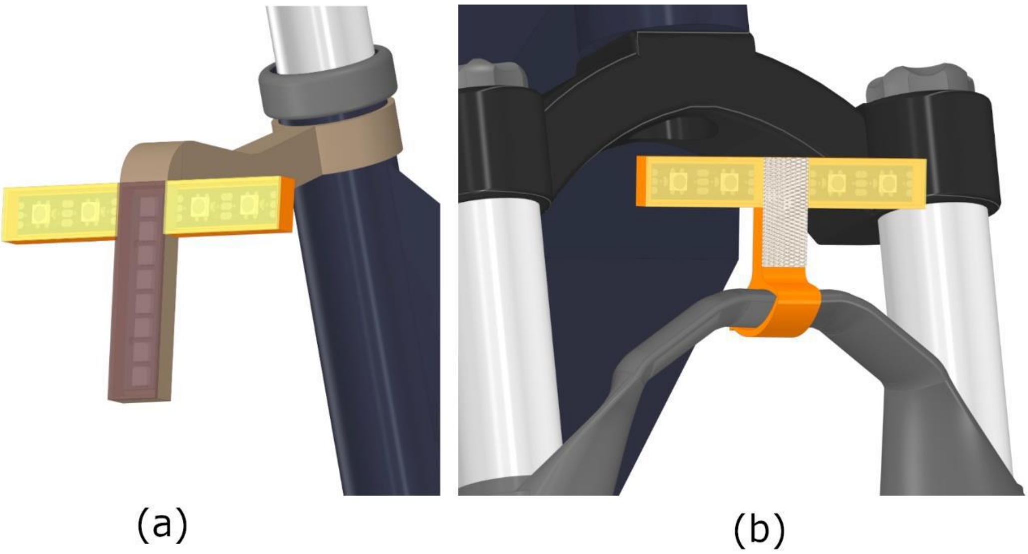

Figure 8. Location of turn signals, a) rear, b) front

(source: own study)

Automatic lighting control requires the use of a U4 light intensity sensor to accurately determine whether the spotlights need to be activated at a given moment. If the controller only used a programmed atomic clock for control, it would be necessary to declare or enter the current date so that, depending on the season, the lights would turn on at dusk. With the appropriate photoresistor circuit, it is possible to enter a variable value which, when exceeded, causes the lighting to turn on or off.

After power is supplied to the microcontroller, it analyzes the readings from the twilight sensor. When the set twilight threshold is exceeded, which suggests that the microcontroller should activate the appropriate lighting mode, it triggers digital outputs D2 and D3. Two switching thresholds are programmed: threshold 1 – triggered when the light intensity falls below 140 lux and above 80 lux, while threshold 2 – interpreted by the microcontroller when the amount of light reaching the sensor is less than 80 lux.

When the first threshold is reached, the microcontroller immediately activates lighting mode 1, then monitors fluctuations and changes in readings from the U4 photoresistor module to check which conditions are met. If the light intensity rises above the upper limit, the T1 countdown begins – this is a delay time during which the controller continuously monitors the level of external lighting in order to eliminate accidental, intense light sources reaching the sensor, such as street lamps or other vehicles. The delay time T1 is set to 5 seconds. If during this time the light intensity falls below 140 lux again, the T1 counter resets and starts counting down again, but if after 5 seconds the external light intensity remains higher, the lighting switches off.

The light intensity sensor is part of a panel built into the steering wheel bridge Figure 9. This location of the photoresistive element eliminates the light source from oncoming vehicles, which, due to its intensity and relatively long exposure time, could effectively interfere with the sensor's operation. When measurements are taken only from sources above the sensor, after dark only street lights have an impact, but when driving, they are passed so quickly that the intensity of the light beam decreases before the delay time T1 or T2 elapses.

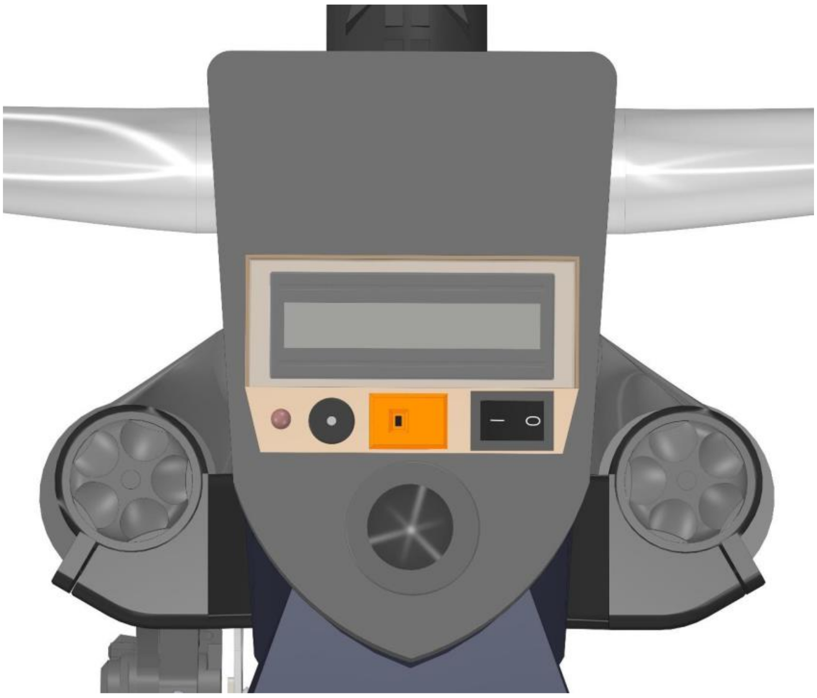

Figure 9. Location of the light intensity sensor

(source: own study)

The main connection diagram shown in Figure 10 contains all electronic system components connected to an Arduino Uno board equipped with an ATmega328 microcontroller.

Assigned digital inputs and outputs of the microcontroller:

- D2 – digital output – LED6 – front headlight;
- D3 – digital output – LED5 – rear position light;
- D4 – digital output – LED4 – right rear turn signal;
- D5 – digital output – LED3 – left rear turn signal;
- D6 – digital output – LED2 – right front turn signal;
- D7 – digital output – LED1 – left front turn signal;
- D8 – digital input – U1 – speedometer (Hall sensor);
- D9 – digital input – S1 – turn signal switch position 1;
- D10 – digital input – S1 – turn signal switch position 2;
- D11 – digital input – S2 – manual lighting control button;
- D12 – digital output – LED7 – obstacle detection system warning LED;
- D13 – digital output – BUZ1 – obstacle detection system warning buzzer.

A4/A5 I2C bus SDA/SCL analog input:

U2 – obstacle detector (distance sensor);

U3 – LCD display;

U4 – automatic lighting control (light intensity sensor).

Assigned analog inputs of the microcontroller:

In addition, the Arduino board has a main switch S0 connected in series between the VIN pin – main power supply, and the power source, thanks to which it is possible to start the entire electronic system with a single switch.

4. Components of a smart bike

The appearance of the single-track vehicle, which is ultimately to be equipped with intelligent electronic systems, does not differ much from a standard bicycle without any electric power-driven amenities. The shape of the smart bicycle presented in the project is similar to many solutions currently available on the market, and it is difficult to confuse it with any other vehicle. A distinctive feature is the support frame, which has been designed with future improvements to the concept in mind and the implementation of an electric drive to assist the cyclist's muscles in situations of increased calorie expenditure. The rectangular shape of the lower tube provides optimal space for equipping the structure with additional, high-capacity batteries, which are the power source for the electric drive Figure 11.

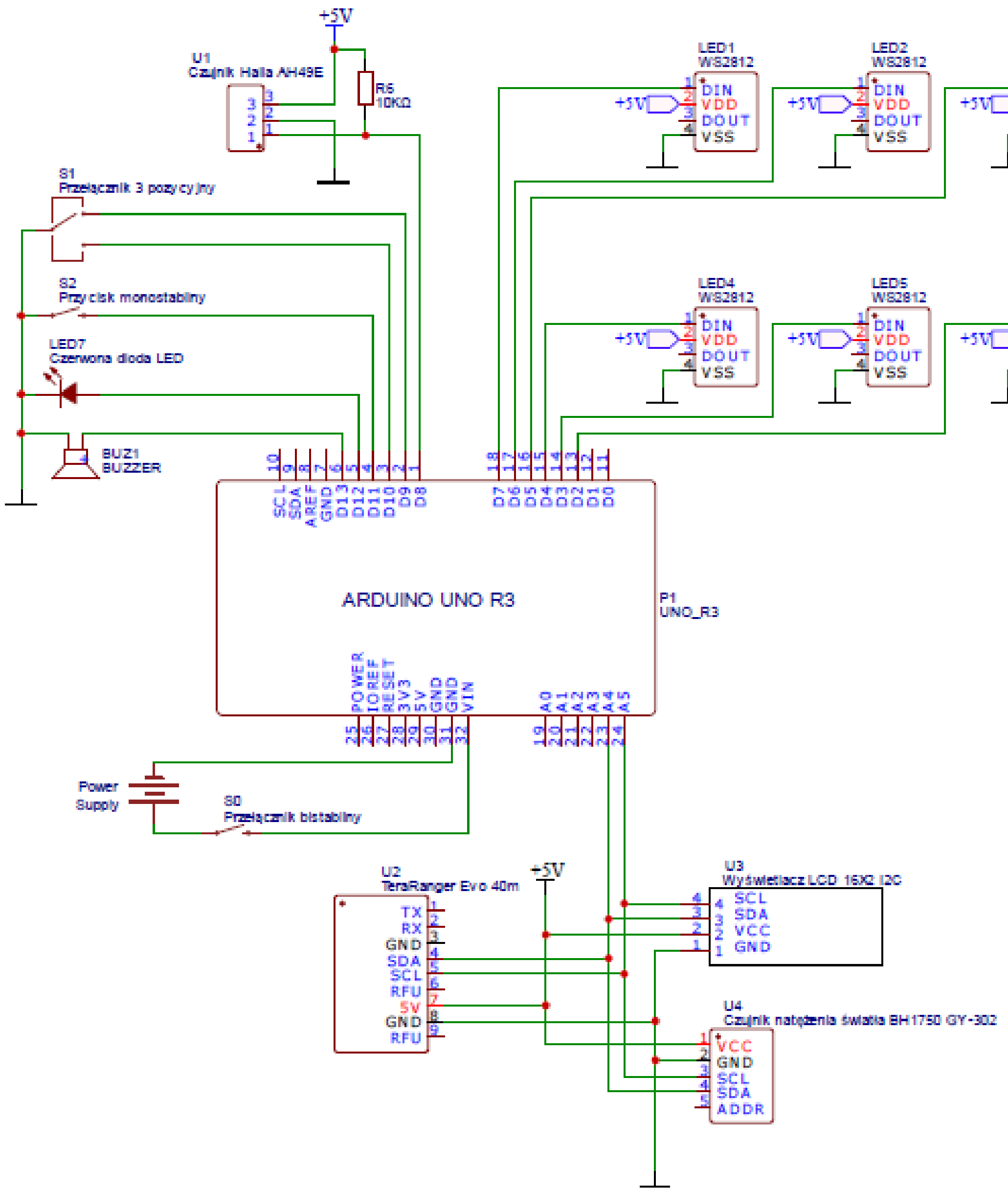

Figure 10. Connection diagram

(source: own study)

Figure 11. Bicycle design

(source: own study)

At the current stage of the project, only the Arduino controller is located inside the bicycle frame, screwed to a prepared bracket in such a way as to ensure convenient access to all connectors of the programmable microcontroller on the printed circuit board. Access to the controller is located on the top of the frame, where a sealed cover is mounted with screws.

A visual representation of the layout of all electronic systems included in the conceptual design of the smart bicycle is shown in Figure 12, which contains detailed groups of systems such as:

- rear lighting, which includes: position light, rear turn signals;
- control panel, including: LCD display, obstacle detection alarms (LED and warning buzzer), main switch, twilight sensor;
- control panel, consisting of: turn signal switch, light switch);
- headlight;
- obstacle detector;
- front turn signals;
- speedometer.

Figure 12. Layout of electronic systems

(source: own study)

5. Conclusions

The proposed topic, "Conceptual design of a smart bicycle", offers a wide range of possibilities for implementing new, innovative solutions or those previously used in other fields of science and technology, which, when simplified and minimized, have the potential to effectively and positively impact the bicycle market. This is a market that is developing rapidly and surprising with its ability to adapt to the prevailing conditions of very fast-paced urban and suburban life. These innovations are needed, especially in cities that are expanding their infrastructure to facilitate the use of two-wheeled vehicles.

The solutions developed for the project focus on improving the safety and ergonomics of bicycle use for people who use bicycles for everyday travel among other road users and pedestrians. This means, among other things, providing the user with a greater sense of psychological comfort by offering technologies that relieve and support their sense of sight, which, in a flood of information, can become a weak point in perceptual-motor function in a critical situation.

The use of a distance sensor that continuously monitors the space in front of the vehicle, processing the signals received by the sensor and then interpreting them in accordance with the control algorithm, issues commands to the executive devices to activate programmed warning signals, alerting the driver to the impending danger. This solution is particularly useful in conditions of limited visibility, for example after dark, when the eyes are constantly exposed to changes in lighting and need a few seconds to readjust to the darkness. In such a case, the obstacle detection system will inform the driver of an undesirable object detected in the sensor's field of view with an optical signal or both an optical and acoustic signal.

The creation of complete lighting on board a bicycle shows that it is essential for safe travel on roads, bicycle paths, or, in exceptional situations, pedestrian paths. Signaling the intention to turn, brake, or generally be present on the road has a huge impact on the safety of all road users, yet two of these signals are not regulated by law and are not used by most cyclists. Using a specially designed lighting system, which, in addition to the standard front headlight and rear position light, also offers front and rear turn signals and an integrated brake light. Turn signals controlled by a switch mounted on the handlebars completely eliminate the need to take your hands off the handlebars while riding, which significantly improves the stability of the vehicle when maneuvering. The brake light is an integral part of the position light and functions independently and completely automatically when a decrease in vehicle speed is detected. An additional element of the lighting system is a twilight sensor, which is responsible for automatically turning on the lights when the intensity of ambient light falls below a specified threshold.

The last element of the electronic system is an LCD display, which collects information useful to the user, such as current speed, temporary distance, total distance, and battery charge level. The displayed data can be used to limit the current speed or draw attention to the number of kilometers traveled in order to suggest the need to visit a bicycle service center for a periodic inspection.

The total estimated cost of purchasing all the electronic components used in the presented concept design does not exceed PLN 1,000 gross per unit. By planning mass production, obtaining wholesale prices or prices directly from the manufacturer for the components, and deducting VAT on goods, it is possible to introduce new technology in bicycles to the market at an affordable price for the end user.

All the systems and components presented, adapted for installation in a smart bicycle, bring certain conveniences and improvements that have been successfully applied in other areas of human life. The manufacturing industry, modern automotive industry, building systems, and many other areas of society are increasingly basing their operations on automation, the use of sensors, and self-adaptation to a given situation. Nowadays, the level of advancement in electronics is admired by enthusiasts and experts in the field, assists people who only use technological goods in their everyday lives, and opens doors for professionals who are constantly looking for new inspiration and solutions.

References

Avina-Bravo, E.G., Cassirame, J., Escriba, C., Acco, P., Fourniols, J.Y., Soto-Romero, G. (2022). Smart Electrically Assisted Bicycles as Health Monitoring Systems: A Review. *Sensors (Basel), 22*(2), 468. DOI: https://doi.org/10.3390/s22020468.

Beeking, M., Wies, H., Steinmaßl, M., Rehrl, K. (2024). How smooth is your ride? Comparison of sensors and methods for surface quality assessment using IMUs. *Traffic Safety Research, 7*. DOI: https://doi.org/10.55329/guai2275.

Boot, M.B., Ulak, M.B., Geurs, K.T. (2024). Using body sensors for evaluating the impact of smart cycling technologies on cycling experiences: A systematic literature review and conceptual framework. *European Transport Research Review, 16*(13). DOI: https://doi.org/ 10.1186/s12544-024-00635-3.

Eisenman, S.B., Miluzzo, E., Lane, N.D., Peterson, R.A., Ahn, G.-S., Campbell, A.T. (2007). The BikeNet mobile sensing system for cyclist experience mapping. In: *Proceedings of the 5th International Conference on Embedded Networked Sensor Systems (SenSys '07*, pp. 87-101). New York: Association for Computing Machinery. DOI: https://doi.org/10.1145/ 1322263.1322273.

Fischer, M.S., Martínez, A., Rojas, R., Vázquez, P. (2024). *Cost-effective, open-source light shutters with Arduino control. HardwareX*. DOI: https://doi.org/10.1016/j.ohx.2024. e00548.

Gómez-Suárez, J., Arroyo, P., Alfonso, R., Suárez, J.I., Pinilla-Gil, E., Lozano, J. (2022). A Novel Bike-Mounted Sensing Device with Cloud Connectivity for Dynamic Air-Quality Monitoring by Urban Cyclists. *Sensors*, *22*(3), 1272. DOI: https://doi.org/10.3390/s22031272.

Henao, A., Apparicio, P., Maignan, D. (2021). One Metre Plus (1M+): A Multifunctional Open-Source Sensor for Bicycles Based on Raspberry Pi. *Sensors, 21*(17), 5812. DOI: https://doi.org/ 10.3390/s21175812.

Jannah, A.N., Moridpour, S., Tay, R., Du, B. (2025). Cyclist safety in the digital age: A review of advanced warning technologies. *Accident Analysis & Prevention, 217,* 108069. DOI: https://doi.org/10.1016/j.aap.2025.108069.

Kapousizis, G., Ulak, M.B., Geurs, K., Havinga, P.J.M. (2022). A review of state-of-the-art bicycle technologies affecting cycling safety: Level of smartness and technology readiness. *Transport Reviews, 43*(3), 430-452. DOI: https://doi.org/10.1080/01441647. 2022.2122625.

Kumar, K.C., Motupalli, R.K. (2020). Arduino Uno based Smart Helmet with Protective Bike System Using IoT. *Journal of Advanced Research in Dynamical and Control Systems, 12*(9), 27-33. DOI: https://doi.org/10.5373/JARDCS/V12I9/20202638.

Lee, D.-Y., Yoo, H.-J., Lee, J.-Y., Jeong, G.-O. (2025). Development of a Bicycle Road Surface Roughness and Risk Assessment Method Using Smartphone Sensor Technology. *Sensors, 25*(11), 3520. DOI: https://doi.org/10.3390/s25113520.

Luo, C., Hui, L., Shang, Z., Wang, C., Jin, M., Wang, X., Li, N. (2024). Portable Arduino-Based Multi-Sensor Device (SBEDAD): Measuring the Built Environment in Street Cycling Spaces. *Sensors, 24*(10), 3096. DOI: https://doi.org/10.3390/s24103096.

Novak, J. (2020). *A Study of Bicycle Frame Customization Through the Use of Additive Manufacturing Technology*. DOI: https://doi.org/10.6084/m9.figshare.12899987.v1.

Omri, A., Benothman, N., Sayahi, S., Tlili, F., Chaabane, F., Besbes, H. (2024). Advancing Cycling Safety: On-Bike Alert System Utilizing Multi-Layer Radar Point Cloud Clustering for Coarse Object Classification. *Sensors, 24*(10), 3094. DOI: https://doi.org/10.3390/s24103094.

Reggiani, G., Salomons, A.M., Sterk, M., Yuan, Y., O'Hern, S., Daamen, W., Hoogendoorn, S. (2022). Bicycle network needs, solutions, and data collection systems: A theoretical framework and case studies. *Case Studies on Transport Policy, 10*(2), 927-939. DOI: https://doi.org/ 10.1016/ j.cstp.2022.03.006.